Influence of flanges on the shear capacity of reinforced non-rectangular concrete members without shear reinforcement

MASTER THESIS

Özge Kiliç | 4621573
TECHNISCHE UNIVERSITEIT DELFT | RIJKSWATERSTAAT

Influence of flanges on the shear capacity of reinforced non-rectangular concrete members without shear reinforcement

By

Ö. (Özge) Kiliç

in partial fulfilment of the requirements for the degree of

Master of Science
in Civil Engineering

at the Delft University of Technology,
to be defended publicly on Wednesday August 23, 2023 at 13:00 PM.

Thesis committee:		
Comittee Chair:	Prof. Dr. ir. M.A.N. Hendriks,	TU Delft
Supervisor:	Dr. ir. Y. Yang,	TU Delft
Supervisor:	Dr. ir. M.A. Roosen,	Rijkswaterstaat
Guest supervisor:	Dr. ir. P.C.J. Hoogenboom,	TU Delft

This thesis is confidential and cannot be made public until August 23, 2023.

An electronic version of this thesis is available at http://repository.tudelft.nl/.

TU Delft

Rijkswaterstaat
Ministerie van Infrastructuur en Waterstaat

Preface

Writing this master thesis on the influence of flanges on the shear capacity of reinforced non-rectangular cross-sections has been a remarkable journey, one that has made an unforgettable impact on both my academic and professional life. It is with great joy, pride and a sense of accomplishment that I present this work and I would like to take a moment to share my personal reflections on this journey.

The decision to delve into this subject was driven by my genuine fascination with its significance in the engineering practice. After hearing that in the Netherlands we are often confronted with the fact that existing structures without shear reinforcement do not comply with the shear force standards and the impact this has on replacement and renovation of these existing structures, I felt a strong desire to contribute to the knowledge surrounding this subject. I went into this research with a sense of purpose and determination.
With this thesis I want to contribute to engineering practice and inspire further research into the complex relationship between flanges and shear capacity. It is my sincere hope that this work will spark curiosity, stimulate innovative thinking and serve as one piece of the puzzle for future research efforts.

During this study I encountered numerous challenges that tested my determination and perseverance. The complexity associated with investigating the influence of flanges on the shear capacity required careful analysis and countless study hours. However, these obstacles were met with enthusiasm and a thirst for knowledge. While immersing myself in the depth of research, I also had a responsibility to properly exercise my career at Rijkswaterstaat and find a balance with this research. It was not always easy to find the harmony between the two, but through perseverance and dedication I managed to find a balance. The support and understanding of my colleagues and executives, Lidewij van Wagensveld and Christine Mak, has been invaluable for which I am deeply grateful.

I must express my deepest gratitude to my supervisors, Marco Roosen and Yuguang Yang, for their unwavering guidance, expertise and patience throughout this research journey. Their invaluable insights and encouragement have played an important role in shaping the direction and quality of this thesis. I am also grateful for the help and cooperation of Max Hendriks.
In moments of self-reflection, I am reminded of the incredible support that has sustained me through this challenging period. My family has been a constant source of encouragement, understanding and love. Their belief in my abilities and infinite support have inspired me to push the limits of my potential.
As I reach the end of this academic chapter of my life, I express my sincere appreciation to all those who have been part of this journey. Your support, mentorship and encouragement have been invaluable and I am truly grateful for any contribution.

Özge Kilic
26-06-2023

Abstract

This master thesis investigates the influence of flanges on the shear capacity of reinforced non-rectangular members without shear reinforcement. The study adapts the evaluation procedure developed by Yang (2014) for rectangular cross-sections to analyze plates with holes, I-beams and T-beams.

Although extensive research has been carried out on reinforced concrete with rectangular cross-sections and without shear reinforcement, little is known about the shear capacity of non-rectangular cross-sections without shear reinforcement. A number of studies have shown that the capacity increases with a T-beam [27, 34, 35, 38], for example, but the positive contribution of the flanges is nevertheless not taken into account in the standards. This conservatism may in some cases lead to unnecessary renovation and possibly replacement of structures. This research will focus mainly on the missing link of the non-rectangular cross-section using the model of Yang as a starting point. The aim is to find an evaluation procedure in order to determine the effective web width for non-rectangular cross-sections, which can possibly be included in the Eurocode 2.

First of all, Yang's evaluation procedure for rectangular cross-sections is adapted for plates with holes, I-beams and T-beams. The results obtained with this modified evaluation procedure are analyzed and then compared with the results of the calculated shear capacity of the web only using Yang's model. In this way, insight is created to determine an effective web width. In addition, the results are also compared with test results, so that the accuracy of the model can be determined.

The study emphasizes the significance of the location of the neutral axis in determining the shear resistance, with members with thick flanges often having the neutral axis inside the flange and thin flanges in the web. However, this depends on the height of the compression zone z_c, which in turn depends on the reinforcement ratio ρ_s
The findings show that members with thinner flanges have approximately 40% less capacity compared to thicker flanges, which is a consequence of the location of the neutral axis, namely in the web. As a result, the effective depth and crack height decreases and the width of the member over the crack height is less than if the major crack would be partly in the flange. The width of the flange plays a crucial role when the neutral axis is in the flange, which has a significant impact on the shear capacity. This is because the upper part of the crack contains the highest shear stresses due to aggregate interlock, which therefore results in higher capacity due to the width of the flange instead of the smaller web width.
In addition, it also appears that the web width has also an important influence on the shear capacity. With a thinner web, the contribution of the aggregate interlock decreases, so also the total shear resistance with approximately 22%. Furthermore, despite the fact that the contribution of the compression zone increases due to larger area of the flange, aggregate interlock plays an important role and contributes most to carry the shear force. The contribution of aggregate interlock varies between 45%-85%

In the Eurocode 2, only the smallest web width is taken into account to calculate the shear resistance of non-rectangular cross-section. To reduce the conservative results because of this assumption in Eurocode 2, a scaling factor is proposed based on the comparison of the results between the modified evaluation procedure for non-rectangular cross-sections and the web-only scenario.
On this basis the study determines the effective web width for plates with holes, which could be determined by $b_{weff} = 1{,}75b_w$. For I-beams with $\rho_s < 1\%$, the effective web width is $1{,}25b_w$ if $h_f/h \leq 0{,}25$, otherwise $4{,}2h_f/h + 0{,}2$. In case of a reinforcement ratio of $1\% \leq \rho_s \leq 2\%$ the effective web width of I-beams becomes

$1{,}35b_w$ if $h_f/h \leq 0{,}25$, otherwise $3{,}5h_f/h + 0{,}5$. For T-beams the effective web width could be determined by $1{,}15b_w$. The general limitations of these models are:

- Only applicable for members within the ranges $0{,}20 \leq b_w/b_f \leq 0{,}60$ for plates with holes; $0{,}10 \leq b_w/b_f \leq 0{,}50$ for I/T-beams and $0{,}15 \leq h_f/h \leq 0{,}40$ for all members;
- Only applicable for member with reinforcement ratio between 0,4% and 2%;
- Only valid for slender members where $a/d \geq 3$.

Comparisons with test results demonstrate the accuracy of the evaluation procedure for non-rectangular cross-sections, as well as the reasonably accurate Eurocode 2 predictions using the simplified effective web width. The average ratio of calculated shear capacity (V_{cal}) to measured ultimate shear capacity during tests (V_u) was 0,94, with a Coefficient of Variation of 16%. In comparison, using the simplified effective web width b_{weff} approach with EC2, the results also showed reasonable accuracy, with an average ratio of 0,79 and a CoV of 21%.

Table of Contents

List of tables

List of Figures

Used symbols

Latin upper case

A_c	Total cross-sectional area of concrete
A_{cc}	Cross-sectional area of the concrete compression zone
A_s	Total cross-sectional area of reinforcement bars
A_x, A_y	Projected contact areas
C_{Rd}	Factor in EC2 to determine the shear strength of members without shear reinforcement
D	Diameter of the holes in reinforced concrete plate
E_c	Elastic modulus of concrete
E_s	Elastic modulus of steel
I	Moment of inertia of a cross-section
M	Bending moment
M_{cr}	Cracking moment
N	Axial force
N_c	Compressive axial force in compression zone
N_{ai}	Normal force component of aggregate interlock along the crack
T_s	Tension force in the reinforcement
V	Shear force
V_{ai}	Shear component of the aggregate interlock along the crack
V_c	Shear component of the uncracked compressive area
V_{cr}	Shear force when the critical inclined crack occurs
$V_{cr,m}$	Shear force which opens the major crack located at x_0 from the support
V_d	Shear force transferred by dowel action
V_u	Maximum shear force in the member before failure

Latin lower case

a	Shear span
a_{eff}	Effective shear span
a_0	Uncracked span from the support
b	Width of a rectangular member
b_f	Total width of the member, also the flange width
b_{ef}, b_n	Netto width at reinforcement level
b_{gem}	Average web width according to RBK
b_w	Smallest web width in the cross-section
b_{weff}	Effective web width
b_{wi}	Width of the web of plate with holes at specific height i
c	Concrete cover
d	Effective height of the member
e_p	Tendon eccentricity
f_c, f_{ck}	Concrete compressive strength
f_{cm}	Mean concrete compressive strength
f_{ct}	Concrete tensile strength
f_{ctm}	Concrete mean tensile strength
h	Total height of the member
h_f	Flange thickness
k	Size effect according to EC2
k_b	Reduction for tensile strength of concrete

k_c	Inclination of the stress line
k_{c1}	Constant factor of 0,5
l_{cr}	Mean crack spacing
$l_{cr;m}$	Spacing of the major cracks
l_t	Minimum crack spacing
n	Number of reinforcement bars
n_e	Ratio between E_s/E_c
r	Radius of the holes in reinforced concrete plate
r_F	Distance between the tip of the crack and the axis where the load is applied
s	Distance of a location on the crack profile measured from the root of the crack
s_{cr}	Stabilized crack height/ Height of the critical crack
sf	Scale factor
w, w_b	Crack width at reinforcement level
w_{max}	Maximum crack width
w_t	Crack width at the tip of a major crack
w_0	Crack width before slip
x	Longitudinal direction of the member
x_{cr}	Distance between the root of the crack and the tip of the crack in longitudinal direction
x_A, x_0	Distance from the root of the crack to the centre of the support
y	Vertical direction of the member/ deflection of the member
z	Internal level arm
z_c, h_F	Height of the uncracked compressive area of the concrete member

Greek upper case

Δ	Vertical crack opening, also shear displacement
Δ_{cr}	Critical shear displacement
Ψ_s	Ratio between the mean crack spacing and the minimum crack spacing at reinforcement level
$\emptyset$	Diameter of reinforcement bars

Greek lower case

α	Grade of fullness
ε	Normal strain
μ	Friction coefficient between aggregate and matrix material
ρ_{eff}	Effective reinforcement ratio
ρ, ρ_s	Reinforcement ratio
σ	Normal stress
σ_m	Normal stress due to bending moment
σ_{pu}	Matrix yielding strength
τ	Shear stress
τ_{bm}	Bond stress between concrete and reinforcement
τ_m	Maximum shear stress in the cross-section

Abbreviations

AI	Aggregate interlock
DA	Dowel action
CZ	Compression zone
EC	Eurocode
CoV	Coefficient of Variation
STA	Shear transfer action
mvd	Shear slenderness ratio calculated by M/Vd

1. Introduction

This chapter describes the problem statement and the scope of the research. The relevance of the research and the structure of the report are also described in this chapter.

1.1 Problem statement

In recent decades, much research has been conducted on the shear design of reinforced concrete members without shear reinforcement [1, 4, 5, 18]. These studies have shown the different shear-transfer actions (STA's) that contribute to the shear strength of these members. Shear is recognized as a potential failure mode that could govern the design at ultimate limit state (ULS) and it is particularly critical due to its limited capacity for deformation and brittleness [19]. Most of the studies on this topic have mainly focused on rectangular cross-sections.

While several studies have shown the benefits of a compression flange in improving the shear capacity of for example T-beams [27, 34, 35, 38], most current codes do not take into account the beneficial effect of the flanges on the shear strength. In many codes of practice, the shear design of members without shear reinforcement mainly relies on empirical equations, for example Eurocode 2 and ACI 318.

Despite the lack of a generally-accepted mechanical model and approach, the understanding of the shear-transfer actions in reinforced concrete has led to the development of several mechanical models for shear design [4, 7, 8, 43, 44]. These models have reached a level of reliability and are starting to be included into codes. It is noteworthy that while the various mechanical models predict comparable shear strengths, they are not in agreement on the governing shear-transfer action carrying the load. This disagreement could be explained by the fact that the mechanical models are often based on the assumption and interpretation of a crack pattern after failure or the measured kinematics prior to failure.

1.2 Scope of the research

The main focus of this master thesis is to investigate the shear capacity of non-rectangular reinforced concrete members without shear reinforcement. Yang's mechanical model [7] will be used as a basis for this research and will be further extended for non-rectangular cross-sections. The aim of this research is to determine the effective width of the cross-section, which could be included in the Eurocode 2 to calculate more accurate shear capacities for non-rectangular cross-sections. The cross-sections that will be studied in this research are: I-beams, T-beams and plates with holes.

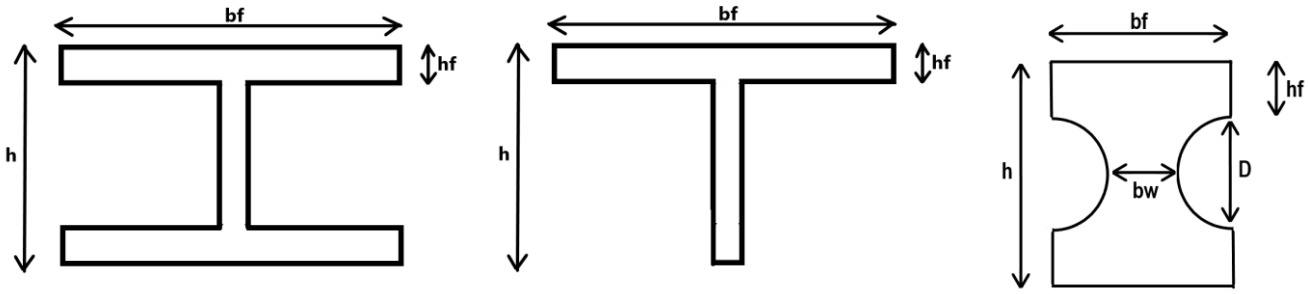

Figure 1: From left to right: I-beam, T-beam and Typical section of plate with holes

The following conditions apply to this study: Yang's method will be extended for a simply supported beam loaded with a point load, without taken into account the effects of the location of the point load or the influence of a distributed load. Research has shown that loads located close to support are transferred directly to the support via another mechanism [8].
The study is limited for concrete elements made of normal concrete mixtures. The effects of high strength concrete and lightweight aggregate concrete on the shear capacity will not be further investigated. The influence of size effect has also not been extensively investigated.

After completion of this research, the results and insights obtained will make it possible to adapt the formulas for determining the shear capacity of members without shear reinforcement in the next-generation Eurocode 2. However, this is not the scope of this research.

1.3 Relevance of the research

Non-rectangular cross-sections such as I and T-beams are used as structural elements in most existing bridges. Another example of structural elements with a non-rectangular cross-section are the plates with holes. Reinforced plates with holes were frequently used in the 1960s and nowadays are still maintained by Rijkswaterstaat. In total there are 731 objects containing plate elements as road deck, however there are an estimation of 15 objects that have a road deck with reinforced plate with holes. Based on the capacity checks according to Eurocode 2, these plates do not have sufficient shear capacity. However, the code only assumes the smallest (web) width of the cross-section, which is a conservative approach based on several researches [27, 34, 35, 38]. This may result in a structure being replaced or renovated, while it may be unnecessary.

1.4 Content

The thesis is structured as follows:

Chapter 2: Literature review
- Overview of shear failure in reinforced concrete structures
- Discussion of shear transfer mechanisms and failure mechanism
- Review of relevant studies and research on shear behaviour of rectangular and non-rectangular cross-sections without shear reinforcement
- Summary of key finding from the literature review

Chapter 3: Analysis of failure mechanism as described by Yang (2014)
- Detailed analysis of the failure mechanism in reinforced concrete members without shear reinforcement based on the work of Yang: “Shear Behavior of Reinforced Concrete Members without Shear Reinforcement, A New Look at an Old Problem”.
- Examination of the assumptions used by Yang

Chapter 4: Adaption of Yang’s evaluation procedure for non-rectangular cross-sections
- Development and description of the modified evaluation procedure for non-rectangular cross-sections based on Yang’s model for rectangular cross-sections
- Explanation of the methodology and adjustments made to account for the specific geometry and characteristics for non-rectangular cross-sections
- Presentation of the equations and evaluation procedure

Chapter 5: Comparison and discussion of the results

- Comparison of the results obtained with the modified evaluation procedure for non-rectangular cross-sections with the shear resistance of the web only
- Analysis of the effects of the cross-sectional parameters, neutral axis location and other parameters
- Identification of any discrepancies or limitations observed in the results
- Comparison of the results with relevant test data

Chapter 6: Conclusion and recommendations

- Summary of the main findings
- Recommendations for further research and potential areas of improvement in the evaluation procedure

2. Shear failure in literature

2.1 Introduction

This chapter contains a literature review of the shear transfer and failure mechanisms.

2.2 Shear transfer mechanism

Several researchers investigated the shear transfer actions after the concrete is cracked. An important study on this was carried out by Kani (1964, 1966), in which he investigated the shear transfer by taking into account the strength of the concrete teeth between two flexural cracks.
Muttoni et al. investigated the shear transfer actions which are possible by this concrete teeth in [A. Muttoni & F. Ruiz 2008]. The influence of the cracking pattern on the shear transfer actions was first investigated by [Fenwick and Paulay 1968]. Others researched the amount of shear that could be transferred by a specific transfer mechanisms. In [S. Campana, F. Ruiz, A. Anastasi & A. Muttoni 2013] Campana et al. investigated the activation of various shear transfer mechanisms for one-way RC members. In his research, Yang has paid attention to the influence of dowelling action on the failure mechanism [Yang, 2014]. Cavagnis (2017) conducted an extensive research on the shear-carrying and failure mechanism of RC members without shear reinforcement.

Although there is no general agreement on the shear failure mechanism of reinforced concrete without shear reinforcement, there is agreement in the literature on the shear transfer actions. The shear force can basically be transferred by the following mechanisms [F. Ruiz, A Muttoni & J. Sagesta 2015]:

- Cantilever action
- Aggregate interlock
- Dowel action
- Residual tensile strength of concrete

The activation of a specific transfer action depends on the shape and kinematics of the critical crack. The development of a critical shear crack does not necessarily mean the failure of the member. Depending on the crack path and geometry of the crack, another shear-carrying mechanism, the arching action, could be developed.
This chapter will take a closer look at the shear transfer mechanisms mentioned above.

2.2.1 Cantilever action

The cantilever action is the ability to transfer the shear force by means of the uncracked concrete in between two flexural cracks, which acts like a cantilever beam or a teeth structure. This structural behaviour was observed by Kani (1964). The shear force is transferred by a compression chord and tension tie within the tooth, strut and tie model as described by Yang (2014).

The shear carrying capacity of this action is reduced or even cancelled when the flexural crack progress with a quasi-horizontal crack, which makes the capacity of the tension tie impossible [A. Muttoni & F. Ruiz 2008] & [F. Cavagnis, F. Ruiz & A. Muttoni 2018]. This phenomenon applies also to the aggregate interlock and dowel action. According to Cavagnis et al. these shear transfer actions induce tensile stresses at the tip of the crack and the reinforcement level. When the tensile stress reaches the tensile strength of the concrete,

the existing flexural crack is extended by a quasi-horizontal crack at the crack tip or a new crack is created at the reinforcement level [A. Muttoni & F. Ruiz 2008].

In uncracked concrete the stress distribution follows the theory of elasticity. According to Yang (2014) the simplified shear stress distribution of Mörsch provides sufficient accuracy in order to calculate the shear force in the compression zone. The shear force in the compression zone could be determined by assuming the contribution of the entire uncracked area. Therefore, the effective width of the concrete member has an important influence on the shear force in the compression zone.

2.2.2 Aggregate interlock

In normal concrete the strength of the hardened cement paste (matrix) is lower than the strength of the aggregate particles. Therefore, crack occurs in the cement paste along the particles at the bond zone, the weakest link. This is the two-phase system described by Walraven in [Walraven 1980, 1981], wherein the matrix is phase I and the collection of aggregate particles phase II, see the crack structure below.

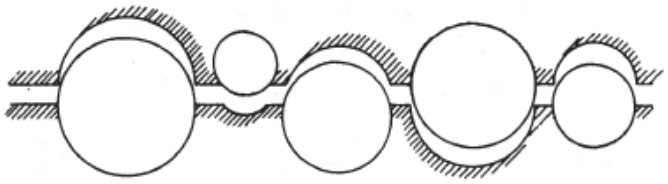

Figure 2: Crack structure

A well-known and extensive research on aggregate interlock has been conducted by Walraven (1980 & 1981). After defining a mechanical model, he verified the validity of it by several experiments. In his study, Walraven concluded that normal stress, shear stress, crack width and shear displacement are all involved in describing the mechanism of aggregate interlock properly.
He assumed spherical aggregate particles with different diameters and distribution. The crack occurs along the particles with crack width w. After this moment the shear displacement takes place. So, he assumed that first the crack opens and then slides. During shear displacement the crack faces make contact, which develops contact areas and interlocking due to the plastic behaviour of the matrix. The aggregate particle at one of the crack face interlocks with the other face and resist the shear displacement. At this contact area normal and tangential stresses are generated due to slip and crushing of the particles, see figure below for the schematic model.

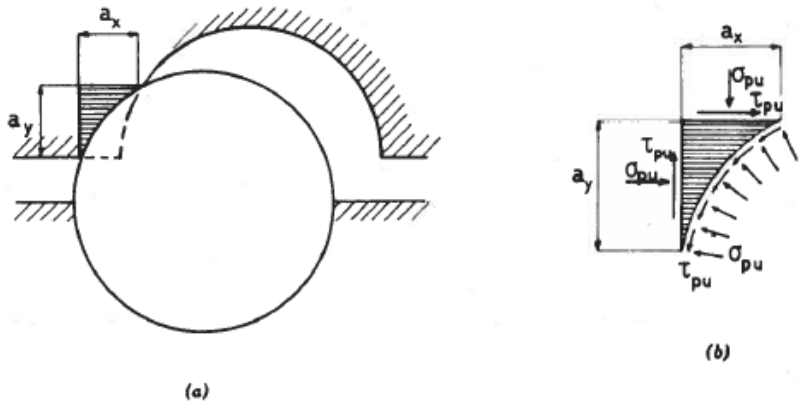

Figure 3: Schematic model Walraven, (a) Contact area, (b) Stress conditions

The (projected) contact areas A_x and A_y depend on the diameter of the aggregates, crack width, shear displacement and the ratio of aggregate volume and concrete volume. This ratio could be considered as the roughness parameter according to [T. Huber, P. Huber & J. Kolleger 2019]. The mechanical model derived is compared with a number of experiments by fitting the theoretical results to the experimental results. According to this, the best result is obtained for a friction coefficient of $\mu = 0{,}40$ (Walraven 1981). For the matrix yielding strength σ_{pu} he found: $\sigma_{pu} = 6{,}39 \times f'^{0{,}56}_{cc}$ MPa.

However, the assumption of that the crack opens (w) prior to sliding (Δ) is doubtful. Taylor (1970) was the first who observed that the opening and sliding of the crack happens simultaneously. Hamadi and Regan also noted in [Y. D. Hamadi & P.E. Regan, 1980] that the crack first opens and then shears with a continuous increase of crack width. Ulaga (2003) and Guidotti (2010) both applied the model of Walraven with different assumptions. Ulaga assumed that the crack opening and sliding occurs simultaneously at a constant angle and recognized a phase of decreasing contact followed by separation. Guidotti assumed that a fraction of the crack width (w_0) develops before the slip, followed by an increase of both at an angle. Comparison of these three methods gives that the method of Walraven leads to an upper bound solution of the aggregate interlock stresses, the kinematics of Guidotti develops intermediate stress values depending on the initial crack width w_0 and the method of Ulaga leads to a lower bound solution [Cavagnis 2017].

Considering the researches done recently, Huber et al. conducted 18 push-off tests and ten shear beam tests in order to determine the influence of aggregate interlock on the shear capacity of RF beams without shear reinforcement in [T. Huber, P. Huber & J. Kolleger 2019]. They investigated the influence of different concrete mixtures on the crack surface roughness. This study confirmed the observations of Cavagnis et al. (2017) that aggregate interlock mostly depends on the crack pattern [F. Cavagnis, M. Fernadez Ruiz, A. Muttoni 2017]. The influence of crack surface roughness was firstly observed by Fenwick et al. [R. Fenwick & T. Paulay 1968]. They showed with direct tests that the influence of aggregate interlock increases with concrete strength and a reduction in crack width. This is in line with the research of Walraven (1980), wherein he observed that the projected contact areas A_x and A_y increase with decreasing crack width w and increasing value of Δ. Also, according to the study of Huber et al. it can be assumed that the roughness of the crack surface is influenced by the concrete strength. Hamadi and Regan (1980) noticed that the stiffness of the interlock action mainly depends on the crack width and aggregate type, while in the same conditions the ultimate shear resistance depends on aggregate type and normal stress.

Contrary to the assumption of Walraven that the crack will propagate along the aggregate particle, it is observed that cracks occur through the aggregate particle in case of high-strength concrete or lightweight aggregates. A crack through the aggregate particle leads to a smooth crack surface, reducing the shear transfer by aggregate interlock. This is shown by Hamadi and Regan in [Y. D. Hamadi & P.E. Regan, 1980]. They used push-off test on concretes made with lightweight (expanded clay) and natural gravel aggregates and T-beam tests. The tests demonstrate that the shear transfer and stiffness is higher with natural gravel aggregates.

Cavagnis et al. observed by measurements on the crack relative displacements that aggregate interlock stresses were mainly developing along the steeper part of the crack, because large crack sliding occurred [F. Cavagnis, M. Fernandez Ruiz, A. Muttoni 2015]. According to Yang (2014), the large crack sliding occurs when a quasi-horizontal branch starts to develop. In some cases, concentration of the aggregate interlock stresses led to the propagation of new crack, which eventually leads to member failure.

As described above, the aggregate interlock depends on the aggregate type, crack width, shear displacement, concrete strength and the ratio of aggregate volume-to-concrete volume, integrated along the crack. Therefore, the effective width of the concrete members has no direct influence on the aggregate interlock mechanism. However, the shear transfer capacity of this mechanism is determined by integration of the aggregate interlock stresses around the crack curve, including the width of the member [F. Cavagnis, M. Fernandez Ruiz, A. Muttoni 2018].

2.2.3 Dowel action

The dowelling action is the resistance of the reinforcement bars to shear displacement (reinforcement bars crossing a crack and loaded perpendicular to their axis). Several studies are conducted to the mechanism and contribution of the dowel action. According to Krefeld and Thurston (1966) failure happens when dowel cracking at reinforcement level occurs. This phenomenon is supported by Yang's findings in [Y. Yang, 2014].

Chana also noticed in his tests that beam failure is predated by dowel cracking at 95% of the ultimate load. According to his research, the crack width opens up with increasing shear force, resulting into increase in the dowel force and tension in the surrounding concrete. This causes splitting cracks in the concrete along the reinforcement bar resulting in loss of bond. At the peak load the crack width is so small that it is unlikely that aggregate interlock mechanism failed, while the dowel crack is in the same of order measured by other researches at the peak load. This indicates that dowel cracking triggered the member failure and that ones the cracking occurs, the restraint between the two beam parts is lost, resulting in an abrupt failure. Therefore, the shear failure mechanism is closely associated with dowel action.

According to Jelic et al. kinking of the reinforcement bars is the only mechanism of dowel action in case of reinforcement with negligible flexural stiffness [I. Jelic, M.N. Pavlovic, M.D. Kotsovos 1999]. In order to provide shear resistance with kinking, the crack surfaces should undergo large shear displacements. They performed several tests on RC beams and compared the results with FEM and observed that the obtained FEM results correspond to the test results, with an underestimation of 5,6% of the failure load. Bearing in mind that the FEM does not take dowel action into account, contrary to the above findings, they concluded that dowel action has a negligible contribution to the shear failure mechanism. Ruiz et al. noticed in [M. Ruiz, A. Muttoni & J. Sagaseta, 2015] that the dowelling action in slender beams is limited, yet not negligible. Jelic et al. also observed that ''as long as the reinforcement cross-sectional area is constant, the ultimate shear capacities of the beams tested are practically identical, irrespective of the bar sizes and steel yield strength''. This is in contrast to the findings of Ruiz et al., who conclude that the dowelling action is affected by strain and size effects depending on mainly the ratio between bar diameter and the effective depth. They noticed that for members without shear reinforcement the dowelling capacity decreases with increasing strains in the reinforcement bars.

According to Cavagnis (2017), the following are the governing parameters of the dowel action: tensile strength of concrete, bar diameter, concrete cover, the net width and the strains in the reinforcement bars. Ruiz et al. noted in [M. Ruiz, A. Muttoni & J. Sagaseta, 2015] that all shear transfer actions in fact depend on the same parameters in mechanical models: strength of concrete, effective depth and width of the member, strains in the reinforcement bars and maximum aggregate size.

Cavagnis et al. (2015) also observed that the influence of the dowelling action is notable for short-span beams with limited distance between the critical shear crack and the edge of the support, which is supported

by the research of Campana et al (2013). Furthermore, cracks related to dowel action lead to increase of the critical shear crack opening, weakening other shear transfer action such aggregate interlock. This behavior was also observed by Yang (2014).
Another observation of Cavagnis et al. (2017) is that if the reinforcement yields partially, the dowelling action is reduced so much, that the contribution of it to the shear strength is negligible.

According to Ruiz et al. (2010) [F. Ruiz, S. Plumey, A. Muttoni] the capacity of the shear transfer capacity of dowel action depends on the concrete effective area around the reinforcement bars. Also the model of Baumann and Rüsch (1970) depends on the effective width of the concrete member at reinforcement level. Based on this, we can assume that the effective width around the reinforcement bars has a significant influence on the shear transfer capacity of the dowel action.

2.2.4 Residual tensile strength of concrete

After concrete has cracked, it still has some capacity to transfer shear forces through the crack, because of the softening residual strength of concrete. Hillerborg (1976) presented a method (fictitious crack model) using fracture mechanics in FEM where stressed are assumed to be transferred through a crack as long as it is narrowly opened. He assumed that the crack starts to propagate when the tensile strength is reached at the crack tip. The stress is not assumed to go down to 0 directly, but to decrease with growing crack width w. In case where $w < w_{max}$, the crack is able to transfer stresses. Therefore, energy is absorbed in the crack. For ordinary concrete w_{max} seems to be in the order of 0,01 – 0,02mm. He showed that the combination of fracture mechanics FEA gives reliable results regarding crack formation, propagation and failure.
According to Yang (2014) tensile stresses could be transferred through cracks when the crack width is smaller than 0,1mm, while according to Cavagnis (2017) this limit is 0,2mm.

Hordijk (1986, 1991) developed a model for the nonlinear material behavior of concrete in the basic principle of the fictitious crack model. This one of the most known and accepted stress-crack width relationship, as well as the one proposed by Reinhardt (1984).

According to Cavagnis et al. (2017) the quasi-horizontal part of the crack is characterized by pure mode I opening response and therefore governing by the residual tensile strength of concrete. Campana et al. (2013) observed that the contribution of this shear transfer mechanism is limited due to the crack widths.

The shear transfer capacity of residual tensile strength depends not directly on the member width. However, integration of the stresses along the crack makes that the shear transfer capacity of this mechanism becomes dependent on the member effective width.

2.2.5 Arching action

Arching action is a plasticity-based shear-carrying mechanism observed by Mörsch (1908), assuming a constant force in the reinforcement and varying depth of the compression zone, which leads to an inclined compression strut. This action is governed by short-span beams where the flexural cracks remain below the compression strut [J. Sagaseta & R.L. Vollum, 2011]. However, Cavagnis (2017) noticed that this shear transfer mechanism could also be governing for slender beams, depending on the height and location of the critical shear crack.

As described for the cantilever action, the shear force in the compression zone could be determined by assuming the contribution of the entire uncracked area. Therefore, the effective width of the concrete member has an important influence on the shear force in the compression zone.

2.3 Shear failure mechanism

2.3.1 Role of cracking pattern on the shear-carrying mechanism

Based on the test results available in the literature, the shear-carrying mechanism will be discussed and described.

Cavagnis (2017) describes four possible regimes governing the shear failure based on his literature review (Kani 1979, Leonhardt & Walther 1962), which is also reflected in the research of Ruiz et al. using Kaní's valley [M. Ruiz, A. Muttoni & J. Sagaseta, 2015]:

- For very short shear spans, the flexural cracks remain below the inclined compression strut and therefore the shear strength depend on the yielding of the longitudinal reinforcement (arching action). This corresponds to the plastic strength of the beam.
- For beams with a rather short span, the arching action is still governing. In this case, the flexural cracks propagate through the compression strut in a stable manner. Assuming the plastic strength may overestimate the shear capacity of the beam, because the strength of the inclined compression strut is reduced due to the flexural cracks through it. The compression strut develops in an elbow shape from the point load to the support. The failure occurs due to crushing of the concrete, because of the reduced compressive strength caused by the crack propagation and transverse tensile stresses. However, it should be noticed that the position of the critical crack is decisive for the shear strength and a large spread in the experimental results has been reported for these type of members.
- In case of larger shear spans, the arching action start to act in combination with the beam shear-transfer actions (aggregate interlock, dowel action, residual tensile strength and cantilever action), which becomes dominant thereafter. For these members, the critical shear crack propagates through the compression strut, leading to a brittle failure.
- In case of very slender members, the yielding of the flexural reinforcement is again governing the shear strength. The beam shear-transfer actions are able to carry sufficient loads, leading to flexural failure.

2.3.1.1 Influence of shear slenderness

Several studies are conducted to the influence of the location of the critical shear crack. Cavagnis et al. observed that the development of the critical crack and the influence of it on the shear strength strongly depends on the shear slenderness ratio in [F. Cavagnis, M. Fernandez, A. Muttoni, 2017], as already noted by Kani (1964). They also observed that for members with values of $a/d > 2{,}5$ the critical cracks propagated through the theoretical compression strut, consequently decreasing the shear strength, which is in line with the observation in literature described above. Another observation in this study was that for slender beams the shear resistance increases when uniformly distributed load is applied. Perez Caldentey et al. showed in their study that the distributed loads near the support are directly strutted to the support, increasing the shear resistance of members subjected to distributed loading. For non-slender beams this influence depends on the location of the critical crack in [P. Caldentey, A. Padilla, M. Fernandez Ruiz, 2012].

A mechanical approach on the size and strain effects has been implemented by Ruiz et al. in [M. Ruiz, A. Muttoni & J. Sagaseta, 2015]. They observed that the contribution of the aggregate interlock and residual tensile strength decreases for increasing openings of the critical shear crack, which occurs due to increasing

strains and sizes. Ruiz et al. also showed that the contribution of dowelling action is limited for slender elements, but not necessarily negligible. It is noted that the dowelling action if affected by size and strain effects.

2.3.1.2 Cracking pattern

Several researchers have studied the kinematics of the crack formation. In [M. Ruiz, A. Muttoni & J. Sagaseta, 2015] the shape of the critical shear crack of slender beams is described. They assume that the crack is composed of three parts: quasi-vertical part, quasi-horizontal part and a delamination crack at the reinforcement level. The quasi-vertical part has mostly a bending origin and extends about to the neutral axis. The quasi-horizontal part develops due to the tensile stresses resulting from the beam shear-transfer actions. The formation of the quasi-horizontal crack leads to rotation of the crack around the crack tip. In the quasi-horizontal part there is only pure opening of the crack (no slip), whereas in the quasi-vertical part there is variable opening and constant sliding along the crack. The vertical component of the displacement at the reinforcement level leads to the formation of the delamination crack, which increases the critical shear crack opening. These observations are in agreement with the test results obtained by other researchers [Yang 2014, Cavagnis et al. 2015].

Cavagnis et al. (2015) describes a similar composition of the crack pattern, but more extensive and detailed:

- Type A: primary flexural cracks under a rather steep slope and normally develop up to the theoretical location of the fibre where the concrete tensile strength is reached, but in all of the cases it develop at least up to 1,5*d*. The angle of this crack type depends on the ratio bending moment – shear force and gets flatter with reduced bending moment. The crack distance between the flexural cracks varies between 0,4*d* and 0,8*d* for all tested beams.
- Type B: secondary flexural cracks located in between two type A cracks or near the support. They initiate at a later stage with increasing load and are usually shorter than crack type A. The spacing between type A and B depends on the amount of reinforcement and the bond conditions.
- Type C: secondary or primary crack merging with another primary flexural crack.
- Type D: Delamination crack at the reinforcement level, with three possible kinematics (see the paper for more details). The delamination crack as described in Yang (2014) and Ruiz et al. (2015) is also observed in this research (type D'' and D'''). These were usually observed to initiate after the maximum load was reached, but not at the maximum load itself or before it.
- Type E: Aggregate interlock induced cracks which could develop at both sides of an (existing) crack type A or B transferring shear by aggregate interlock. The development of this crack type is studied by Jacobsen et al. (2012). According to this study, when an existing crack mode I (pure tension) is then subjected to a shear displacement, inclined cracks initiate due to the aggregate interlock forces. These inclined cracks develop according to the geometry of the existing crack and possibly at both sides of the crack.
- Type F: Growth of a primary flexural crack (type A) into the compression chord, named quasi-horizontal part in [M. Fernandez Ruiz, A. Muttoni & J. Sagaseta, 2015]. The length of this crack type at maximum load was varying between 0,05d and 0,8d and the angle between 5º and 50º. In cases of crack type F became critical the angle varied between 5º and 30º. However, the length of crack type F is limited by the distance to the load introduction area. The development of this crack type strongly depends on the ratio acting bending moment – shear. It was observed that this crack type developed close to failure for low values of bending moment (area near the support or point of moment inflection) and also in cases of relatively low loading when the bending moment was significant.

- Type G: Crack development within the compression chord, not originated from a crack type A. Develops due to local bending of the compression chord or near the load introduction area.

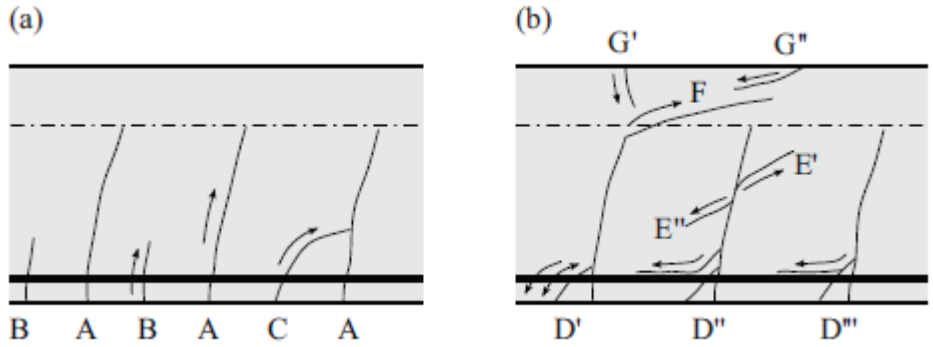

Figure 4: Crack types according to Cavagnis et al.: a)primary and secondary crack; b) cracks due to shear transfer actions

Yang (2014) also pays attention to the crack pattern in his study. According to him, the concrete starts to crack when the tensile strength of concrete is reached, at crack moment M_{cr}. After this moment (crack height s_1), the crack becomes unstable and further development of the crack height does not require any loading, until the moment resistance of the cross section gets higher. At this point (crack height s_2), the crack becomes stable. The values of s_1 and s_2 depends on the reinforcement ratio and fracture energy of concrete, with a higher reinforcement ratio resulting in a lower stabilized crack height $s2$ and a lower critical moment M_1.
He also noted that with increasing load multiple flexural cracks over the span will initiate and makes difference between cracks which are able to develop to the stabilized crack height s_{cr} (called major cracks) and those are not. The stabilized crack height is assumed to be independent to the crack shape and depends on the moment in the cross section. Ones the moment in the cross section reaches M_{cr}, a crack with height s_{cr} will develop. The value of s_{cr} could be calculated if the reinforcement ratio and the beam height is known.

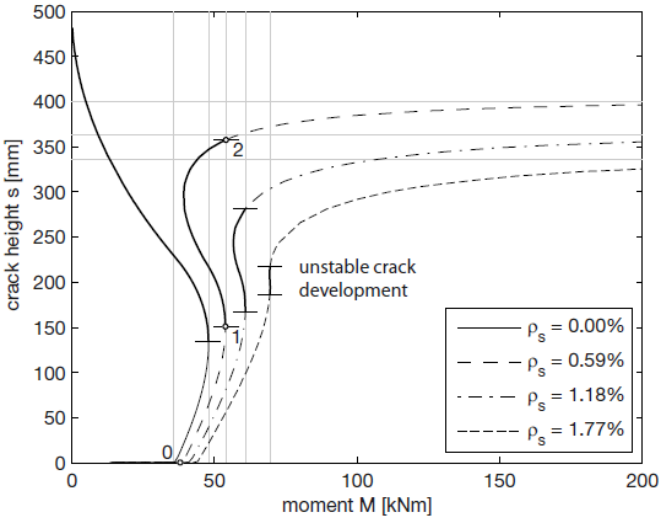

Figure 5: Crack height vs cross-sectional moment for beams with differential reinforcement ratios (Yang 2014)

According to Yang, major cracks have a spacing of s_{cr} / k_c, where k_c is the inclination of the stress line with k_c=1,28 for 52° in Krips (1985). He observed that the results of this theory compare well with the test results. Comparing the results of beams with different heights (3000mm, 1000mm and 100mm) he noticed that the cracks at reinforcement level for a beam h= 3000mm have a limited crack height, while the crack height in beam with h= 1000mm develop to a larger height. This observation confirms the theory of the crack distribution. Another important observation is that 100mm seems to be a lower bound of the effective height, so the crack pattern of the major crack is not influenced by tension softening behaviour of the concrete.

Cavagnis (2017) observed that the distance between two major cracks varies between 0,4d to 0,8d, with an average value of 0,56d in agreement to other researches. The assumption of Yang described above is also within this range, with a value of around 0,63d for a beam 300x500 with 3- ∅32 reinforcement.

2.3.1.3 Location of the critical shear crack

According to Yang (2014) the critical shear crack for beams with high shear slenderness ratio (a/d) will develop in the vicinity of the loading point. However, for small values of M_{cr}/V_{cr} the critical section will be close to the support.

Cavagnis et al. (2018) observed that the distance between the tip of the critical shear crack and the loading point varies between d and 2d for slender beams, which is also observed by Leonhardt and Walther. Cavagnis et al. also noticed that the shear capacity does not significantly differ between the investigated sections $x_A = d$, $x_A = 0{,}5a$ en $x_A = a - d$ (x_A is distance from the support). However, the contribution of the shear transfer actions show some levels of variation. Increasing shear slenderness ratio leads to different position of the critical crack, where the critical crack for less slender members is close to mid-span 0,5a. This is logical and in agreement with the observation of Yang, where the arching action becomes more dominant for less slender members.
Furthermore, the research has shown that for increasing reinforcement ratio the governing location of the critical crack shifts towards mid-span. Other parameters, for example the depth d, have low influence on the location of the critical shear crack.
Considering the test results, it is noticed that the curves around the minimum shear capacity is very flat between 1,5d and 2,5d from the load introduction plate (and between 0,4a and 0,6a). In order to adapt a fixed control section, Cavagnis assumed $x_A = 0{,}5a$ based on the considerations of Reineck et al. [K. Reineck, E.C. Bentz, B. Fitik, D.A. Kuchma, O. Bayrak, 2013]. This assumption is not very in line with the assumption of Yang. This difference can be explained by the fact that Yang's method is theoretical and that of Cavagnis is based on the test results.

2.3.2 Influence of compression flange

As described above, the effective width of the beam has an important influence on the shear transfer capacity of the transfer mechanisms. The presence of the flanges could also influence the crack pattern and kinematics. Gonzales et al. (2017) recently did a research on the influence of flanges on the shear-carrying capacity of RC without web reinforcement. They analysed the cracking pattern and kinematics, compared this with that of a rectangular cross section.

The crack does have a similar crack propagation process as for rectangular cross sections. The first cracks are bending cracks and extend approximately to the neutral axis. With increasing load, the quasi-horizontal branch develops above the neutral axis in the same way. These two steps were also observed by Thamrin et al. (2016) for both rectangular cross sections and T-beam.

Until the interface of web-to-flange is reached. For T-beams with large flange, the crack develops horizontally at the interface as this corresponds to the weakest area of the tension tie. They observed two patterns in most of the T-beams without shear reinforcement, based on the data collected from the literature:

- Diagonal shear crack in the web continued as a delamination crack at the interface, causing bending in the flange. This allows the development of the arching action or the strut and tie model with the elbow-shaped strut. This model allows the concrete strut to deviate by activating tensile forces in the concrete, as described by Muttoni and Schwartz (1991) and observed during measurements performed by Ribas and Cladera (2013). Thamrin et al. also observed this phenomenon, the maximum compression strain of T-beams is smaller than rectangular cross sections. Consequently leading to higher tensile strain of the reinforcement in T-beams. This shear transfer action fails in case of failure of the concrete flange in tension, leading to collapse of the beam.
- Diagonal shear crack in the web continued in the flange as an inclined crack. Failure occurs due to collapse of the strut and tie model, where dowel action is required which is not available.

Gonzales et al. (2017) also noticed during their study that the strut and tie models acting in the two patterns above neglect the aggregate interlock in the inclined branch of the crack in the web. This seems also in line with the observations for rectangular beams, where the quasi-horizontal branch has no slip and thus no aggregate interlock.

Thamrin et al. (2016) noted that the maximum load for T-beams is higher than that for rectangular cross sections (5 to 20% higher), confirming that the flange affects the shear stress distribution and initiation of the diagonal cracks in the web. Comparison between load-deflection curves confirmed that the contribution of the flange in the compression zone results in higher capacity and stiffness of T-beams. They observed that for T-beams with higher reinforcement ratio the height of the flexural crack remain relatively small. This indicates that the ratio of longitudinal reinforcement influences the crack formation, see figure below for the crack patterns from their research. They noticed that the reinforcement ratio also affects the crack angle in the shear span zone (second branch). This angle decreases with increasing reinforcement ratio for both rectangular cross sections and T-beams.

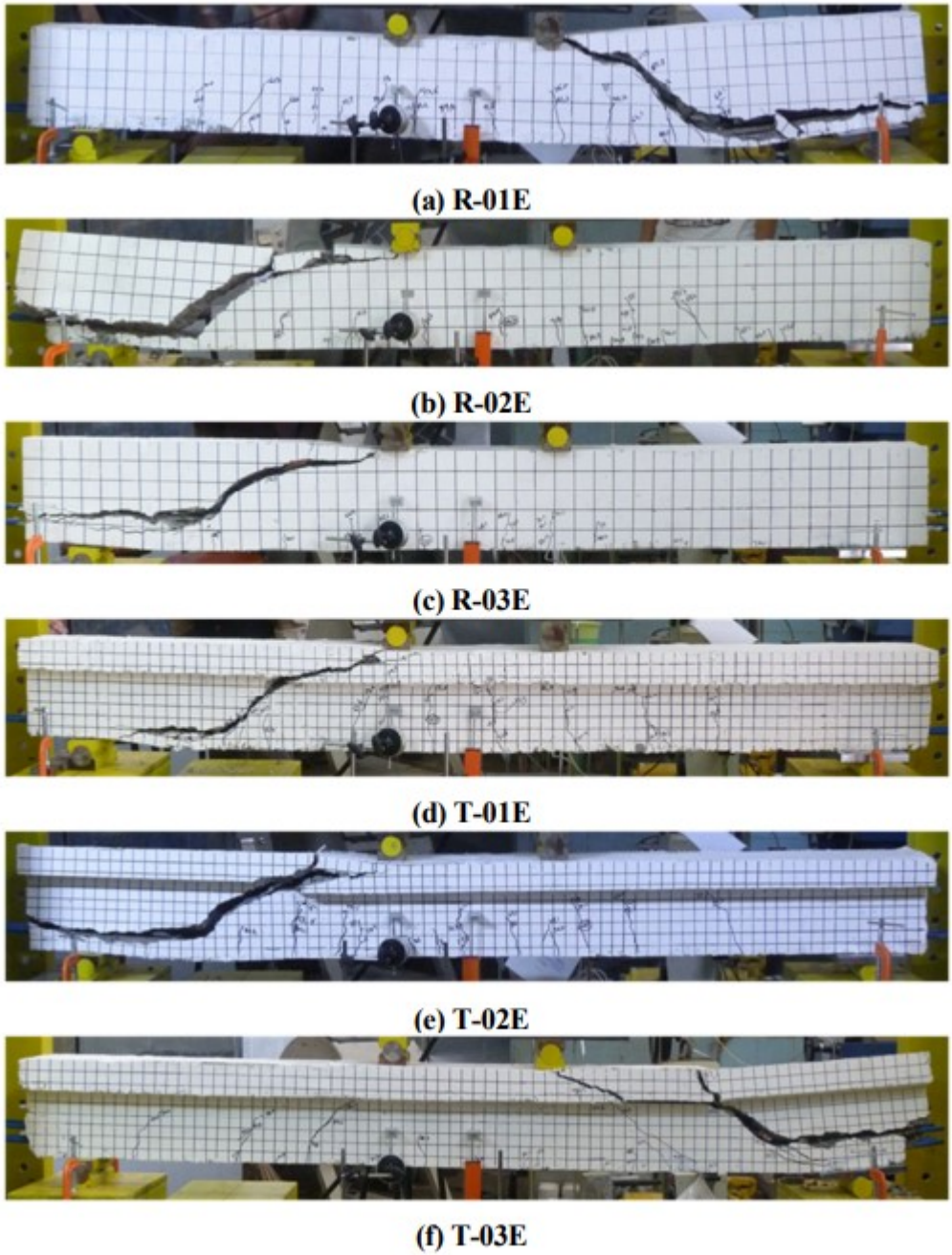

Figure 6: Crack patterns from Thamrin et al.

As described above, for rectangular beams with a shear span ratio of $a/d < 2{,}5$, the force can be directly strutted to the support. For beams $a/d > 2{,}5$ the shear transfer actions become governing. Gonzales et al. noted a similar behaviour for T-beams using the data from the literature. In case of a crack pattern with a delamination crack, the force could be directly strutted to the support for more slender beams compared with rectangular cross sections. This gives a shift in the limit value from $a/d = 2{,}5$ to $a/d = 4$.

A.K. Tureyen and R.J. Frosch (2003 & 2006) developed a design model to determine the shear strength of reinforced concrete with rectangular cross-section and T-beams without transverse reinforcement. In their research they only assume the concrete contribution to the shear strength of reinforced concrete beams.

According to Tureyen and Frosch, it was hypothesized that a RC beam without shear reinforcement fails in shear when the principal tensile stresses in the compression zone in a cracked region within the shear span of the beam exceed the concrete tensile stress. The results of the design model are validated with several test results.
They observed that the effective shear area does not include the total flange area in compression, but a part of it. In order to determine this, they developed two methods: form factor and shear-funnel. For detailed information about this, see [A.K. Tureyen, T.S. Wolf and R.J. Frosch, 2006].
The form factor is a multiplication factor on the design model, which is determined as $\sqrt{(b_w/b_f)}$ based on test results. The angle of the shear funnel is conservatively taken as 45 degrees. The shear funnel method gives more conservative results compared to the form factor.

2.3.3 Influence of prestressing

A number of studies have been conducted on the influence of normal force on the shear capacity of reinforced concrete members. Considering prestressing as an external action, these researches are relevant to this study.

Bui et al. (2017) observed that the strength of specimens loaded with axial compression increased. For specimens without axial loading the stiffness after cracking (about 300 kN shear force) reduced strongly, while for members with axial compression the stiffness remained constant and later reduced slightly. According to Bui et al. this can be explained by the fact that the compression forces delay the crack development. Therefore, axial compression give greater shear resistance. However, when the member was loaded with a high compression force a sudden drop was observed in the force-displacement diagram after the post-peak phase. This behaviour corresponds to the brittle shear failure.

Muttoni and Ruiz (2008) also noticed that when axial force is present, the critical crack width may be increased (tension) or diminished (compression). This in accordance with the observations of Bui et al. According to Muttoni and Ruiz, the effective shear span is smaller than the geometric span in presence of an axial compressive force. In order to determine this effective shear span $a_{eff,}$ the effect of the axial force on the arching action should be accounted:

$$a_{eff} = a + \frac{Nh}{2V} \tag{2.1}$$

According to Ruiz et al. [M. Fernandez Ruiz, S. Campana and A. Muttoni 2009] the shorter effective shear span is due to the fact that prestressing doesn't allow flexural cracks to the support area. Therefore, a_{eff} could be determined by:

$$a_{eff} = a - \frac{Pz}{V} \tag{2.2}$$

Cavagnis (2017) also studied this phenomenon and came up with the following formula in order to determine the influence of a compressive axial force:

$$a_{eff} = a + \frac{N}{V}\frac{d}{3} \tag{2.3}$$

In case of prestressing, formula (2.3) could be replaced by:

$$a_{eff} = a - \frac{P}{V} \cdot (\frac{d}{3} + e_p) \quad (2.4)$$

Furthermore, Cavagnis (2017) noted that the crack angle decreases due to a_{eff}, which leads to a reduction of the shear capacity. However, the decreasing shear span leads to an increase of the shear strength which is dominant on the global response.

2.3.4 Mechanical models

There are several mechanical models in order to determine the shear capacity of reinforced concrete beam without shear transfer [4, 7, 8, 43, 44]. In this chapter only two relevant models will be discussed: models of Yang (2014) and Cavagnis (2017).

According to Cavagnis the total shear strength V_u can be calculated by summing the contribution of the various shear transfer actions: Aggregate interlock, dowel action, compressive area and residual tensile capacity of concrete.

Also following Yang the shear resistance is a summation of the contribution of the shear transfer actions, but he does not include the residual tensile capacity of concrete in his model. The reason for that is that the contribution of this shear transfer action is only present in case of small crack width and in case of failure the crack width is much larger. So the contribution of the residual tensile capacity is according to Yang negligible.

Although the general assumption of both mechanical models is almost the same, there are also differences between the assumed contributions of each shear transfer actions. In the following, these differences will be discussed.

2.3.4.1 Dowelling action

Yang uses the method of Baumann and Rüsch (1970) in his mechanical model:

$$V_d = 1{,}64 \emptyset b_n f_{ck}^{1/3} \quad (2.5)$$

According to Cavagnis the dowelling force causing a splitting failure can be calculated by:

$$V_d = 2n f_{ct} k_b b_{ef} \emptyset \quad (2.6)$$

where b_{ef} = min(b/n-$\emptyset$, 4-c) and k_b is a reduction factor for the tensile strength of concrete
$k_b = (0{,}063\varepsilon_s^{-1/4} \leq 1)$

However, research of Autrup et al. (2020) showed that both methods above predict the dowel cracking load inaccurately. Therefore, the contribution of the dowelling action requires further research which is beyond the scope of this study.
Also, both models are applicable to rectangular cross-sections and should be extended to non-rectangular cross-sections.

2.3.4.2 Compressive area

Yang assumed the classic beam theory (according to the theory of Mörsch 1909) in order the determine the contribution of the uncracked concrete compressive area for rectangular cross sections:

$$V_c = \frac{2}{3}\frac{z_c}{z}V \tag{2.7}$$

where $z_c = d - s_{cr}$, s_{cr} is the crack height of the critical shear crack

Cavagnis (2017) has derived a formula based on test results:

$$V_c = \frac{k_{c1}\frac{h_F}{r_F}}{(1-k_{c1})\frac{h_F}{r_F}} \tag{2.8}$$

where k_{c1} is a constant approximately 0,5, obtained by fitting, r_F is the distance between the tip of the crack and the axis where the load is applied and h_F is the thickness of the compression zone above the tip of the crack.

Also for this case the models are only valid for rectangular cross-sections and therefore needed to be extended for a non-rectangular shape.

2.3.4.3 Aggregate interlock

Both Yang and Cavagnis used the model of Walraven as a basic assumption, but Cavagnis considered the kinematics of Guidotti in his model. The kinematics of Guidotti is that there is an initial opening w_0 followed by a combination of opening w and sliding γ.

Yang simplified the model of Walraven into:

$$V_{ai} = f_c^{0,56} s_{cr} b_w \frac{0,03}{(w_b - 0,01)}(-978\Delta^2 + 85\Delta - 0,27) \tag{2.9}$$

where b_w is the web width, w_b is the crack width and Δ is the shear displacement.

The final formula of Cavagnis is:

$$\frac{V_{Agg}}{\sqrt{f_c}\cdot b}=\int_{l_1}^{l_2}\frac{\sin\beta_{AB}\cdot c_3\cdot\overline{\delta}_A^{4/3}}{\left(c_2\cdot\psi\cdot\frac{\xi}{d_{dg}}\right)^{1.8+c_2\cdot\overline{\delta A}}}-\frac{\cos\beta_{AB}\cdot c_4\cdot\overline{\delta}_A^{7/3}}{\left(c_2\cdot\psi\cdot\frac{\xi}{d_{dg}}\right)^{3+c_2\cdot\overline{\delta A}}}d\xi+\int_{l_1}^{l_3}\cos\beta_{AB}\cdot\left(1-\left(\frac{\psi\cdot\xi}{w_c}\right)^{c_1}\right)d\xi=$$

$$=\sin\beta_{AB}\cdot\frac{c_3\cdot\overline{\delta}_A^{4/3}}{\left(c_2\overline{\delta}_A+0.8\right)\cdot\left(\frac{u_A}{d_F}\cdot\frac{c_2}{d_{dg}}\right)^{1.8+c_2\overline{\delta}_A}}\cdot\frac{l_2^{\,0.8+c_2\overline{\delta}_A}-l_1^{\,0.8+c_2\overline{\delta}_A}}{\left(l_2\cdot l_1\right)^{0.8+c_2\overline{\delta}_A}}+$$

$$-\cos\beta_{AB}\cdot\frac{c_4\cdot\overline{\delta}_A^{7/3}}{\left(c_2\overline{\delta}_A+2\right)\cdot\left(\frac{u_A}{d_F}\cdot\frac{c_2}{d_{dg}}\right)^{3+c_2\overline{\delta}_A}}\cdot\frac{l_2^{\,2+c_2\overline{\delta}_A}-l_1^{\,2+c_2\overline{\delta}_A}}{\left(l_2\cdot l_1\right)^{2+c_2\overline{\delta}_A}}+$$

$$+\cos\beta_{AB}\cdot\left[l_3\cdot\left(1-\frac{1}{1+c_1}\cdot\left(\frac{u_A\cdot l_3}{d_F\cdot w_c}\right)^{c_1}\right)-l_1\cdot\left(1-\frac{1}{1+c_1}\cdot\left(\frac{u_A\cdot l_1}{d_F\cdot w_c}\right)^{c_1}\right)\right]\cdot\frac{f_{ct}}{\sqrt{f_c}}$$

where $\overline{\delta}_A=\frac{\delta_A}{d_{dg}}=\frac{\sqrt{u_A^{\,2}+v_A^{\,2}}\cdot\sin\theta_A}{d_{dg}}$, $v_A=\frac{u_A}{d_F}\cdot\left(l_F\cdot\cos\beta_{BF}+l_A\cdot\cos\beta_{AB}\right)$ and $\theta_A=\beta_{AB}-\operatorname{atan}\frac{d_F}{l_F\cdot\cos\beta_{BF}+l_A\cdot\cos\beta_{AB}}$

For the used notification of this formula, see research of Cavagnis (2017).

Both models are valid for rectangular cross-sections. Since aggregate interlock is develop in the steeper part of the crack and the contribution is determined by integration over this height, the formula is also applicable for non-rectangular cross-sections with a constant width over this height. In case of plates with holes, the b_w should be changed into a formula that describes the width over the height.

2.4 Conclusion and discussion

Despite the fact that there is no general agreement about the governing shear failure mechanism, most studies have shown the same with regard to the contribution of aggregate interlock and the influence of dowel action on the failure of a reinforced concrete beam. It has been proven that aggregate interlock has a significant contribution to the transfer of shear force in slender members. Due to the increasing tensile stresses in concrete at reinforcement level, dowel crack along the reinforcement bar occur. This crack leads to an increase of the (critical shear) crack width, reducing the contribution of other mechanisms. In particular, the contribution of aggregate interlock declining sharply. This leads to the failure of the member.

Furthermore, the researchers agree on the possible failure regimes according to Kani's valley and the cracking pattern. The crack is composed of three parts: quasi-vertical part, quasi-horizontal part and a delamination crack at the reinforcement level. Several studies have shown that an average value of $0{,}56d$ for crack spacing is a safe assumption. Despite differing beliefs regarding the location of the critical shear crack, research of Cavagnis has shown that this has little impact on the shear capacity.

Research has shown that for reinforced T-beams without shear reinforcement the crack does have a similar crack propagation process as for rectangular cross sections. It is also observed that T-beams have a higher shear capacity compared to rectangular cross-sections. A possible reason to this is the flange in compression, which makes it possible to activate the arching action. However, it is noted that using the full width of the compression flange leads to conservative results. The effective shear area does not include the total flange area in compression, but a part of it.

It is generally accepted that the effective shear span is smaller than the geometric span in presence of an axial compressive force (prestress). A smaller shear span leads to an higher shear capacity. The proposed formulas in order to calculate a_{eff} (effective shear span) differ little from each other.

Although extensive research has been carried out on reinforced concrete with rectangular cross-sections and without shear reinforcement, little is known about the shear capacity of non-rectangular cross-sections without shear reinforcement. A number of studies have shown that the capacity increases with a T-beam [27, 34, 35, 38], for example, but the positive contribution of the flanges is nevertheless not taken into account in the standards.
In addition, little research has been conducted into the effect of prestress on the shear capacity.
This research will focus mainly on the missing link of the reinforced non-rectangular cross-section using the model of Yang as a starting point. The aim is to find an evaluation procedure in order to determine the effective web width for non-rectangular cross-sections, which can possibly be included in the EC2.

3. Analysis of the failure mechanism

Because the model of Yang will be used as a starting point, it is important to fully understand the assumptions of this model. In this chapter the failure mechanism as described in Yang's research is studied and compared to other relevant studies.

3.1 Crack development

Several experimental studies in the past have shown that the shear force capacity strongly depends on the crack pattern in the shear span [7, 8]. Therefore it is important to gain insight into the crack pattern of the structure.

3.1.1 Crack height

The first cracks start to initiate from the ultimate tensile fibre, where the tension capacity of concrete is reached. The initiating of the crack and the crack height are related to the stress distribution, thus to the bending moment in the cross-section. Using the layered model principle of (Hordijk 1991), Yang has shown that at the cracking moment M_{cr} the crack becomes unstable and short after the cross sectional moment M has exceeded the cracking moment M_{cr}, the crack becomes stable again. At this point, the increase of the moment does not lead to the change of the crack height and thus means that the stabilized crack height s_{cr} is reached. The assumption of this method is a linear strain and stress distribution in the cross-section. Therefore, this method is also applicable for non-rectangular cross-sections. By calculating the force and moment equilibrium per layer, the stabilized crack height can be calculated.
The stabilized crack height s_{cr} is expressed by:

$$s_{cr} = (1 - 1{,}05(\rho_s n_e)^{0{,}45})d \tag{3.1}$$

According to the experimental results obtained by Cavagnis et al. (2015), the crack extends at least up to $0{,}5d$. Assuming a reinforcement ratio of 1% and $n_e = 5{,}7$, s_{cr} becomes $0{,}71d$, which is in agreement with the observations of Cavagnis et al..

However, it should be noted that both theories are based on rectangular cross-sections and with some changes, can also be used for non-rectangular cross-sections. So the methods cannot be adopted directly, which will be discussed in more detail in the following paragraphs.

3.1.2 Crack spacing

When a crack develops, the tension stress in the adjacent areas decreases. This decrease of stresses prevents new cracks from developing within this area. With increasing moment above M_{cr}, new cracks are formed at a specific distance depending on the bond conditions and stress τ_{bm} between concrete and reinforcement. The minimum crack spacing l_t is calculated by:

$$l_t = \frac{f_{ctm}\emptyset}{4\tau_{bm}\rho_{eff}} \tag{3.2}$$

The maximum crack spacing is equal to 2 times l_t. According to the literature, the mean crack spacing l_{cr} at the reinforcement level at the tension side can be calculated by $l_{cr} = \psi_s l_t$, where the value of ψ_s differs from 1,3 to 1,5. However, according to Yang, a concrete beam with reinforcement at the tensile side behaves differently than a tensile member. In the former case the stressed area of the uncracked part must build up again over a certain length from the area adjacent to the reinforcement level at the crack face, see figure below for an overview.

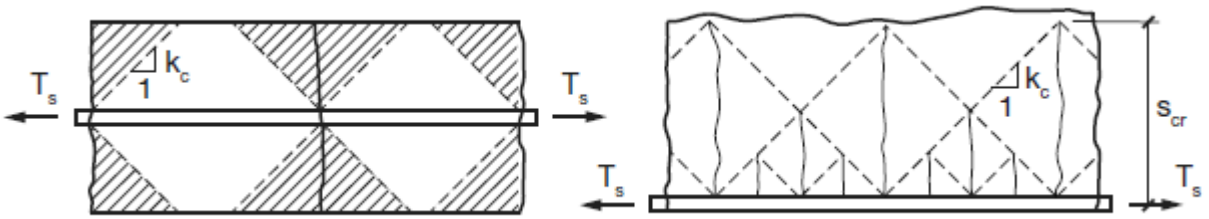

Figure 7: Stress lines and crack patterns: left) with reinforcement bars in the middle; right) at the bottom (Yang 2014)

The boundary of this stressed area could be simplified by a stress line k_c, which represents the part of the member where the stresses can develop. The geometry of the stress line shows that not all cracks can grow to the neutral line. This phenomena has also been seen in experiments Cavagnis et al (2015). In Yang's research, the ones that can develop till s_{cr} are called major cracks. Considering the stress line, the spacing of the major cracks could be determined by:

$$l_{cr,m} = \frac{s_{cr}}{k_c} \tag{3.3}$$

When the crack spacing between l_t and $2l_t$ is reached, increase of the load only leads to the growth of the crack width. Yang confirmed the theory of crack height and spacing described above with a FEM analysis using $k_c = 1{,}28$ (52°). He observed that 100mm is a lower bound of the effective height where the crack pattern of the major cracks is influenced by the tension softening behaviour, which means in that case the theories above could not be used.
According to the test results obtained by Cavagnis et al. (2015), the spacing differs between $0{,}4d$ and $0{,}8d$ for all values of slenderness, load types and reinforcement ratios. The average value is $0{,}56d$. Assuming the example of $\rho_s = 1\%$ and $s_{cr} = 0{,}71d$, $l_{cr,m}$ becomes $0{,}56d$. This is equal to the average value obtained by experiments.

3.1.3 Inclination of the crack

For the inclination of the crack, several theories are present in the literature. The most well-known is the theory of elasticity. Here the inclination depends on the direction of the principal stresses. Since the maximum shear stress is at half of the height, the inclination of the crack should depend on this. The most commonly accepted value here is 45°. However, test results show that this is not always the case. According to the experimental results obtained by Cavagnis et al. (2015), for high values of *M/Vd* (values > 3) the angle becomes steeper, to a maximum value of 85° as shown in Figure 8. For values < 1 the angle of the crack becomes flatter. This will mainly occur nearby the supports.

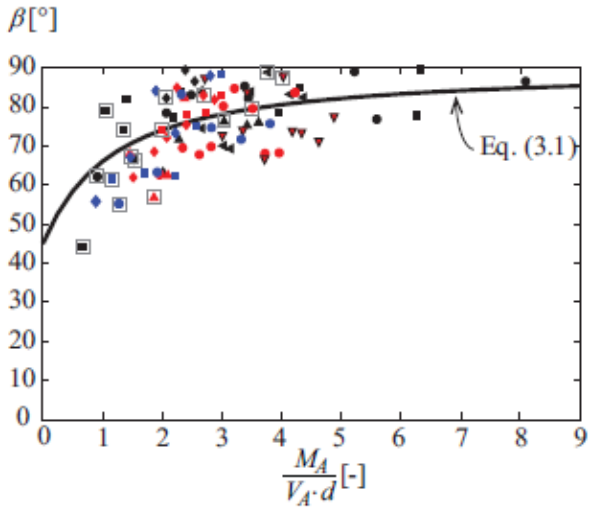

Figure 8: Angle of major cracks (Cavagnis et al. 2015)

Also, according to Yang, the value of *M/Vd* (which is equal to shear slenderness ratio in case of a simple supported beam) at a specific location will directly affect the inclination of the crack generated on that section. This is in line with the experimental observations of Cavagnis (2017). *M* and *V* are the bending moment and the shear force where the flexural crack intercept the reinforcement.

3.1.4 Equilibrium system of a crack

Once the shape of the major crack is defined, a part of the concrete along the crack close to the support could be taken out in order to determine the internal forces using a free body diagram, see figure below. In this free body, the forces should be in equilibrium.

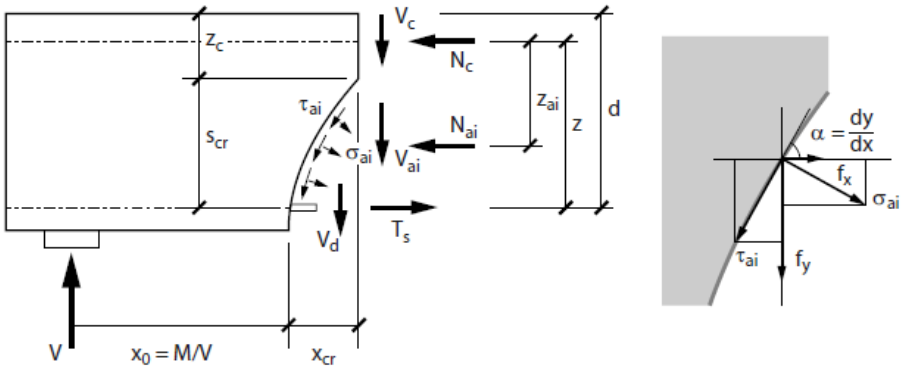

Figure 9: Free body diagram (Yang 2014)

The following vertical forces are acting on the free body diagram:

- V_c: shear component of the uncracked compressive area;
- V_{ai}: shear component of the aggregate interlock along the crack;
- V_d: shear force transferred by dowel action;
- V: support reaction.

The following horizontal forces are acting on the free body diagram:

- N_c: normal force component of the uncracked compressive area;
- N_{ai}: normal force component of aggregate interlock along the crack;
- T_s: tension force in the reinforcement bars.

The following equilibrium conditions should be satisfied:

Vertical force equilibrium: $V = V_c + V_{ai} + V_d$
Horizontal force equilibrium: $N_c + N_{ai} + T_s = 0$
Moment equilibrium around N_c: $V(x_0 + x_{cr}) = V_d x_{cr} - N_{ai} z_{ai} + T_s z + V_{ai} x_{ai}$

The contribution per component will be further studied in chapter 4.

3.2 Development of the critical inclined crack

The further increase of the load does not influence the crack pattern, but the kinematics of the major cracks. In case the major crack does not change from kinematics, it is not possible to achieve force equilibrium at the crack. Therefore, an additional shear displacement Δ must occur. After the vertical opening of the crack, the shear resistance of the cross-section increases, which is linked to aggregate interlock. This process is described below.

3.2.1 Critical inclined crack and failure mechanism

After the major cracks are formed, increasing the load leads to the formation of secondary crack branches. On the compression side, a secondary crack branch at the crack tip in longitudinal direction is propagated in order to generate a shear displacement to balance the shear force. This phenomena is also observed by Cavagnis et al. (2015), see crack type F in Figure 4. Another secondary crack branch forms at the reinforcement level, the dowel cracking (type D'' and D''' in Figure 4). When the tensile strength of concrete is exceeded, delamination cracks develop towards the support along the reinforcement bar. The formation of the secondary crack branches leads to an increase of the crack width of the major crack, becoming an unstable opened crack. This is defined as the critical inclined crack.
In order to achieve an unstable failure, the contribution of the aggregate interlock should be reduced. Therefore, the longitudinal crack width w has to increase, which reduces the contact area of the aggregates. As mentioned before, short before failure delamination crack starts to develop at reinforcement level (dowel cracking). This causes the detachment of the reinforcement from the concrete and increase of the crack width. Increase of the crack width w results in the reduction of the aggregate interlock, leading to unstable failure of the beam. This is also observed by Cavagnis (2017) during the experiment. Therefore, the occurrence of the dowel cracking is directly linked to the unstable failure of the member.

However, according to Yang the maximum dowel action is easily reached during the loading process while the crack stays stable. The reason for this is the fact that the contribution of the dowel action is limited. Therefore, the force as a failure criterion is not acceptable to determine the moment that the crack becomes unstable. Instead the shear displacement Δ is assumed as a criterion, because it depends on the shear force and also determines the contribution of other shear transfer mechanisms such as aggregate interlock.

3.2.2 Location of the critical inclined crack

It is also important to understand where the critical inclined crack could occur on the member. As mentioned earlier, the crack pattern depends on the value of *M/Vd*. This value is also an important value in order to determine the location of the critical inclined crack. Experimental results of Yang and den Uijl 2011 showed that the minimum shear displacement occurs between *M/Vd* = 1 and *M/Vd* = 2, see figure below for the test results of several beams with different shear capacities. For a simple supported beam loaded with point load, this means that the crack will occur in the area below the point load, because this area will reach the value of Δ_{crit} (value of Δ when the critical inclined crack develops) earlier.

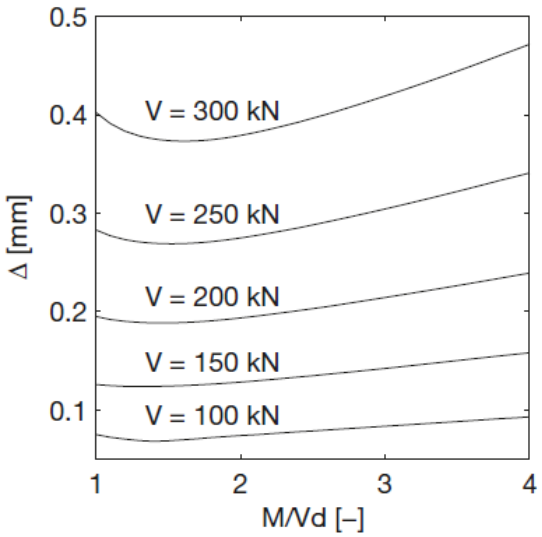

Figure 10: Shear displacements for beams with different shear capacities (Yang 2014)

However, for smaller values of *M/Vd* than that of the lowest point (left side from the lowest point toward *M/Vd* =1) the shear displacement Δ increases. According to Yang this means that the cracks that develop at sections closer to the supports can transfer less shear force than those further away.
This sounds contradictory with the test results of beams with short shear span *a/d*, where the beam can achieve high shear capacities. This is due to the arching action, where the shear force is transferred through the uncracked area. As long as the crack does not disturb this area, the beam can achieve plastic strength. According to Yang, this could be explained as follows:
Assuming that the major crack starts to form when reaching cracking moment M_{cr} and that the crack is x_0 away from the support, the cracking shear force $V_{cr,m}$ must be:

$$V_{cr,m} = \frac{M_{cr}}{x_0} \tag{3.4}$$

Yang plotted this value of $V_{cr,m}$ against every location of the beam, see Figure 11.
The shear resistance is represented by the section between where the load is applied and the intersection with the cracking shear force line. After the intersection point (towards the support) the shear resistance is replaced by the cracking shear force line. The location with the lowest value of the shear resistance is where the critical inclined crack will develop. Based on this, for beams with high shear slenderness ratio (*a/d*) it is a safe assumption that the crack will occur below loading point. However, according to Yang it is also necessary to check the uncracked span from the support a_0:

$$a_0 \leq \frac{M_{cr}}{V_{cr}} \tag{3.5}$$

In case the value of a_0 is very small based on the formula above, then there is a high chance that the critical inclined crack is close to the support.

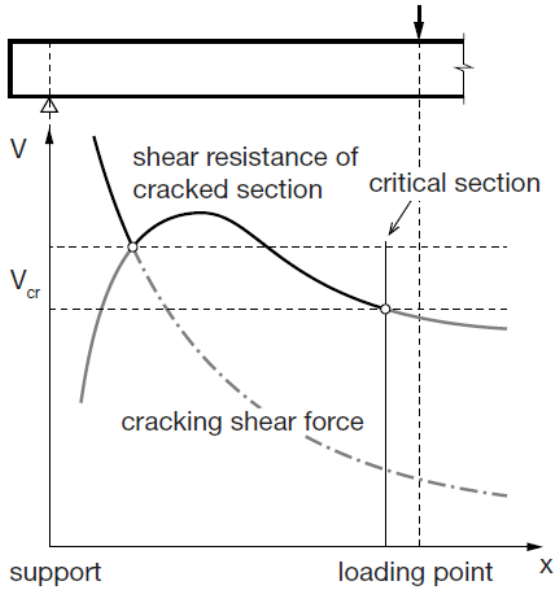

Figure 11: Overview of shear resistance versus cracking force at shear failure (Yang 2014)

4. Evaluation of the shear capacity of non-rectangular cross-sections

It was noted in the previous chapter that the failure occurs when dowel cracks and cracks in the compression zone develop, which has also been observed in experiments. In chapter 4, this failure mechanism will be translated into an analytical model in order to determine the shear resistance of the member.

It was also noted in the previous chapter that the shear force is carried by three mechanisms: aggregate interlock V_{ai}, compression zone V_c and the dowel action V_d. These mechanism together form a parallel system, so that the total shear force can be transferred to the supports. In this chapter, the contribution of each of them will be determined for plates with holes and I-beams. For T-beams, see chapter 5.

4.1 Compression zone

In this paragraph, the method and derivation of Yang for the compression zone will be analysed. After this, the method will be adapted for the plate with holes.

4.1.1 Rectangular cross-sections

Since the compression zone is the only uncracked area in compression in the cross-section, it is likely that this whole area will contribute to carrying the total shear force. The stress distribution in the uncracked compression zone could be described by the classic beam theory. Yang's method is based on Mörsch's theory (1909), which investigated the amount of shear force carried by the compression zone. Mörsch assumes that the maximum shear stress τ_m in de compression zone is equal to the difference in normal force. Assuming a small length of Δx, the shear stress could be determine by $\tau_m = dN/dx$. The compressive force in the cross-section is equal to $N_c = M/z$. The substitution of these 2 functions results in the following formula:

$$\tau_m = \frac{dM}{dx}\frac{1}{bz} = \frac{V}{bz} \tag{4.1}$$

According to the theory of Jourawski, the maximum shear stress in elastic beams with any cross-section can be determined as follows:

$$\tau_m = \frac{VS}{bI} \tag{4.2}$$

where S is the first moment of area (also called statical moment of area) and I the moment of inertia.

For rectangular cross-sections, the maximum shear stress could be determined as follows:

$$S = \frac{1}{2}bh \cdot \frac{1}{4}h = \frac{1}{8}bh^2 \tag{4.3a}$$

$$I = \frac{1}{12}bh^3 \tag{4.3b}$$

$$\tau_m = \frac{V \cdot \frac{1}{8}bh^2}{b \cdot \frac{1}{12}bh^3} = \frac{3}{2}\frac{V}{bh} \tag{4.3}$$

Rewriting this in the terms of *V* for the compression zone formula (4.4) is obtained. The factor *2/3* in this formula is the degree of fullness of the shear stress diagram for specifically rectangular cross-section, because it depends on the shape of the cross-section.

$$V_c = \frac{2}{3}\tau_m z_c b \tag{4.4}$$

The substitution of (4.1) and (4.4) gives the amount of shear force which could be transferred by the compression zone of a rectangular cross-section:

$$V_c = \frac{2}{3}\frac{z_c}{z}V \tag{4.5}$$

This means that the contribution of the compression zone depends on the height of the compressive zone and the total shear force *V*. However, this formula is only suitable for rectangular cross-sections. Therefore, it will be adapted for non-rectangular cross-sections, focusing on plates with holes and I-beams.

4.1.2 The approach

In this research, three types of non-rectangular cross-sections are studied to determine the influence of flanges, namely: plates with holes, I-beams and T-beams. Structural elements with these cross-sections are often used in engineering practice and are therefore relevant for research. Especially with emphasis on existing structures with the plates with holes without shear reinforcement, which seem to have insufficient shear capacity according to current standards. To determine the stresses in the cross-section of a plate with holes, a typical section is taken from the cross-section, see figure below. The cross-sectional parameters of this typical section are also showed in Figure 12.

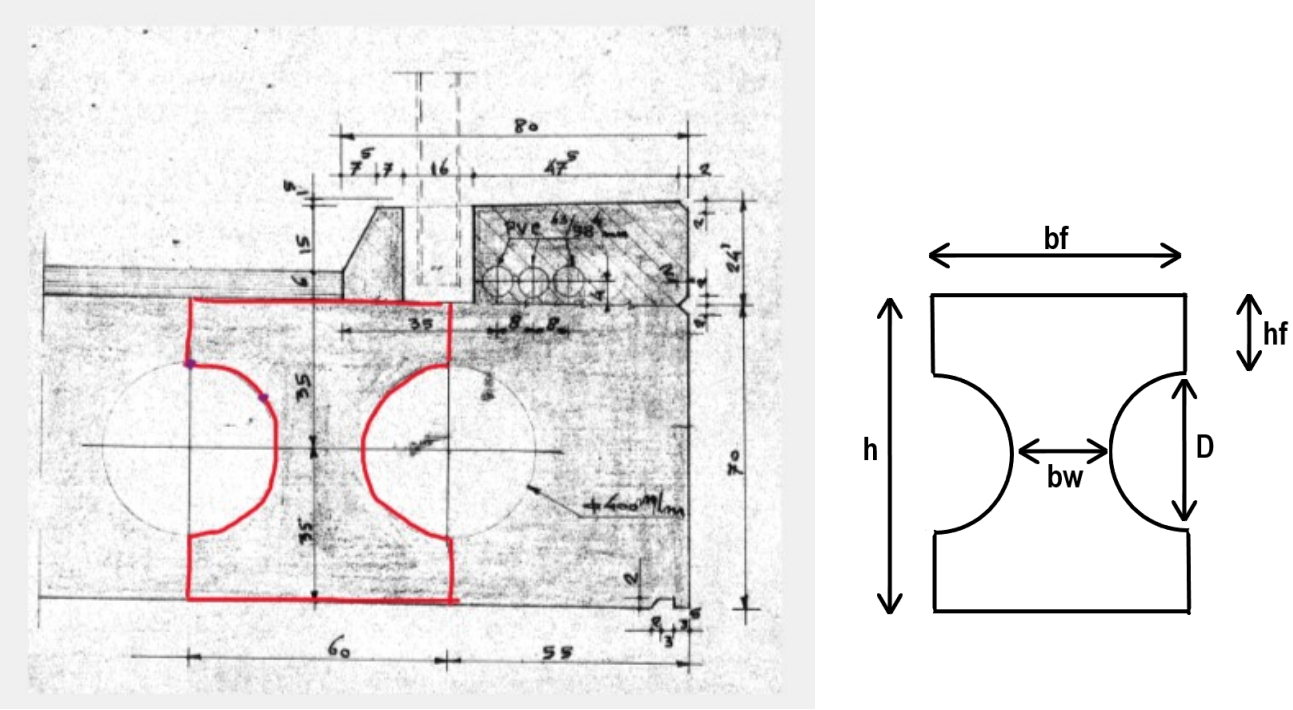

Figure 12: Example of a typical section of plate with holes and the cross-sectional parameters.

Following the steps as described in 4.1.1 it is possible to determine the shear stress in any type of cross-section. However, for a non-rectangular cross-section, the degree of fullness factor is not easy to determine analytically by following the previous steps, which results in long and complex formulas. The reason is that these cross-sections depend on several cross-sectional parameters, for example the flange width and thickness, web height and thickness, centre of gravity etc...
Therefore, the following approach is used to determine the degree of fullness for a non-rectangular cross-section, with formula (4.4) as a starting point. Doing this, the formula for rectangular cross-sections is translated into a formula for non-rectangular cross-sections. Calling the degree of fullness α, the formula becomes:

$$V_c = \alpha \tau_m z_c b_w \tag{4.6}$$

Expressing (4.6) into terms of degree of fullness α, it becomes:

$$\alpha = \frac{V_c}{\tau_m z_c b_w} \tag{4.7}$$

This makes it possible to determine the degree of fullness of each type of cross-section. To be able to do this, the shear force in the compression zone V_c and the maximum shear stress at neutral axis level τ_m must first be determined. These unkowns can be determined in a layer model using Jourawski's theory (formula (4.2)).
A layer model divides the cross-section into small elements of approximately 10mm. This allows per layer to calculate the first moment of area S, second moment of inertia I and the shear stress τ (with $\tau = VS/bI$). In order to do this, a unit load of $V = 100$ kN is assumed as shear force in the cross-section in this layer model. Now the shear stress per layer could be calculated and so the shear force in every layer with:

$$V_i = \tau_i b_i h_i \tag{4.8}$$

where i is the number of the specific layer. With this data it is possible to determine the degree of fullness per cross-section using equation (4.7). The calculations with the layer model are attached in appendix I.
To determine the height of the compression zone and then to calculate the degree of fullness, a number of cross-sections are assumed, see Table 1.

Table 1: Input parameters for the height effect

Member	h_f [mm]	b_f [mm]	b_w [mm]	h [mm]	r [mm]	h/D [-]
1	100	400	200	400	100	2,0
2	200	400	200	600	100	3,0
3	300	400	200	800	100	4,0
4	100	500	200	500	150	1,7
5	200	500	200	700	150	2,3
6	300	500	200	900	150	3,0
7	100	600	200	600	200	1,5
8	200	600	200	800	200	2,0
9	300	600	200	1000	200	2,5
10	100	800	200	800	300	1,3
11	200	800	200	1000	300	1,7
12	300	800	200	1200	300	2,0
13	100	700	200	900	350	1,3
14	200	700	200	1100	350	1,6
15	300	700	200	1300	350	1,9
16	100	1000	200	1000	400	1,3
17	200	1000	200	1200	400	1,5
18	300	1000	200	1400	400	1,8
19	100	1100	200	1100	450	1,2
20	200	1100	200	1300	450	1,4
21	300	1100	200	1500	450	1,7

where: h_f is the thickness of the flange; b_f is the flange width; b_w is the web width at $0{,}5h$, also smallest width in the cross-section of non-rectangular members; h is the height of the members; r is the radius of the opening and h/D is the ratio between height and diameter of the hole. See also Figure 12 for an overview.

The minimum flange thickness used is 100mm, because the reinforcement bars in the flange needs a minimum cover of 30mm at both sides. So in principle the minimum flange thickness could be 60mm, but because this is not really common in engineering practice, 100mm has been assumed.
Furthermore, the diameter of the holes varies from 100mm to 900mm. In reality, diameters of 300mm to 500mm are usually used in engineering practice. The other assumed values are used to capture the size effect. The width and the height of the members depend on the diameter, flange height and web width.

Based on this, the following ranges for height h and width b are possible:

$1{,}2D \leq h \leq 4D$ and $1{,}1D \leq b \leq 3{,}0D$, where D is the diameter of the hole.

The width of the member has no influence on the grade of fullness. This only depends on the location of the neutral axis, which in turn depends on the effective height and reinforcement ratio.

4.1.3 Height of the compression zone

The height of the compression zone z_c is an important parameter to determine the amount of shear force in the compression zone. The test results obtained by the research of Cavagnis (2017) showed that the height of the compression zone varies between 0,2d (for members with reinforcement ratio $\rho_s < 1\%$) and 0,4d (for $\rho_s > 3\%$). He concludes that an assumption of 0,3d for the height of the compression zone is on the safe and realistic side. Since the plates with holes generally have a reinforcement ratio of around 0,4%, this would mean that the height of the compression zone should be assumed to be 0,2d.

Yang's method has a more theoretical approach. Here the stabilized crack height s_{cr}, and thus the height of the compression zone, is calculated by determining the equilibrium of the forces in the cross-section assuming a linear stress distribution. As mentioned in 3.1.1, the crack height s_{cr} depend on the reinforcement ratio and the effective height d. To compare this assumption with the test results of Cavagnis, the degree of fullness of different cross-sections from Table 1 has been determined for both methods. The comparison of the plate configurations for different values of z_c are shown the overview on the next page.

Yang's method

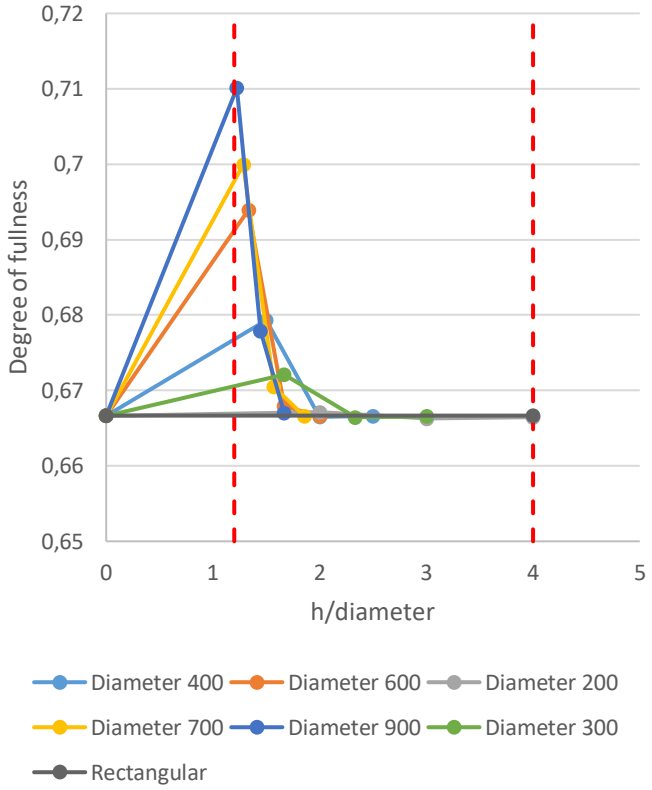

Cavagnis' test results

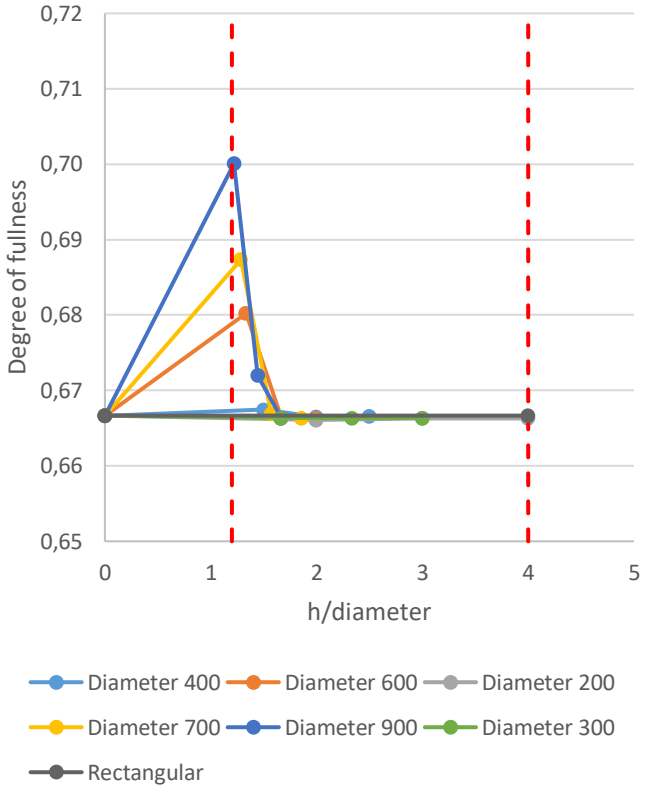

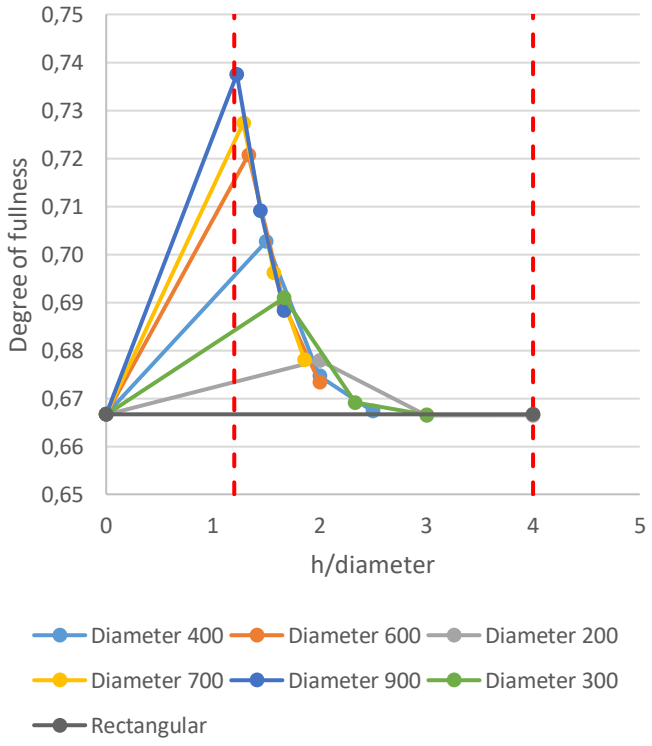

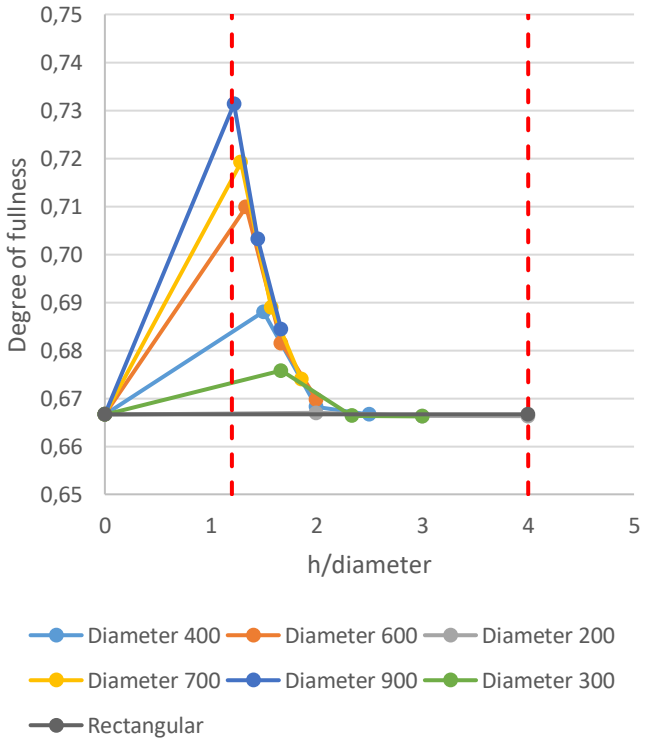

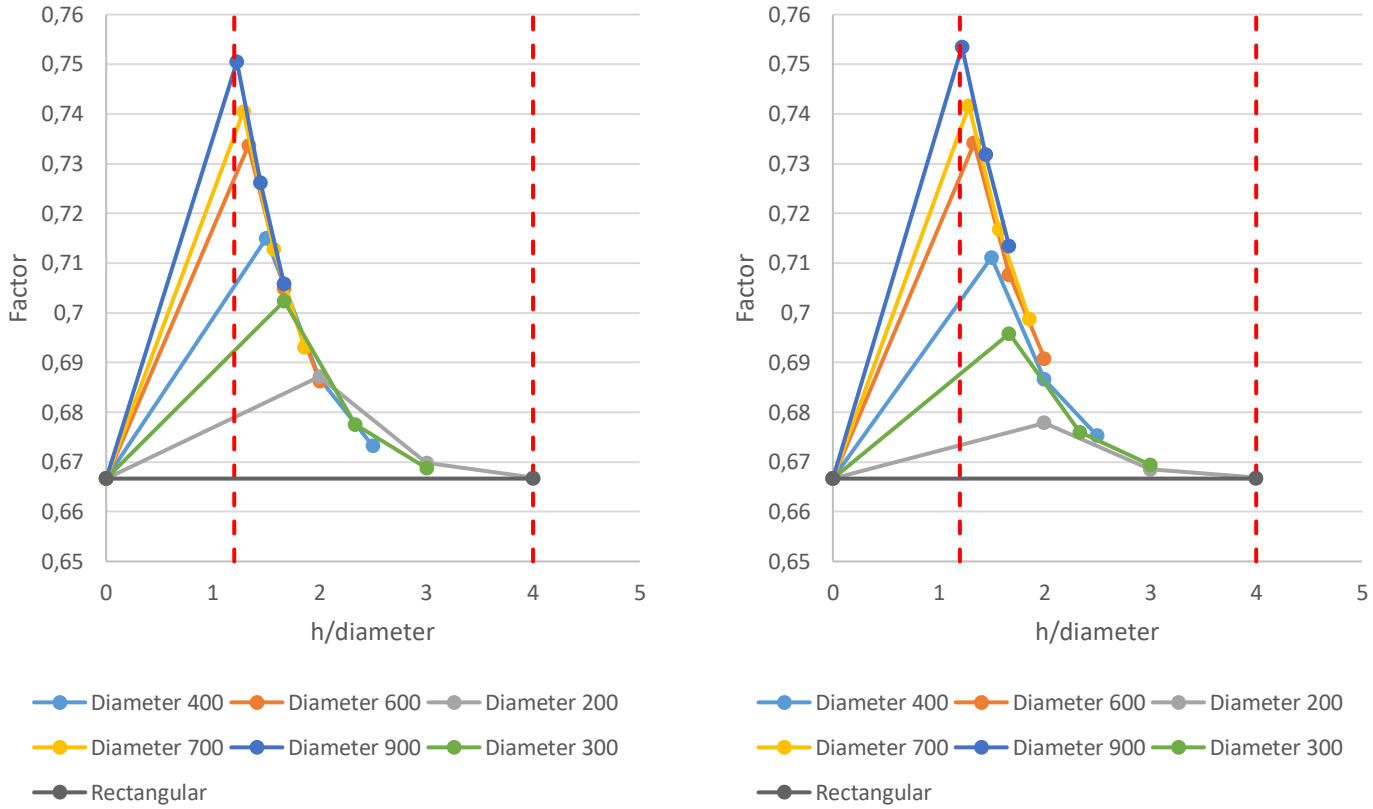

Figure 13: Overview of the height effect for different values of zc, from top left to bottom right: ρ = 0,4%; z_c = 0,2d; : ρ = 1,0%; z_c = 0,3d; : ρ = 1,5%; z_c = 0,4d;

The vertical lines in Figure 13 represents the limit values of h/D which are feasible and realistic. For example, $h/D = 1$ means that the diameter equals the beam height, which is not possible.

Figure 13 shows that there are small differences between the values of grade of fullness calculated with z_c = 0,2d and z_c calculated with Yang's method assuming 0,4% reinforcement ratio. However, these differences are so small (on average 0,01) that they are negligible. So this means that the z_c calculated by Yang's method assuming ρ_s = 0,4% agrees well with $z_c = 0{,}2d$ based on the test results Cavagnis obtained. The overview also shows that for plates with a diameter of 200mm to 400mm, assuming $z_c = 0{,}2d$ always results in the neutral axis being in the flange. For the other plates (500mm < D < 900mm) the grade of fullness grows very limited, to a maximum of 0,70, for a small range of h/D. This means that in most cases the neutral line is in the flange or just below it, where the shape of the compression zone is almost equal to a rectangular cross-section. So in case of $z_c = 0{,}20d$ the compression zone of all studied plates is (almost) equal to a rectangular cross-section (the flange area). As a result the grade of fullness does not change.

From the overview in Figure 13 it can be deduced that assuming a compression zone of $0{,}3d$ corresponds much to a compression zone calculated with the method of Yang by using 1% reinforcement ratio. In case of $h/D \leq 1{,}5$, the grade of fullness differs between 0,69 to 0,73 depending on the diameter of the hole. A compression zone of $0{,}4d$ almost corresponds to z_c calculated using 1,5% reinforcement ratio according to Yang's method. For $h/D \leq 2{,}0$ the grade of fullness is higher than 0,69. It can be observed that for all values of z_c the compression zone of plates with D < 400mm is in the flange or just below it (flange area).

However, it should be noted that the methods of Cavagnis and Yang are both based on solid rectangular cross-sections. As explained earlier, Yang determines the height of the compression zone using force balance in the cross-section. However, when the neutral axis is outside the flange, this force balance is no longer correct and so the height of z_c is not correct either. This is because the area of the compression zone is smaller compared to a rectangular cross-section based on the flange width. This is demonstrated by means of a simple calculation:

Based on a linear (normal) stress distribution the compressive force in the compression zone N_c of a rectangular cross-section could be determined by $N_{c;rect} = \sigma_m b z_c$, where $z_c = 0{,}2d$. So $N_{c;rect} = 0{,}2\sigma_m bd$. In case of a non-rectangular cross-section the compressive force could be calculated by $N_{c;non\text{-}rect} = \sigma_m \sum b z_c$. By equating these 2 equations, the z_c for a non-rectangular cross-section could be determined. This has been calculated in a layer model for a number of examples where $h_f < 0{,}2d$ (so the neutral axis is below the flange):

Table 2: Evaluation of z_c

Member	b_w [mm]	b_f [mm]	h_f [mm]	h [mm]	D [mm]	0,2d [mm]	$A_{cc;rect}$ [mm^2]	z_c [mm]
1	200	400	50	300	200	52	20.800	0,20d
2	200	600	100	600	400	112	67.200	0,21d
3	200	600	50	500	400	92	55.200	0,25d
4	200	800	100	800	600	152	121.600	0,24d
5	200	900	100	900	700	172	154.800	0,26d
6	200	1100	100	1100	900	212	233.200	0,31d

From Table 2 it can be deduced that if the neutral axis is just below the flange, this has little influence on the height of the compression zone. The reason for this is that the width just below the flange is not much smaller than the flange width itself. However, the further the neutral line is from the flange, the higher the height of the compression zone. In most cases this results for plates with holes up to a compression zone height of 0,25d on average. The combination of a large diameter and slender flanges is also a good approximation of an I and T-beam.

Based on the results shown in Table 2, in case of a reinforcement ratio of 0,4%, the compression zone height z_c is assumed to be 0,2d if the neutral axis is in the flange. For plates with holes, in case of flange thickness $h_f < 0{,}25d$, z_c is assumed to be 0,25d. For I-beams and T-beams this becomes 0,3d to balance the internal force balance due to smaller web width compared to plates with holes.

For reinforcement ratio $\rho > 1\%$ the compression zone height becomes 0,3d if the neutral axis is in the flange, 0,35d for plates with holes and 0,4d for I and T-beams in case the neutral axis is in the web.

4.1.4 Contribution of the compression zone

The height of the compression zone is described and determined in 4.1.3. With this assumption, the definitive graphs for the members in Table 1 have been determined, see figure below.

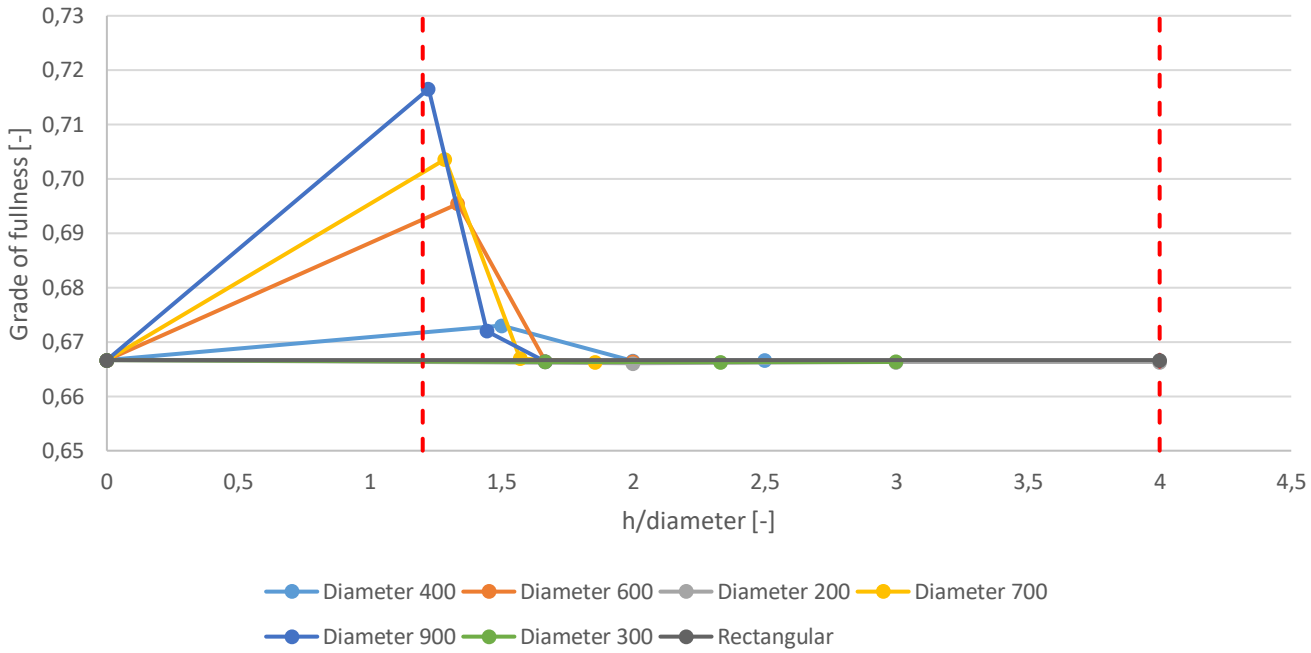

Figure 14: Influence of height effect on the contribution of compression zone of plates with holes

For rectangular cross-sections the degree of fullness is equal to 0,67. For values of $h/D > 1{,}4$ the degree of fullness is (almost) equal to 0,67. This means that the neutral axis is located in the flange of just below it. So the shape of compression zone is rectangular. Therefore, formula (4.4) is applicable to determine the contribution of the compressive zone.

Figure 14 shows that between a range of $1{,}2 < h/D < 1{,}4$ the degree of fullness differs between 0,69 and 0,72. This is an increase of 5% compared to rectangular cross-sections. Because the degree of fullness only increases in a very small range, formula (4.4) will also be used conservatively in this case to determine the contribution of the compressive zone.

In order to generalize the influence of the flanges, the degree of fullness of several I-beams according to Table 1 is studied. The height of the compressive zone is assumed to be $0{,}3d$ ($\rho = 0{,}4\%$). As shown in Figure 15 the degree of fullness of I-beams is in the most cases higher than 0,70, with an average of 0,75. On this basis, the contribution of the contribution zone for I-beams and T-beams is determined as follows:

$$V_{c;I} = \frac{3}{4}\frac{z_c}{z}V \qquad (4.9)$$

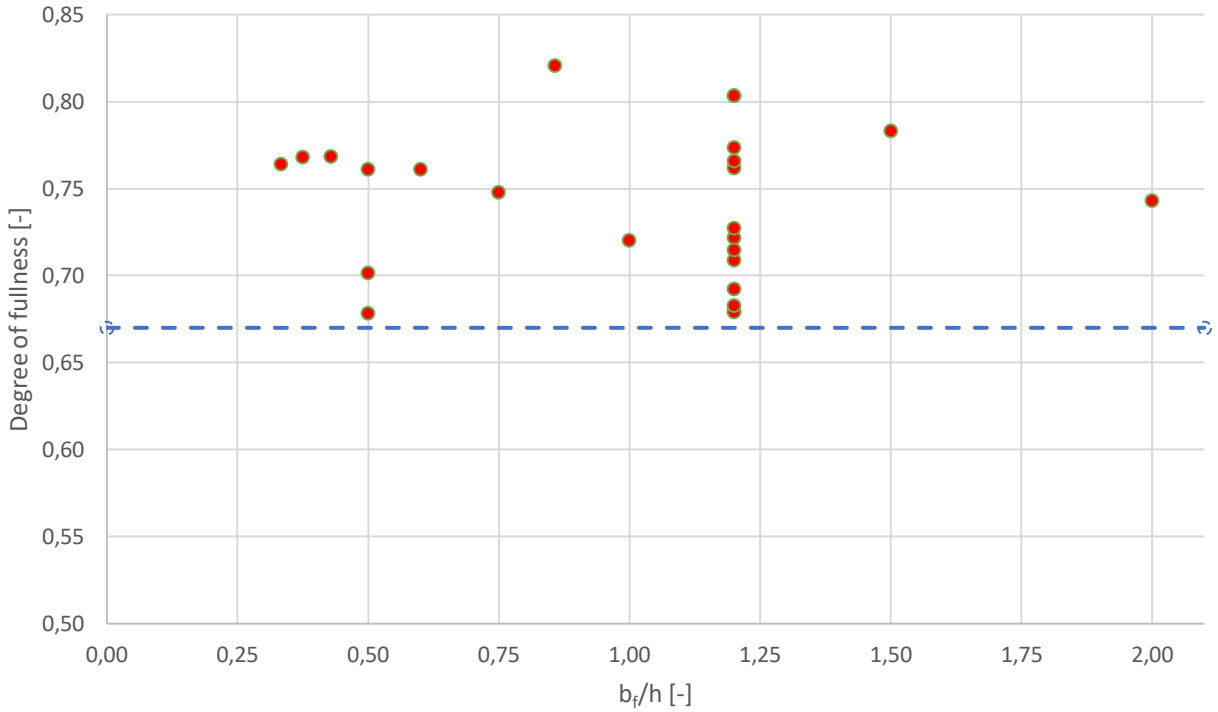

Figure 15: Degree of fullness of I-beams, also valid for T-beams

4.2 Aggregate interlock

To determine the contribution of the aggregate interlock, Walraven's method (1980 & 1981) is applied. The method describes the relationship between the normal stress, shear stress and the crack opening in normal and tangential directions. The contribution of the aggregate interlock could be calculated by integration of Walraven's formula along the crack height. However, because of the complexity it is not possible to calculate this analytically. Therefore the method of Walraven is not directly applicable in engineering practice.

In his research, Yang translated the method into a simplified relationship between V_{ai}, w and Δ. In this section the approach of Yang is first studied, then the method is adapted for non-rectangular cross-sections.

4.2.1 Rectangular cross-sections

In order to simplify the method of Walraven, Yang studied the critical inclined crack at failure. He simplified the crack profile observed during tests into straight lines, see figure below.

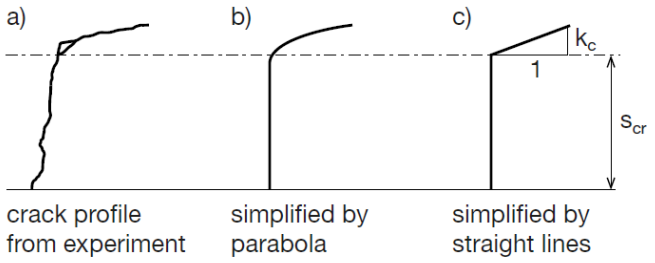

Figure 16: Simplification of the crack profile (Yang 2014)

The comparison of simplifications b) and c) showed that there are hardly any differences in the calculated stresses. Also, the contribution of the secondary branch appears to be small. This in accordance with the observations of Cavagnis (2017). Therefore the contribution of this secondary branch is neglected in simplification c). The crack width at reinforcement level is assumed to be:

$$w_b = l_{cr,m}\varepsilon_s \tag{4.10}$$

The term $l_{cr,m}$ is the crack spacing which could be determined by equation (3.3). ε_s is the average strain of the reinforcement. At the top of the crack the crack width depends on the rotation around the crack tip, so on the shear displacement Δ. Yang made a rough estimation of w_t = 0,01mm based on previous studies. The crack opening w could now be described by a linear distribution along the crack height s_{cr}:

$$w(s) = w_t + \frac{w_b - w_t}{s_{cr}} s \tag{4.11}$$

Based on all the assumptions above the contribution of V_{ai} for rectangular cross-section could be determined with:

$$V_{ai} = \sigma_{pu} b \int_0^{s_{cr}} A_x\big(\Delta, w(s)\big) - \mu A_y\big(\Delta, w(s)\big) ds =$$
$$V_{ai} = \sigma_{pu} b s_{cr} \int_0^{1} A_x\big(\Delta, w(s')\big) - \mu A_y\big(\Delta, w(s')\big) ds' \tag{4.12}$$

The failure criterion Δ_{cr} is determined by Yang (2015) by a regression analyses between Δ_{cr} (obtained during the tests) and effective height d:

$$\Delta_{cr} = 3{,}3555 \cdot 10^{-5} d + 0{,}005 \quad (4.13)$$

Another important boundary condition is that the maximum value of Δ_{cr} could not be higher than 0,025mm to limit the influence of the specimen size.

4.2.2 Non-rectangular cross-sections

The assumptions made in 4.2.1 are in principle also valid for non-rectangular cross-sections. The difference is in the shape of the cross-section. The contribution is determined by integration over the crack height and multiplied by the width. With a rectangular cross-section, the width is constant, but this will nog be the case with a non-rectangular cross-section.
In the case of plates with holes, the width from the flange varies over the height. Therefore, the constant term b in (4.12) should be changed and replaced in the integral. The width of a typical section of a plate with holes could be described by using Cartesian coordinates for the holes. The x-coordinate defines the width, y-coordinate the height and r is the radius of the hole. The centre of the coordinate system is located at half the height of the cross-section on both left and right sides, see Figure 17.
Remark: this coordinate system is only used to determine the varying width.

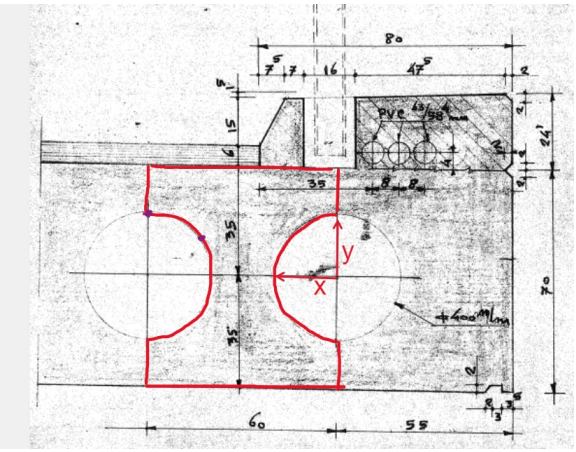

Figure 17: Cartesian coordinate system to determine the varying width

Based on this the width above the flange could be determined by:

$$b_{wi} = b_f - 2\sqrt{r^2 - y^2} \quad (4.14)$$

Formula (4.12) can now be adapted for plates with holes:

$$V_{ai} = \sigma_{pu}\{b_f \int_0^{h_f} A_x(\Delta, w(s)) - \mu A_y(\Delta, w(s))ds + \int_{h_f}^{scr}[A_x(\Delta, w(s)) - \mu A_y(\Delta, w(s))]b_{wi}(s)ds\} \quad (4.15)$$

In order to generalize the result, a comparison is also made with an I-beam. Therefore, for an I-beam, the contribution of aggregate interlock is also determined:

$$V_{ai;I} = \sigma_{pu}\{b_f \int_0^{h_f} A_x(\Delta, w(s)) - \mu A_y(\Delta, w(s))ds + b_w \int_{h_f}^{scr} A_x(\Delta, w(s)) - \mu A_y(\Delta, w(s))ds\} \quad (4.16)$$

4.3 Dowel action

To determine the contribution of the dowel action, the method of Baumann and Rüsch (1970) is assumed by Yang. Baumann and Rüsch showed the relationship between the vertical crack opening and the dowel force (resistance from dowel action), which is linear elastic before the maximum dowel force V_{dmax} is reached. After V_{dmax} is reached, contribution of dowel action becomes constant for any increasing displacement. Baumann and Rüsch also observed that at the peak dowel force V_{dmax} the vertical crack opening Δ was 0,08mm. The contribution of the dowel action for rectangular cross-sections could be determined with:

$$V_d = 1{,}64 b_n \emptyset \sqrt[3]{f_c} \tag{4.17}$$

Where: $b_n = b - n\emptyset$ (the netto width at reinforcement level)

For non-rectangular cross-sections formula (4.15) is not directly applicable. The starting point of formula (4.15) is that in case of a rectangular cross-section, the dowel crack will occur at the weakest point in the cross-section. This is at the reinforcement level where the net width of the cross-section is the smallest.
Based on this, with an I-beam the dowel crack will occur in the web just above the flange, because this is the weakest point of the cross-section:

$$V_{d;I} = 1{,}64 b_w \emptyset \sqrt[3]{f_c} \tag{4.18}$$

However, with the typical cross-section of plates with holes, this is somewhat more difficult to determine. This behaviour should be determine with test results. It is way too conservative to assume that the crack will occur at where the web width is smallest (b_w), because this is about half the height in the cross-section. It is likely that the dowel cracking will occur at the bottom closer to the longitudinal reinforcement. Given that previous studies (Cavagnis 2017) have shown that dowel action only has a small contribution to the total shear capacity, it is conservatively assumed that the crack will occur just below the smallest web width b_w, with $b_n = 1{,}25 b_w$.
This results in the following formula to determine the contribution of dowel action for plates with holes:

$$V_d = 1{,}64(1{,}25 b_w) \emptyset \sqrt[3]{f_c} = 2{,}05 b_w \emptyset \sqrt[3]{f_c} \tag{4.19}$$

4.4 Evaluation procedure

Now that the contribution of all mechanisms are defined and the failure criteria are known, it is possible to determine the shear capacity of reinforced concrete plates with holes without shear reinforcement under a point load. The steps that should be taken are the same as defined by Yang (2014):

Step 1: Calculate the maximum shear force carried by dowel action:

$$V_d = 2{,}05 b_w \emptyset \sqrt[3]{f_c} \tag{4.19}$$

Step 2: Start with a shear force value V_u, calculate the moment at the design cross-section, and the crack width w_b at that cross-section:

$$M_d = V_u d \frac{M}{Vd}, w_b = \frac{M_d}{z A_s E_s} l_{cr,m} \tag{4.20}$$

Step 3: Determine the critical shear displacement Δ_{cr}:

$$\Delta_{cr} = 3{,}3555 \cdot 10^{-5} d + 0{,}005 \tag{4.13}$$

Step 4: Evaluate the shear force carried by aggregate interlock effect with the calculated Δ_{cr} and w_b:

$$V_{ai} = \sigma_{pu}\{b_f \int_0^{h_f} A_x(\Delta, w(s)) - \mu A_y(\Delta, w(s)) ds + \int_{h_f}^{S_{cr}} [A_x(\Delta, w(s)) - \mu A_y(\Delta, w(s))] b_{wi}(s) ds\} \tag{4.15}$$

Step 5: Calculate the shear force carried in the concrete compressive zone:

$$V_c = \frac{2}{3}\frac{z_c}{z} V \tag{4.5}$$

Step 6: Update the overall shear force V_u of the whole cross-section and repeat this from step 2 to step 6 till the value of V_u converges:

$$V_u = V_{ai} + V_c + V_d \tag{4.21}$$

To determine the shear capacity of reinforced I-beams without shear reinforcement, the same steps should be taken with the contributions specifically determined for this cross-section in 4.1, 4.2 and 4.3.
The shear capacity must be determined iteratively with the procedure described above.

5. Comparison and discussion of the results

In this chapter the results obtained with the evaluation procedure are shown. The evaluation procedure is implemented in a Matlab code with which the shear capacity can be determined, see appendix II. The results of non-rectangular cross-sections are compared to rectangular cross-sections. With this comparison, a proposal is made to apply as effective width in the Eurocode 2. Furthermore, the results are compared with test results from the literature.

5.1 Results

In this section the results for plates with holes, I-beams and T-beams will be showed and discussed.

5.1.1 Plates with holes

To achieve a reliable final result, 27 different cross-sections of plate with holes were calculated. The corresponding parameters of these members are shown in the table below:

Table 3: Cross-sectional parameters plate with holes

	Assumpties				Beam parameter						
Member	mvd	d_a	d_r	f_c	h_f	h	b_f	r	d	z_c	b_w
1	3	16	16	34	200	800	600	200	720	144	200
2	3	16	16	34	100	600	600	200	540	135	200
3	3	16	16	34	200	800	500	200	720	144	100
4	3	16	16	34	300	1000	600	200	900	180	200
5	3	16	16	34	300	1000	500	200	900	180	100
6	3	16	16	34	200	1000	800	300	900	225	200
7	3	16	16	34	150	900	800	300	810	203	200
8	3	16	16	34	300	1200	800	300	1080	216	200
9	3	16	16	34	200	1000	700	300	900	225	100
10	3	16	16	34	75	450	500	150	405	101	200
11	3	16	16	34	75	450	400	150	405	101	100
12	3	16	16	34	150	600	500	150	540	108	200
13	3	16	16	34	200	900	700	250	810	203	200
14	3	16	16	34	400	1300	700	250	1170	234	200
15	3	16	16	34	400	1300	600	250	1170	234	100
16	3	16	16	34	200	1100	900	350	990	248	200
17	3	16	16	34	300	1300	900	350	1170	234	200
18	3	16	16	34	200	1100	800	350	990	248	100
19	3	16	16	34	200	1200	1000	400	1080	270	200
20	3	16	16	34	100	1000	1000	400	900	225	200
21	3	16	16	34	300	1400	1000	400	1260	315	200
22	3	16	16	34	200	1200	900	400	1080	270	100
23	3	16	16	34	200	1200	1000	400	1080	270	200
24	3	16	16	34	200	600	400	100	540	108	200
25	3	16	16	34	300	800	400	100	720	144	200
26	3	16	16	34	200	600	300	100	540	108	100
27	3	16	16	34	75	350	400	100	315	79	200

All the members have a reinforcement ratio of 0,4%. In this section the results obtained for plates with holes are shown and discussed. Also, contribution of each shear transfer mechanism is determined, which is shown in the figures below.

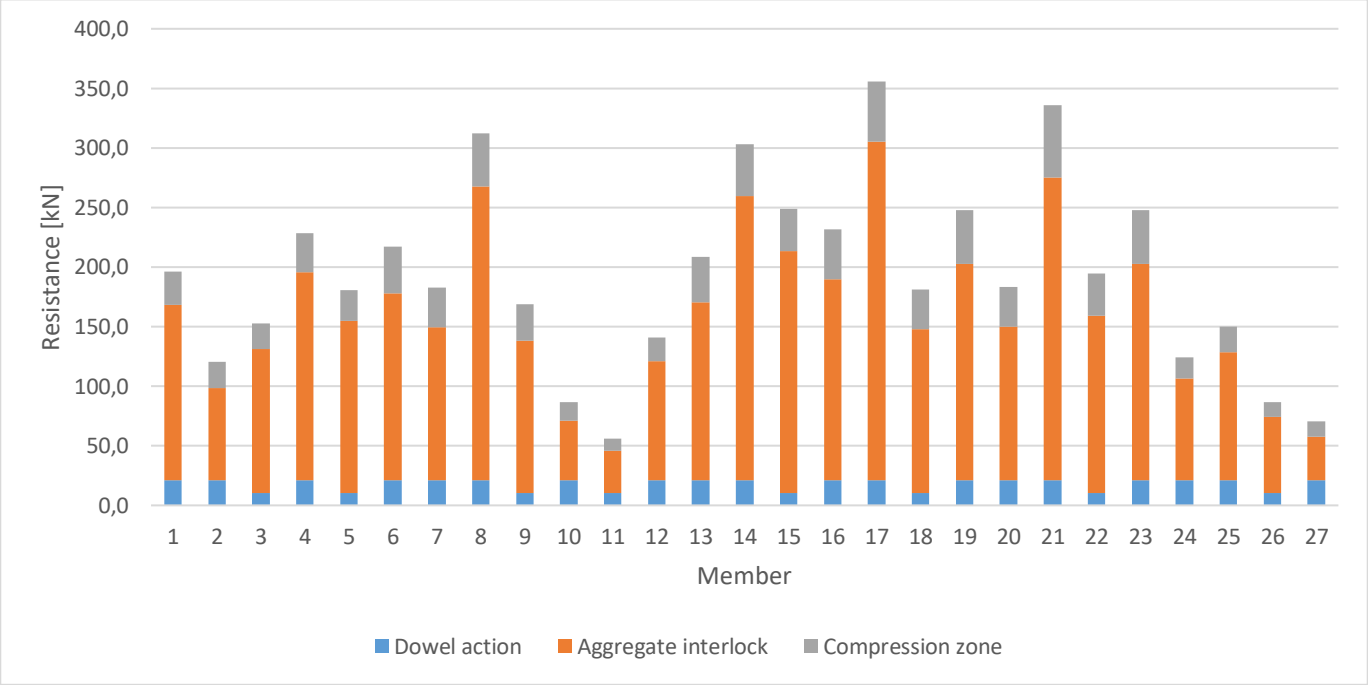

Figure 18: Overall results plate with holes

Figure 18 shows an overall overview of the calculated resistance per member. It shows that members 10, 11, 26 and 27 have the lowest shear resistance. A similarity between members 10, 11 and 27 is that they have very slender flanges, namely 75mm. Member 26 has a flange thickness of 200mm. The diameter of the holes is small, for members 10 and 11 this is 300mm and members 26 and 27 200mm. So the member height h and effective depth d is also limited, as it depends on the diameter of the hole. These 4 members all have a shear resistance of less than 100 kN.

Members with a resistance higher than 250 kN are 4, 8, 14, 15, 17 and 21. All these members have in common that the flanges are 300mm or thicker, see table 3. Member 17 has the highest shear resistance, with a flange thickness of 300mm. The diameter of the holes vary between 400mm and 800mm.
All other members have a shear resistance between 100kN and 250kN. The flange thickness and web width b_w varies between 100mm and 200mm. The results show that a smaller web width leads to a smaller shear resistance, see Figure 19. This is logical, because the contribution of aggregate interlock and dowel action decreases due to thinner web. As a result, the total shear resistance V_u also decreases. This in turn has a small influence the contribution of the compression zone, as it depends on the ratio z_c/z and the total resistance V_u in the evaluation procedure.

It also appears that a thinner flange thickness leads to a lower shear resistance, see Figure 20 which shows the overall results in terms of flange thickness.
An explanation is the fact that aggregate interlock decreases, because the crack height s_{cr} decreases due to a higher compression zone as explained in 4.1.3. For non-rectangular cross-sections the height of the compression zone increases if the neutral axis falls outside the flange. This is the case with thin flanges, where the ratio z_c/z increases because of the shift, see example below. So in case the neutral axis is outside

the flange, the contribution of the compression zone increases by 4% in proportion to the total shear resistance. This seems logical, because the compressive area also increases. However, it should be noted that the total shear resistance is lower in case of thinner flanges. So at the bottom line the real contribution of compression zone with thinner flanges is less. The location of the neutral axis affects the distribution of the shear transfer action contributions.

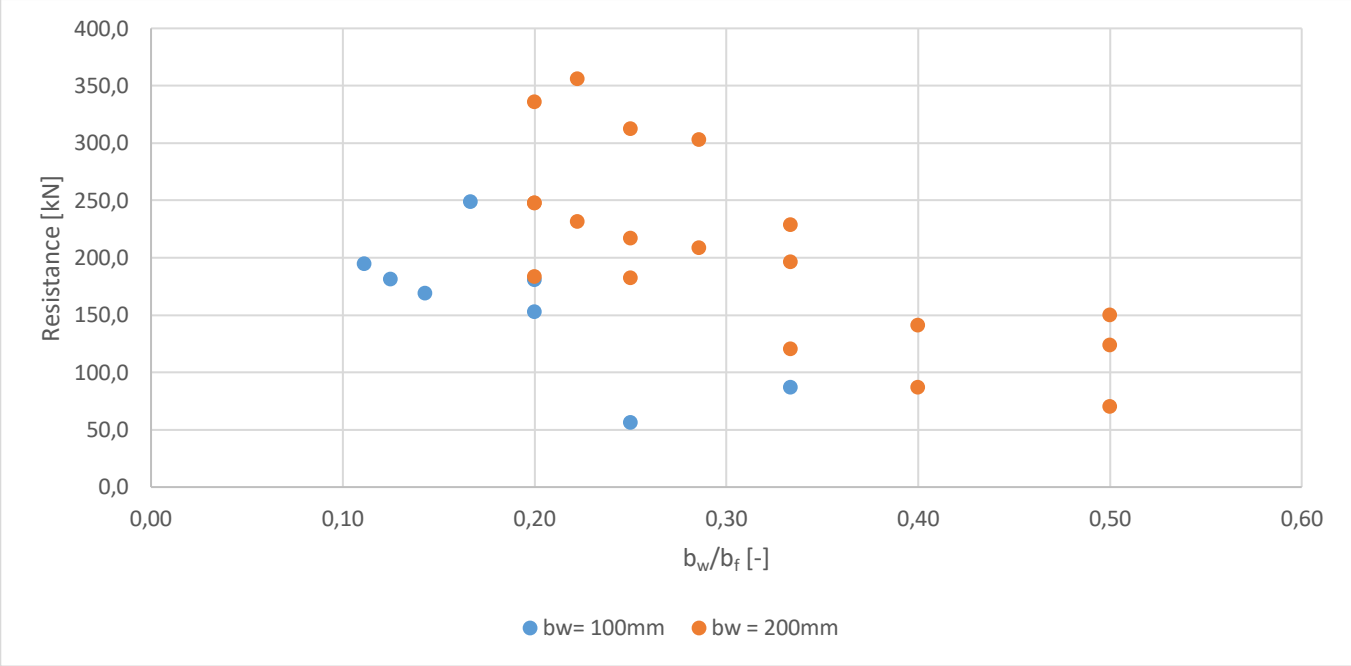

Figure 19: Influence of web width on the shear resistance

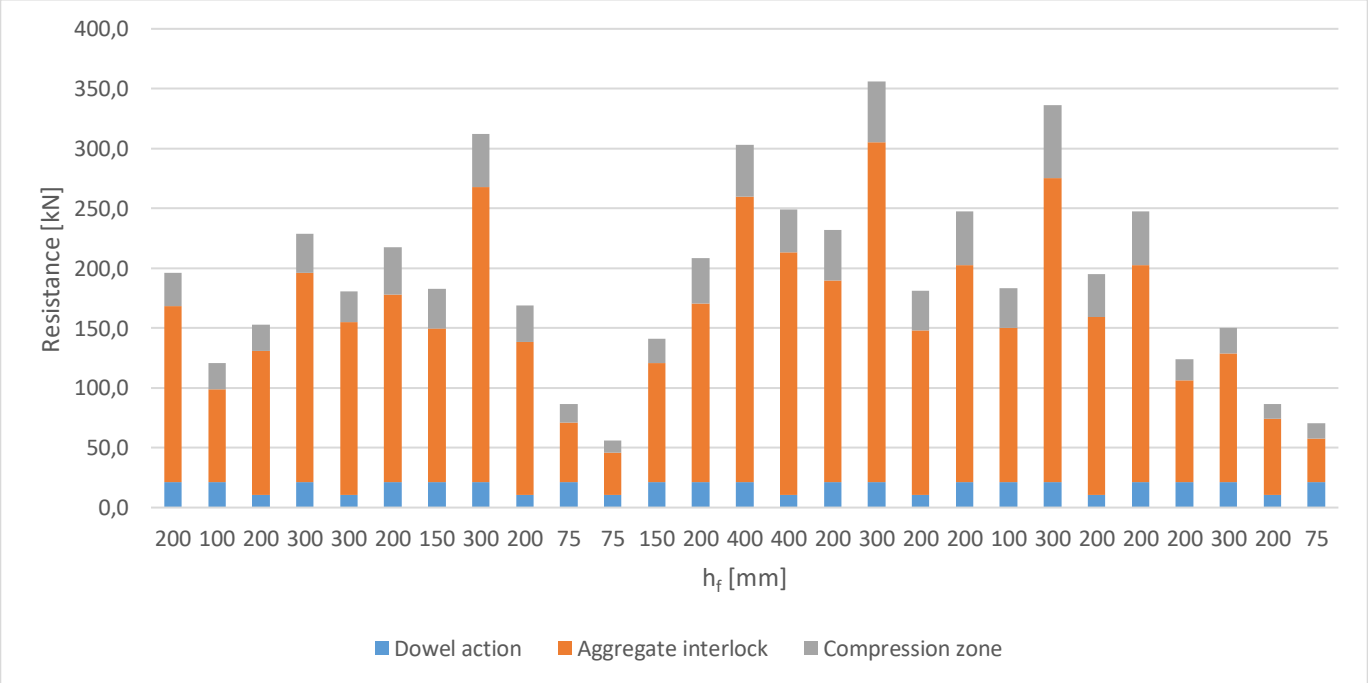

Figure 20: Overall results plates with holes in terms of flange thickness

Example of the ratio z_c/z:

Member 1: $h_f = 200mm$; $z_c = 144mm$; $d = 720mm$; $z = d - 1/3z_c = 672mm$
$z_c / z = 144 / 672mm = 0,21$ [-]

Member 2: $h_f = 100mm$; $z_c = 135mm$; $d = 540mm$; $z = d - 1/3z_c = 495mm$
$z_c / z = 135 / 495mm = 0,27$ [-]

The main reason of the lower shear resistance is that the neutral axis is below the flange. If the neutral axis is in the flange, the top part of the major crack is also in the flange. This part of the crack has the largest shear stress due to aggregate interlock, hence the largest contribution, see Figure 23. If the major crack is partly in the flange, the contribution of aggregate interlock grows enormously because of the flange width. In the evaluation method the compression zone depends on the total shear resistance and not directly on the web or flange width. The shear resistance increases strongly due to aggregate interlock, which increases due to the influence of the flange width. So the effect of the flange width on the compression zone is simulated through iterations in the evaluation method.

The observations described above indicate that the flange thickness and the location of the neutral axis are an important parameter for determining the shear resistance of non-rectangular cross-sections. Therefore, the calculated shear capacity is plotted against the parameter h_f/h, see Figure 21.

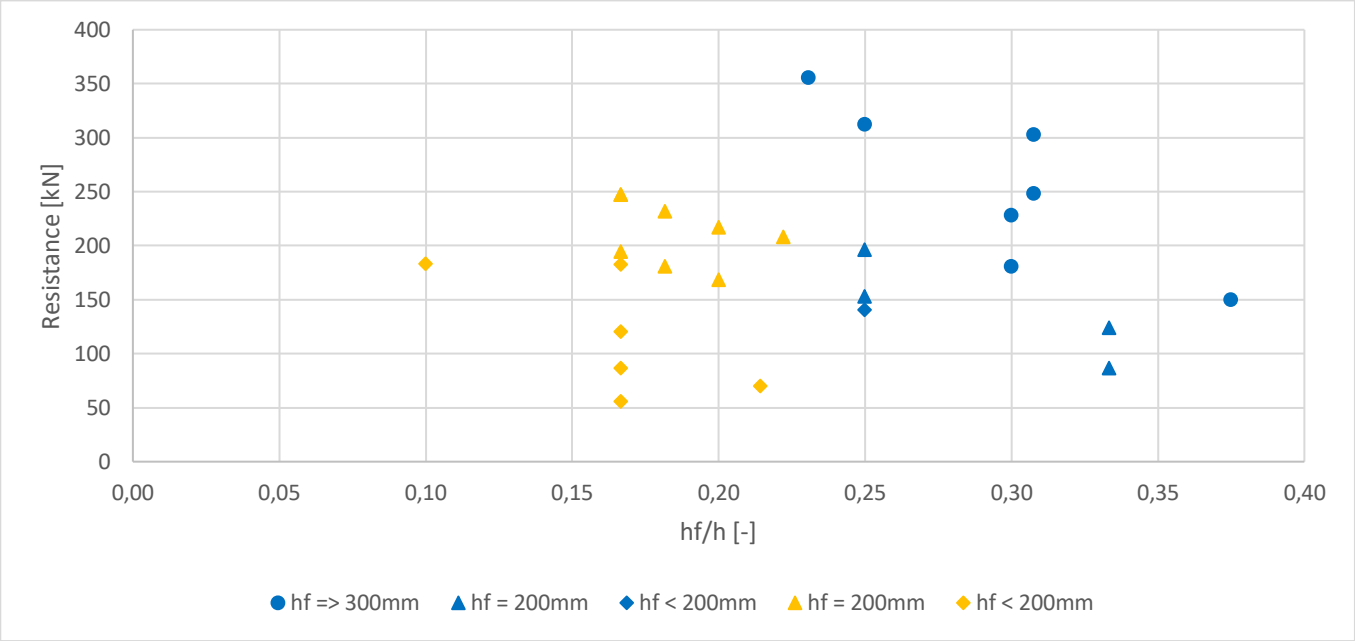

Figure 21: Shear capacity plotted against h_f/h. Blue: neutral axis is inside the flange; Yellow: neutral axis is below the flange

Figure 21 shows a clear separation between members where the neutral axis is inside the flange (blue) and where it is below the flange (yellow). This shows that the members with the neutral axis in the flange have a higher shear capacity. In cases where the shear capacity is less than 150 kN, the limiting factor on the shear capacity is the limited member height h.

From Figure 18 it can be concluded that for members 1, 3, 4, 5, 8, 12, 14, 15, 17, 24, 25 and 26 the contribution of the compression zone is 14%. The neutral axis of all these members is located in the flange. In the evaluation procedure, the contribution of the compression zone is a certain ratio of the total shear resistance. As shown in the example above, the ratio z_c/z is equal to 0,21. The grade of fullness of a rectangular compression zone is 2/3 and the multiplication of these 2 parameters gives 0,14, which explains the contribution of 14% for the compression zone.
The contribution of aggregate interlock and dowel action varies between 63% - 81% and 4% - 19% respectively. Members 5 and 15 have the highest contribution of aggregate interlock in percentages (81%). These members have in common that they both have thick flanges, 300mm and 400mm respectively, with a thin web of 100mm. Members 4 and 14 have the same flange thickness, but a web width of 200mm. The latter have higher total shear resistance, but a different ratio of contributions where aggregate interlock is slightly less and dowel action is slightly more. This can be easily explained by the fact that in case of a thinner web the contribution of the dowel action decreases, so does the contribution ratio in %.

For the other members the contribution of the compression zone is approximately 18%, explained by the multiplication of 0,27 x 2/3 = 0,18. The contribution of aggregate interlock and dowel action varies between 48%/74% and 8%-34% respectively. Member 27 has the largest contribution of dowel action relative to other shear transfer actions, followed by members 2, 10 and 11. All these members have thin flanges, which explains the large contribution of dowel action: The contribution of aggregate interlock and compression zone decreases, but the contribution of dowel action remains unchanged.
As explained in section 4.3, dowel action reaches the plastic limit of V_{dmax} when the shear displacement is 0,08mm. This is quickly reached during loading the member. After this the value of V_{dmax} remains the same for increasing shear displacements.

In summary, the location of the neutral axis is an important parameter, which also determines the height of the compression zone z_c. In case the neutral axis is in the flange, the height of the compression zone for plates with holes is $0{,}2d$. When the neutral axis is below the flange, z_c becomes $0{,}25d$ to ensure the internal force balance. This causes an increase in the contribution of the compression zone, because the compressive area becomes larger. The calculations have shown that if the neutral axis is located in the flange, the width of the flange is used optimally. In this case, the top of the major crack is in the flange, where the shear stresses due to aggregate interlock are highest and the width of the cross-section is greatest. This increases the contribution of aggregate interlock enormously and therefore the total shear capacity.
In addition, it appears that the width of the web and the flange also play an important role in calculating the shear capacity. A smaller web width, and if the neutral axis is in the flange also the flange width, leads to a smaller capacity. The results also show that aggregate interlock contributes the most to the total shear capacity of the cross-section.

5.1.2 I-beams

For the I-beams the same parameters as Table 3 have been applied, whereby the parameter *r* (radius of the holes) is omitted. This is done so that a one to one comparison can be made with plates with holes. It should be noted, however, that a shear lag effect could occur, whereby the full flange width cannot be used with wide flanges. This will be discussed further in the remainder of the study.

In addition, it has been found in 4.1.3 that the compression zone for I-beams with $\rho_s = 0{,}4\%$ is equal to $0{,}3d$ if the neutral axis is below the flange.

Table 4: Cross-sectional parameters I-beams

Member	Assumptions				Beam parameter					
	mvd	d_a	d_r	f_c	h_f	h	b_f	d	z_c	b_w
1	3	16	16	34	200	800	600	720	216	200
2	3	16	16	34	100	600	600	540	162	200
3	3	16	16	34	200	800	500	720	216	100
4	3	16	16	34	300	1000	600	900	180	200
5	3	16	16	34	300	1000	500	900	180	100
6	3	16	16	34	200	1000	800	900	270	200
7	3	16	16	34	150	900	800	810	243	200
8	3	16	16	34	300	1200	800	1080	324	200
9	3	16	16	34	200	1000	700	900	270	100
10	3	16	16	34	75	450	500	405	122	200
11	3	16	16	34	75	450	400	405	122	100
12	3	16	16	34	150	600	500	540	162	200
13	3	16	16	34	200	900	700	810	243	200
14	3	16	16	34	400	1300	700	1170	234	200
15	3	16	16	34	400	1300	600	1170	234	100
16	3	16	16	34	200	1100	900	990	297	200
17	3	16	16	34	300	1300	900	1170	351	200
18	3	16	16	34	200	1100	800	990	297	100
19	3	16	16	34	200	1200	1000	1080	324	200
20	3	16	16	34	100	1000	1000	900	270	200
21	3	16	16	34	300	1400	1000	1260	378	200
22	3	16	16	34	200	1200	900	1080	324	100
23	3	16	16	34	200	1200	1000	1080	324	200
24	3	16	16	34	200	600	400	540	108	200
25	3	16	16	34	300	800	400	720	144	200
26	3	16	16	34	200	600	300	540	108	100
27	3	16	16	34	75	350	400	315	95	200

The results of the I-beams are shown in the figures below.

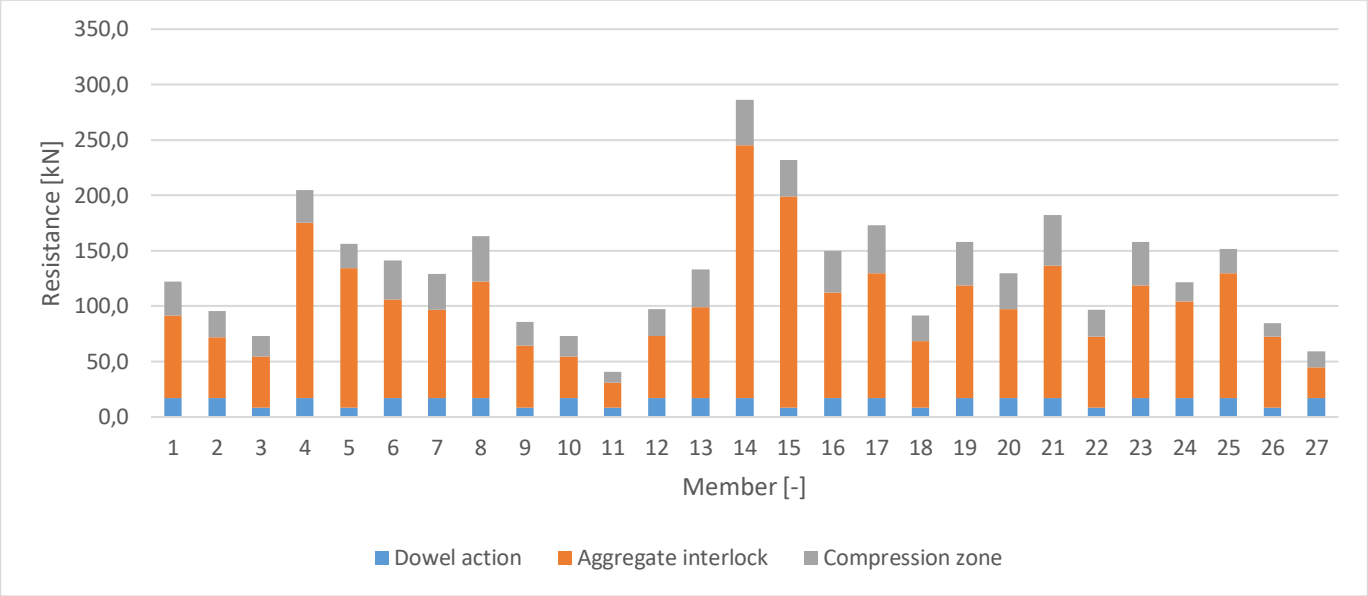

Figure 22: Overall results I-beams

The results from Figure 22 show the same patterns and observations as for plates with holes, with some minor difference. This is discussed further in section 5.2.
It can be deduced that the contribution of the compression zone varies between 14% and 25% for I-beams. For members where the neutral axis falls in the flange, the contribution of compression zone of I-beams is the same as plates with holes, because the compression zone has a rectangular shape. This is the case for members 4, 5, 14, 15, 24, 25 and 26, where the contribution of the compression zone is 14%.
The neutral axis of the other members is below the flange, with the contribution of the compression zone increasing proportionally to 25% due to larger compressive area. As a result, the aggregate interlock decreases slightly, because the crack height s_{cr} decreases slightly due to higher compression zone z_c.
To further explain and highlight the influence of the location of the neutral axis, a comparison made between members 1 and 24. The effective heights are 720mm and 540mm respectively. The neutral line of member 1 is below the flange, while that of member 24 is inside the flange. The thickness off the flange and the web width are the same for both members. The results of both members are given in the table below:

Table 5: Results of member 1 and 24

Member	**V_d**	**V_{ai}**	**V_c**	**V_u**
1	17 kN, 15%	68, 60%	28, 25%	114 kN
24	17 kN, 14%	84, 71%	17, 15%	118 kN

The contribution of the dowel action is the same, because the web thickness is the same.
Although member 24 has a smaller effective height and overall width b, it has almost the same shear resistance as member 1. This is due to the location of the neutral axis in the cross-section. As explained earlier, the flange width of the member is best used when the neutral axis is in the flange. This is shown by the shear stresses due to aggregate interlock, see Figure 23. The shear force is equal to the area under the shear stress distribution.

As it can be seen in the figure below, the shear stress is highest at the top of the crack and decreases sharply towards 0 towards the root of the crack. If the neutral axis is in the flange, a part of the peak shear stress will be multiplied with the flange width b in order to calculate the shear force. This results in a favourable contribution of the aggregate interlock, which can be seen in the results of Table 5.

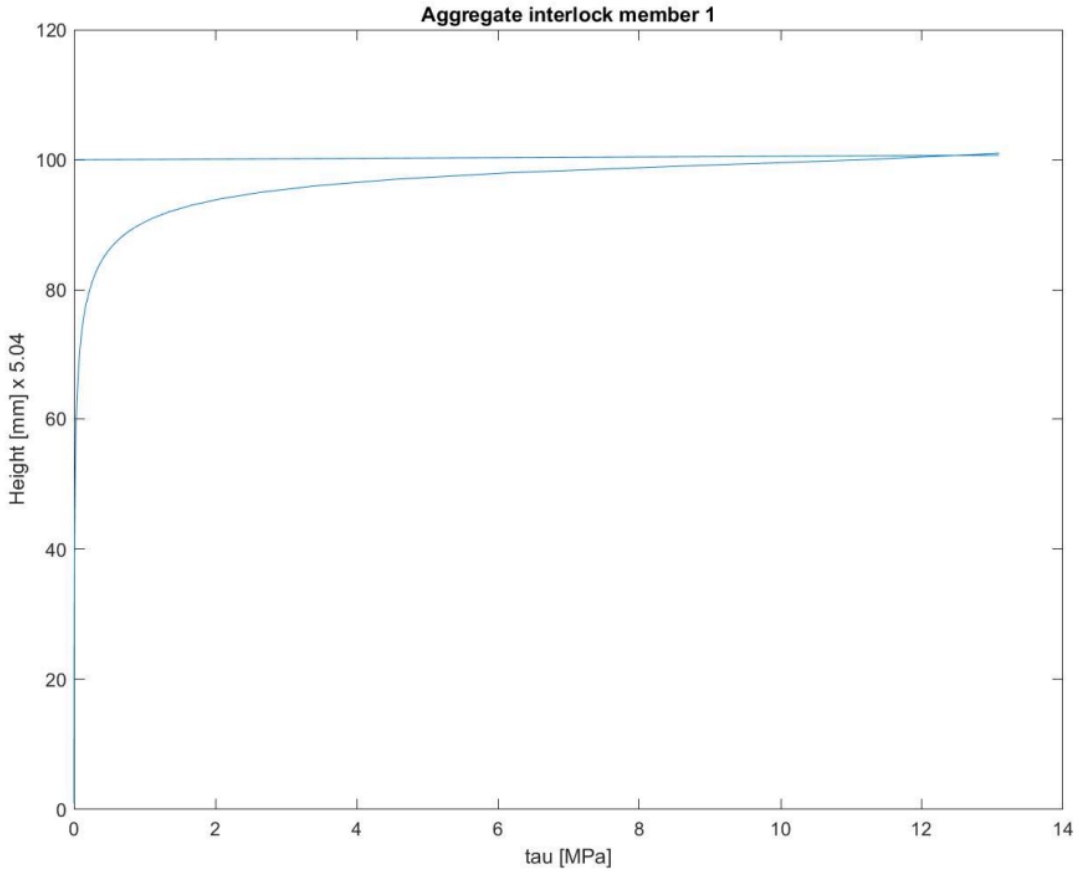

Figure 23: Shear stresses due to AI member 1
Remark: although a large part of the shear stresses from figure 23 appear to be 0, this is not the case. The stresses are very low (but not 0), which creates a distorted picture.

5.1.3 T-beams

By comparing the results of I-beams with T-beams, it is possible to determine the added value of the bottom and top flange. In order to do that, the same cross-sectional parameters as in Table 4 is assumed for the T-beams. The influence of shear lag effect will be discussed later.

There are small differences between a T-beam and I-beam in the evaluation procedure. One of these changes is the dowel action. Instead of the web width, the net width of the web should be taken, because the reinforcement is located in the web in case of a T-beam. Therefore, formula (4.16) should be replaced by formula (4.15).

The change into a T-beam from an I-beam also leads to the omission of the term for the bottom flange in the calculations of aggregate interlock:

$$V_{ai;T} = \sigma_{pu}\{\cancel{b_f \int_0^{h_f} A_x(\Delta, w(s)) - \mu A_y(\Delta, w(s)) ds} + b_w \int_{h_f 0}^{s_{cr}} A_x(\Delta, w(s)) - \mu A_y(\Delta, w(s)) ds\}$$

The comparison of these two cross-sections is shown below.

There is a slight difference in the total shear capacity between I-beams and T-beams. The biggest differences can be seen with members with thick flanges. This is because the contribution of a thick lower flange is eliminated in case of T-beams.

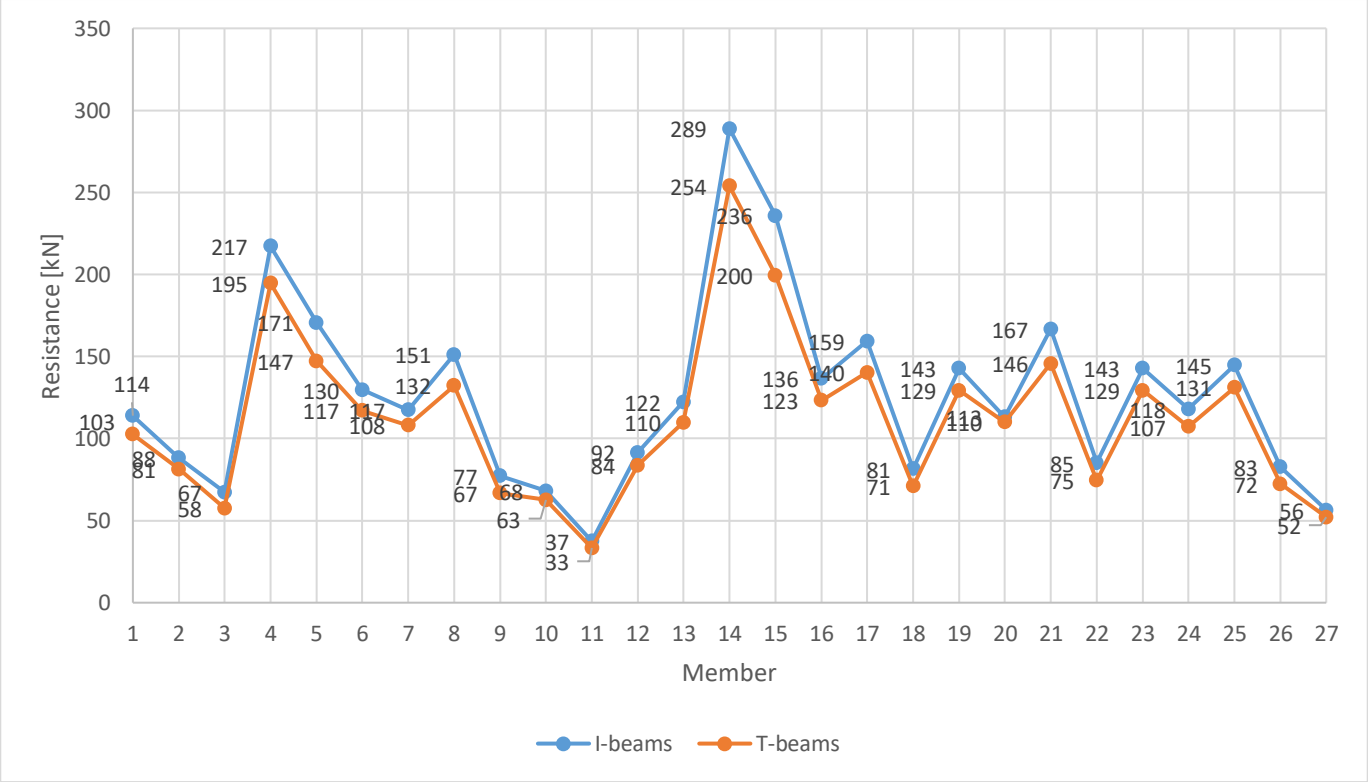

Figure 24: Comparison of I-beams and T-beams

Zooming in further on shear transfer action level appears that the dowel action decreases, which is logical because of the reduced net width of the web. In addition, small differences can be seen in the aggregate interlock and compression zone. The reason of a small decrease in the contribution of the compression zone is because it depends on the total shear force V_u in the evaluation procedure. This doesn't quite make sense since a bottom flange should not affect the compression zone since it is at the top flange. But given the fact that this is small (5 kN) this is accepted.

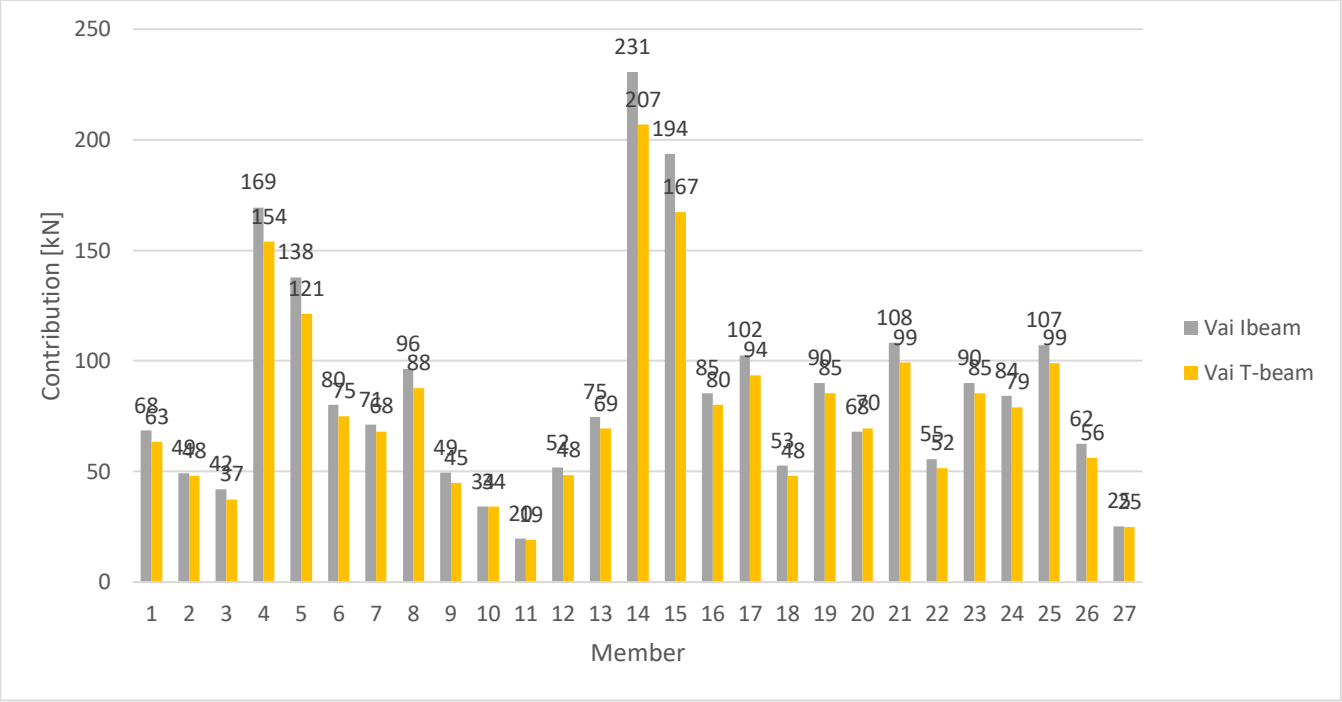

Figure 25: Comparison of AI for I-beams and T-beams

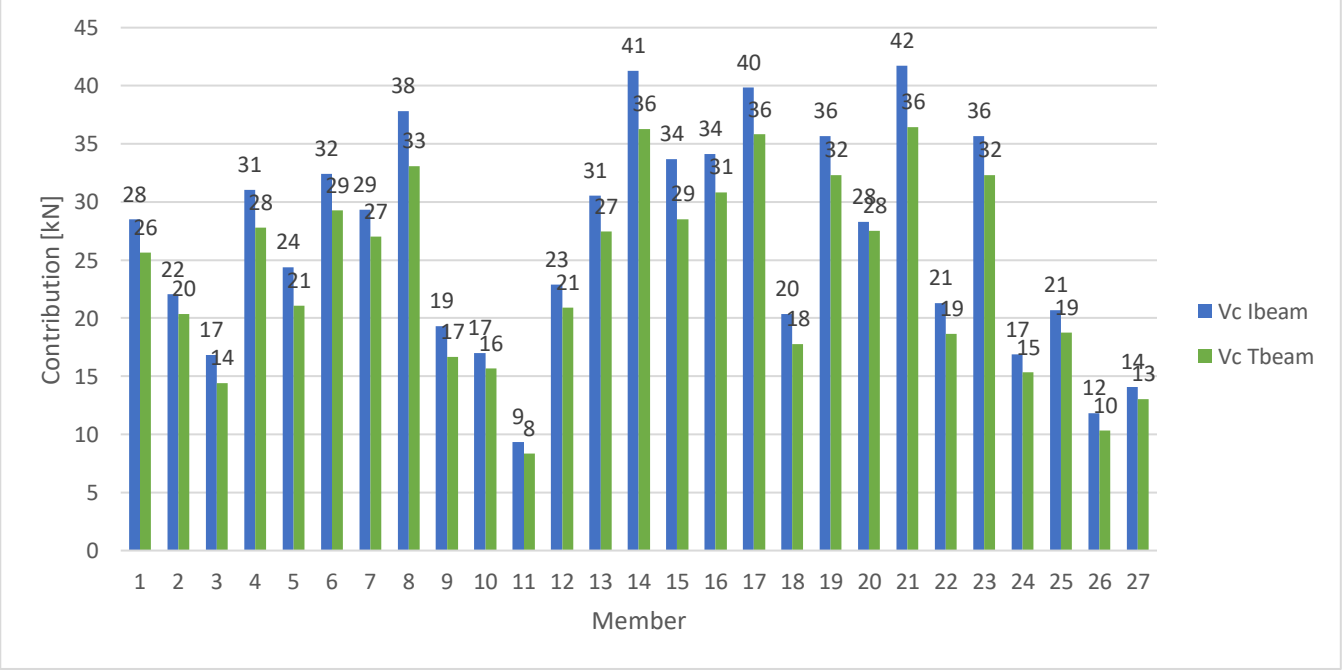

Figure 26: Comparison of CZ for I-beams and T-beams

It can therefore be concluded from the above that the bottom flange has little added value for the shear capacity of non-rectangular cross-sections. The absence of a bottom flange leads to a small decrease in capacity.
However, unlike the bottom flange, the contribution of the top flange will be crucial, because the contribution of the compression zone depends entirely on it. If the neutral axis is in the top flange, the aggregate interlock also strongly depends on the width and thickness of the top (compression) flange.

5.2 Comparison with rectangular cross-sections

In order to determine the contribution of flanges, the shear force capacity of the web alone is also determined. For plates with holes, this web alone area is shown with a orange region in the figure below.

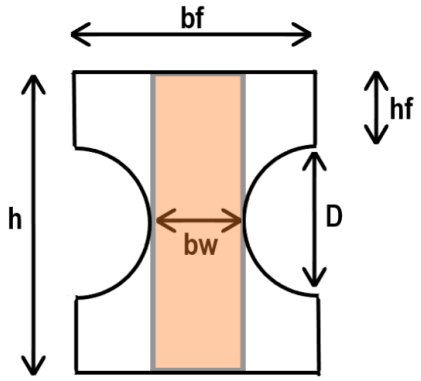

Figure 27: Web only area of plates with holes

The web alone area results is a rectangular cross-section with width b_w and height h according to tables 3 and 4. In this section, the results of the rectangular cross-sections will be compared to non-rectangular cross-sections. The results of rectangular cross-sections per member are shown below.

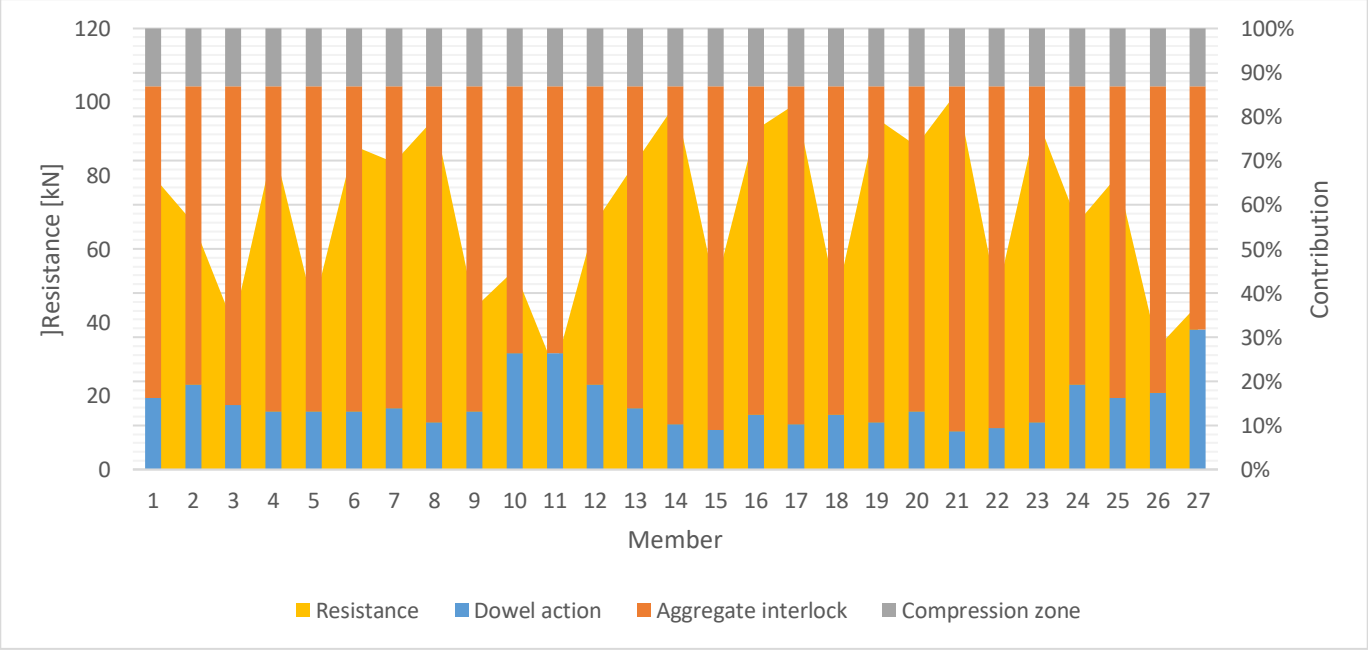

Figure 28: Results of only web

5.2.1 Comparison of the results

The comparison of the total shear resistance of the web with non-rectangular cross-sections is shown in Figure 29: Overall comparison of the shear resistance.

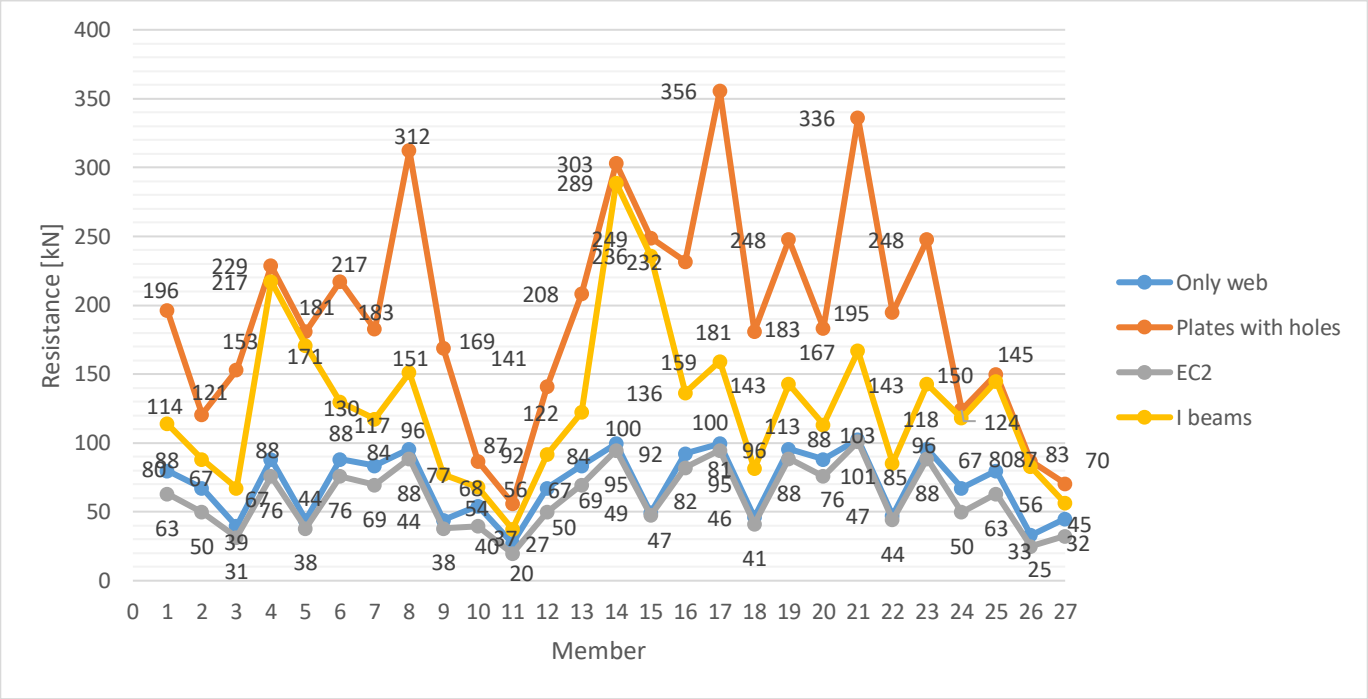

Figure 29: Overall comparison of the shear resistance

Figure 29 also includes the resistance according to EC2 for comparison. The equation from Eurocode 2 section 6.2a to calculate the shear resistance of beams without shear reinforcement is:

$$V_{EC} = C_{Rd;c} k \sqrt[3]{100 \rho_s f_{ck}} bd \tag{5.1}$$

where,

$$k = 1 + \sqrt{\frac{200}{d}} \leq 2{,}5 \quad \text{and} \tag{5.2}$$

$$C_{Rd;c} = \frac{C_{Rd}}{\gamma_c} \tag{5.3}$$

According to EC2, the value of C_{Rd} is equal to 0,18 and γ_c is 1,5, leading $C_{Rd;c}$ = 0,18/1,5 = 0,12. The background of these values are given in the study of Walraven [52].

For non-rectangular cross-sections, the smallest width in the cross-section should be used for the width b. As can be seen in Figure 29, this results in conservative results for plates with holes and I-beams, therefore also for T-beams. Also, it shows that the results of the web only (rectangular cross-section) using evaluation procedure of Yang (2015) and the Eurocode are almost identical.

The smallest difference of the shear resistance between web and web including flanges can be seen in members 10, 11 and 27. These members have in common that the flanges are very thin (75mm). The greatest differences are observed in case the neutral line is in the flange.

Furthermore, there are also differences between the resistance of I-beams and plate with holes. These differences are mainly observed in members with thick flanges. The reason for this is the change of the compression zone height z_c in case of I-beams. If the flange thickness h_f is smaller than $0{,}25d$ for plates with holes or $0{,}3d$ for I-beams, the neutral axis is below the flange. This causes the neutral axis to be outside the flange more often in case of I-beams, slightly reducing the shear resistance due to the decrease of aggregate interlock. Taking into account the shear lag effect, this difference will only increase.

Contrary to what the Eurocode 2 prescribes, the Dutch Guideline for the Assessment of Existing Bridges (RBK) states that an average width (b_{gem}) for non-rectangular cross-sections may be used in (5.1), with an upper limit of $1{,}25b_w$. For the procedure to determine b_{gem}, please refer to the RBK [53].
According to this procedure, the upper limit of b_{gem} applies to plates with holes, resulting in to an underestimation of the shear capacity. The upper limit value is also applied for the I-beams. Figure 30 shows that in most cases this gives a reasonable estimate of the shear capacity of I-beams. However, if the neutral axis is in the flange, the RBK approach leads to an underestimation.

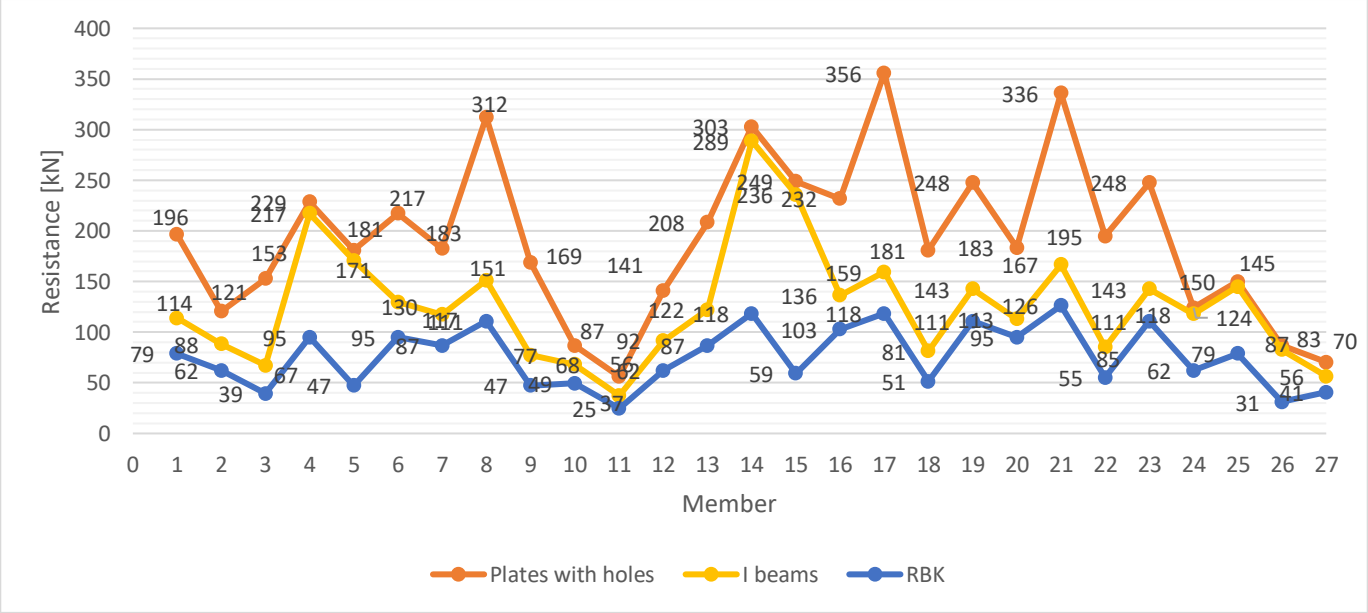

Figure 30: Comparison of the calculated results with RBK method

Before an extensive comparison is made, attention should be paid to the influence of shear lag on the shear capacity of I-beams with wide flanges. According to the research of Zanuy et al. [54], for slender beams where b_f/L <0,20 loaded with a point load at $0{,}5L$, the shear lag effect is nil and therefore negligible. This study only focusses on slender beams with a shear slenderness lower bound of $a/d = 3$. This results in a b_f/L value of up to 0,20 for the members shown in Table 3. However, despite this outcome, it has been decided to limit the width of the flange to $3b_w$ when calculating the shear capacity. The influence of this is shown in the figure below. In most cases it leads to little or no decrease in shear capacity. However, if the neutral axis is in the flange, the capacity decreases by approximately 40%. It is therefore decided to take the shear lag effect into account for I and T-beams in the remainder of the study.

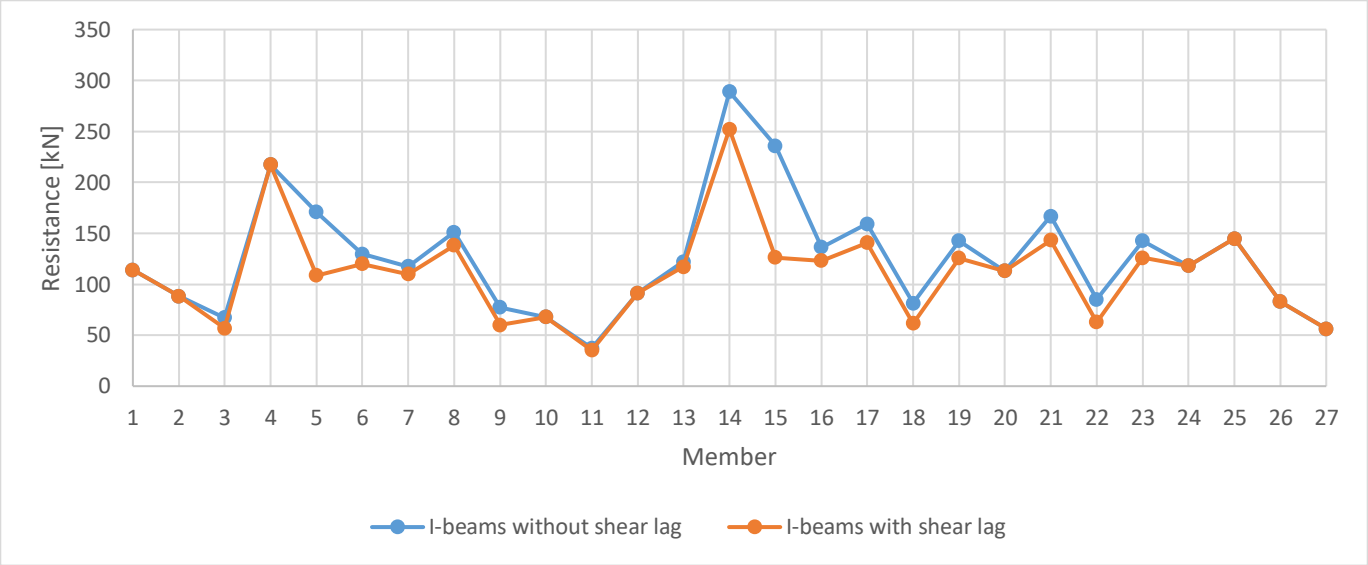

Figure 31: Influence of shear lag on the shear capacity of I-beams

Back to the comparison between non-rectangular cross-sections and rectangular cross-sections, the contributions of the shear transfer actions are discussed in more detail, see figures below.

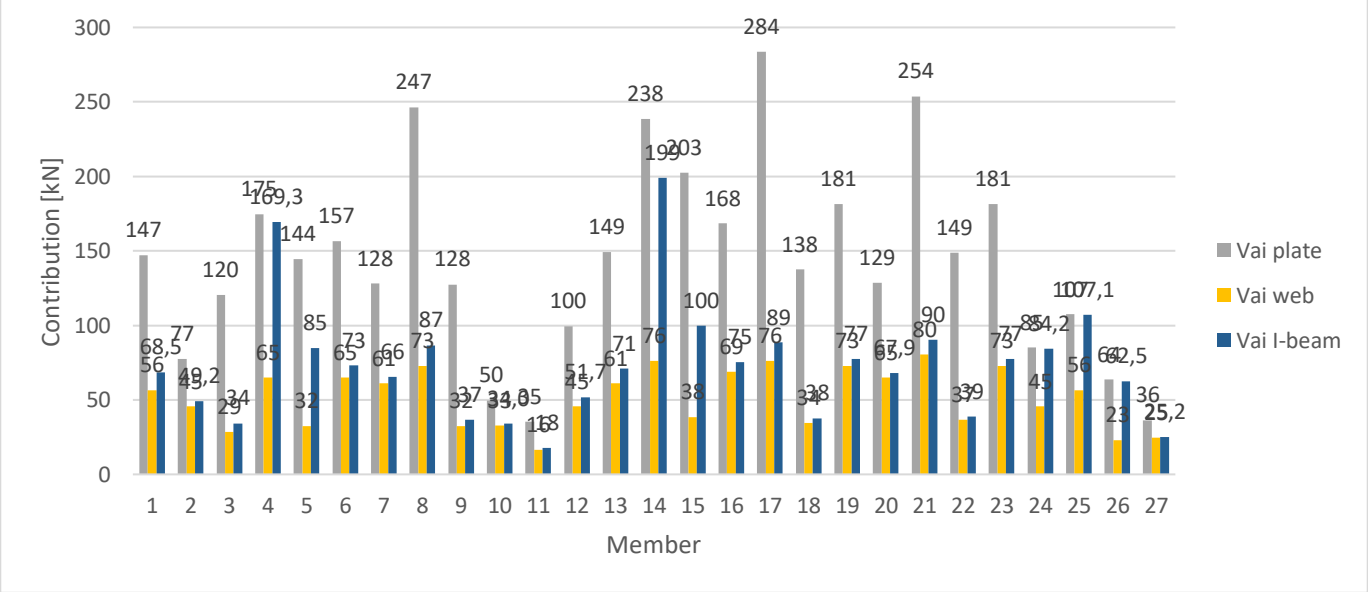

Figure 32: Comparison of AI

Figure 32 shows that aggregate interlock increases the most for members where the neutral axis is in the flange. The smallest increase in aggregate interlock is seen for members with thin flanges, which makes sense. The neutral axis is in these cases in the web, so the contribution of the flanges on the aggregate interlock is then minimal, which approximates the web-only scenario. However, in case the neutral axis is in the web, I-beams still show a greater contribution of aggregate interlock compared to web alone. This is caused by the small contribution of the bottom flange.
The difference between plates with holes and I-beams is caused by the varying width of plates with holes, which increases the contribution of aggregate interlock for plates with holes. This is also the reason for the

huge increase and difference in aggregate interlock compared to web-only scenario. In addition, the shear lag effect on I-beams also creates differences between plates with holes and I-beams.

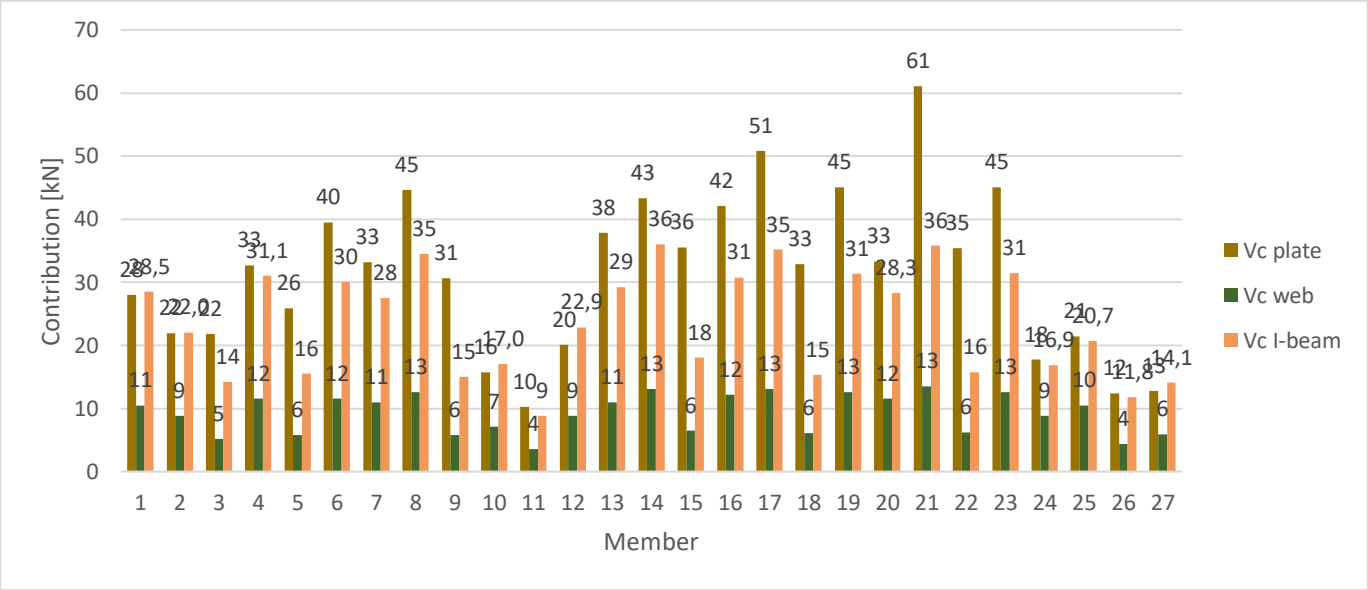

Figure 33: Comparison of compression zone

The contribution of the compression zone also increases, proportionally much more than the aggregate interlock. This is because the area of the compression zone is increased by the flanges compared to web-only scenario.

Figure 34 on the next page compares the contribution of dowel action. The contribution of plates with holes is the highest due to the varying width of the web. This is more favorable compared to I-beams, where the web width b_w is decisive. As a result, the increase in dowel action of I-beams compared to web alone is limited. The width is the same in both cases, but in the case of only the web, the net width b_n is used in the calculation.

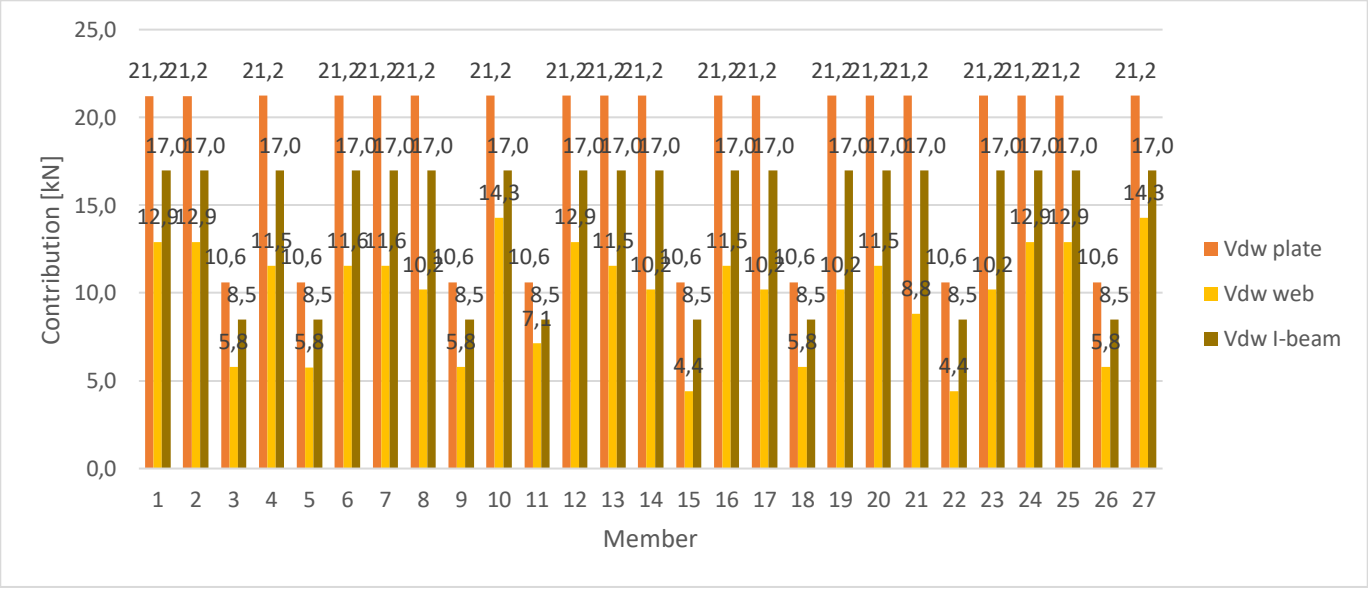

Figure 34: Comparison of dowel action

5.2.2 Scale factor

The effective web width b_{weff} is determined for each member by dividing the calculated shear resistance for non-rectangular cross-sections by the shear resistance of the web only. This determines a scaling factor for the effective width per member, which could be used in the EC2.

The calculated scale factor for plates with holes per member are shown in Figure 35. The scale factor is plotted against h_f/h and b_w/b, because it was shown in section 5.1 that the resistance strongly depends on the flange thickness, flange width and web width. Of course, the member height and thus the effective depth is also an importance factor to calculate the shear resistance. The overview shows that members with a thin web width lead to a large spread in the data, because the scale factor is much higher than the average. Given that this research aims to serve as an aid to engineering practice, it is decided to maintain a realistic range of cross-sectional parameters. This range is shown with a red box in Figure 35.

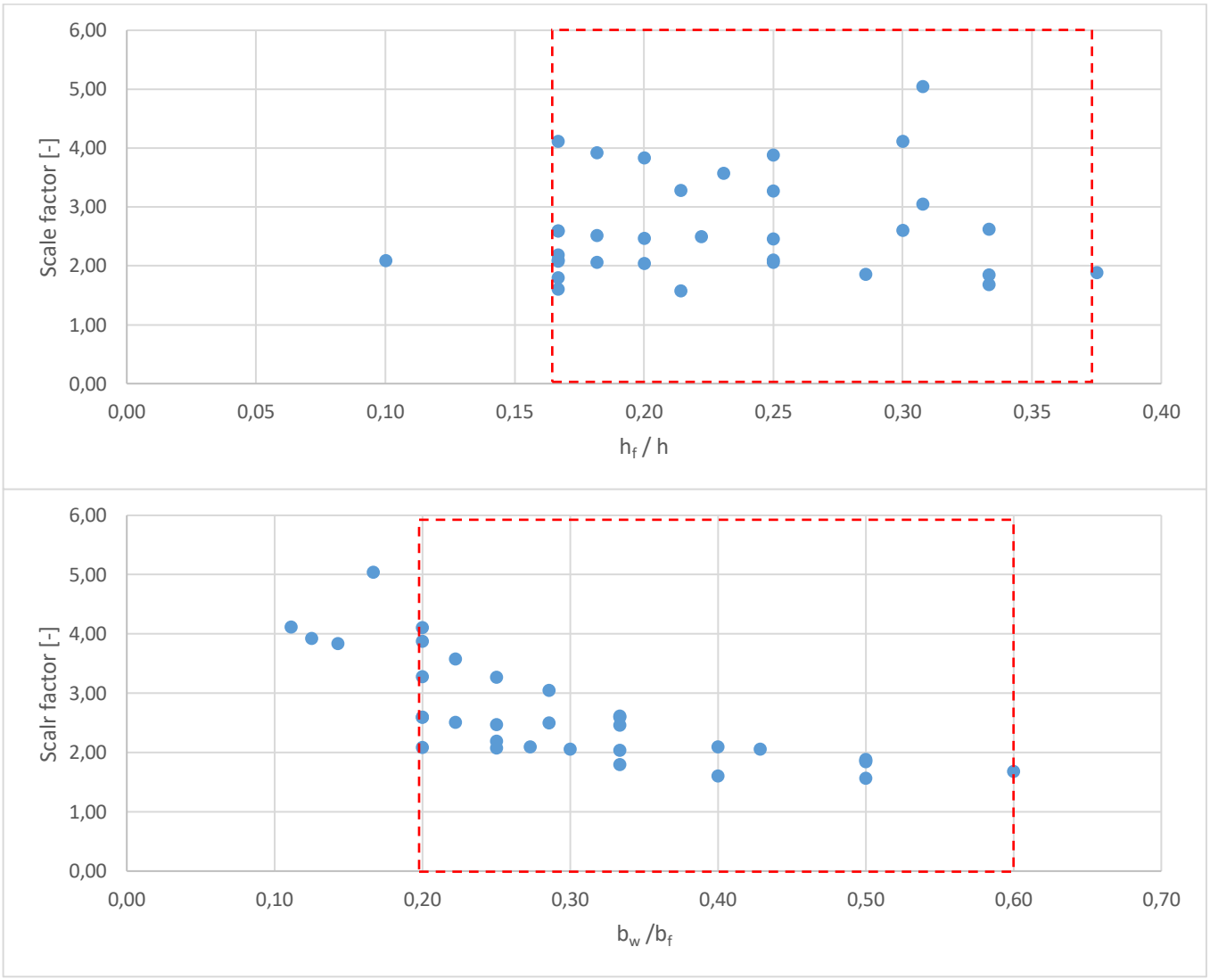

Figure 35: Effective web width of plates with holes, top: flange thickness divided by height; bottom: web width divided by width. The red box indicates the realistic range of cross-sectional parameters.

Figure 35 shows that for an increasing value of h_f/h the scale factor increases, which means that the resistance of non-rectangular members increases more compared to the web alone. With an increasing factor h_f/h the neutral axis is most likely in the flange. This also explains the fact that the scale factor increases, because previous results have already shown that the resistance increases sharply when the neutral axis is located in the flange.
However, the shear resistance of non-rectangular cross-sections also depends on the web width. Figure 35 shows that with an increasing value of b_w/b_f the scale factor decreases, so also the resistance for non-rectangular cross-section compared to only the web.

5.2.3 Parameter study

The scale factors calculated in 5.2.2 are only based on a number of specific parameters, such as reinforcement ratio of 0,4%, shear slenderness ratio of 3 and concrete compressive strength of 34 MPa. This section examines the influence of these parameters on the scale factor. To determine this, the parameters are changed on a case-by-case basis: the reinforcement ratio becomes 2%, the shear slenderness becomes 5 and the concrete compressive strength becomes 60 MPa. The results of these changes are shown on the next page.

The overview in Figure 36 shows that changing the concrete compressive strength or the shear slenderness ratio has hardly any influence on the scale factor. It can therefore be concluded that the effect of these parameters on the scale factor is negligible. However, it appears that the reinforcement ratio does influence the scale factor. For plates with holes, a higher reinforcement ratio leads to a lower scale factor. This is because the height of the compression zone increases with higher reinforcement ratio, so the neutral axis falls outside the flange in most cases. As a result, the capacity of plates with holes decreases sharply, resulting in a lower scale factor.

For I-beams and T-beams, the increase in reinforcement ratio leads to a small increase in scale factors when the neutral axis was in the web with $\rho_s = 0{,}4\%$. For cases where the neutral axis was in the flange and with a higher reinforcement ratio move into the web, this change leads to a decrease in the scale factor as noted by plates with holes.

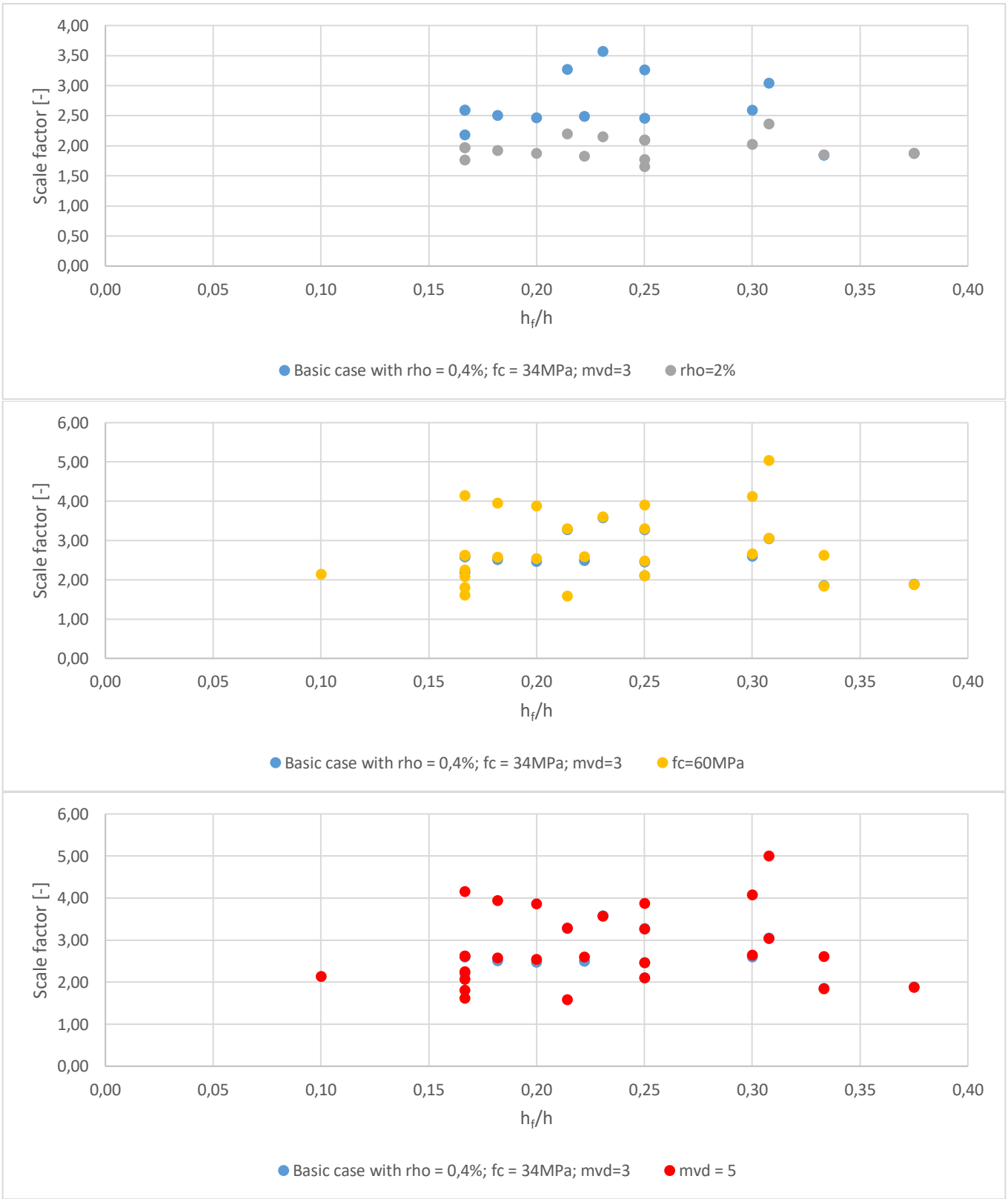

Figure 36: From top to bottom influence of reinforcement ratio, concrete compressive strength and shear slenderness ratio on the scale factor for plates with holes

5.2.4 Determining effective web width

With the results shown previously, it is possible to calculate the effective web width b_{weff}. This width can then be used for non-rectangular cross-sections to calculate the shear resistance according to the EC2 with formula (5.1), which is comparable with the RBK approach. The calculated scale factors are generalized in this section to a uniform factor formula, with which a general b_{weff} can be determined. A distinction is made here between reinforcement ratios <1% and >1%, so that the spread of the data is smaller.
To determine the dependence of the scale factor with parameters b_w/b_f and h_f/h, a multiple linear regression analysis is performed. The effective web width can be determined using the scale factor:

$$b_{weff} = sf \cdot b_w \tag{5.4}$$

Plates with holes:
The regression analysis resulted in the following relationship for ρ < 1% for plates:

$$sf = 2{,}9 + 7{,}4\frac{h_f}{h} - 7\frac{b_w}{b_f} \tag{5.5}$$

Limitations:

- Formula (5.5) is only applicable for members within the ranges $0{,}20 \leq b_w/b_f \leq 0{,}60$ and $0{,}15 \leq h_f/h \leq 0{,}40$. Outside these ranges, the formula may lead to incorrect results.
- Formula (5.5) is only applicable for member with reinforcement ratio lower than 1%, but not lower than 0,4%, because in these cases flexural failure will be decisive.
- Formula (5.5) is only valid for slender members where $a/d \geq 3$.

The regression analysis resulted in an average of 1,01 ($sf_{cal}/sf_{regression}$) with a Coefficient of Variation (CoV) of 10%. This means that formula (5.5) gives a good approximation of the scale factor.
The results of this regression model is shown below in Figure 37. The calculated shear capacity using the evaluation procedure from this research is named V_{cal} and calculated according to EC2 using b_{weff} in EC2 is called $V_{EC2;new}$. The mean value of the adapted model using formula (5.4) for b_{weff} is 1,11 (V_{cal}/V_{EC2}), with a CoV of 18%. The standard Eurocode 2 approach (taking the minimum web width b_w) has an average of 2,73 with a CoV of 16%. The model thus provides better results compared to the current approach.

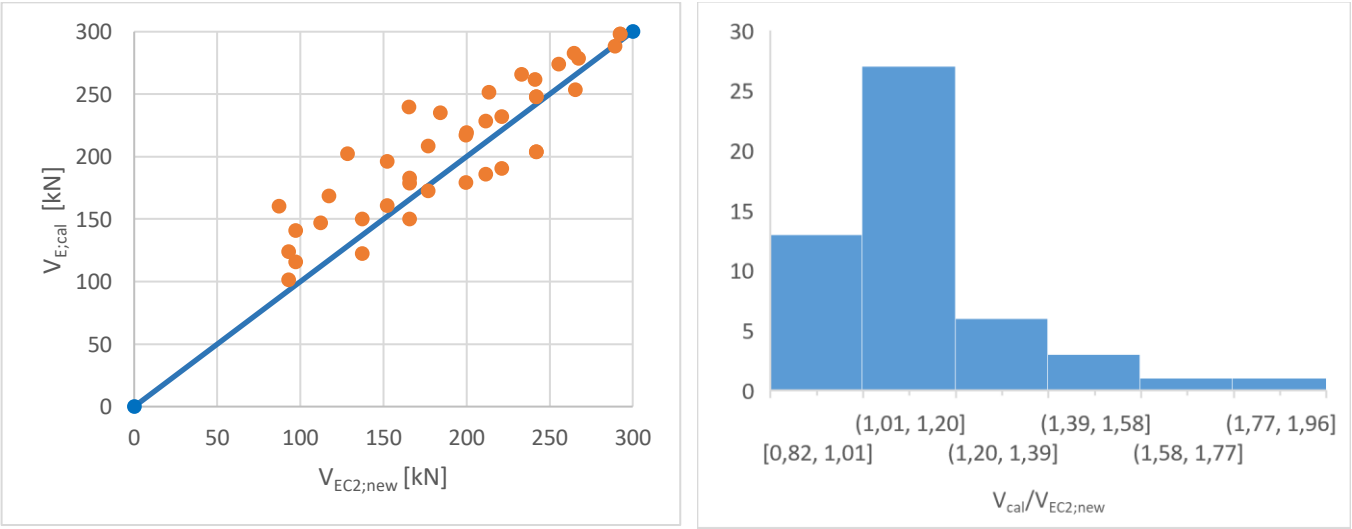

Figure 37: Distribution of $V_{cal}/V_{EC2;new}$ using formula (5.5)

However, in 23% of the cases this model leads to an overestimation of the shear capacity. This is a significant portion. Therefore, a lower limit value is sought. Figure 36 shows that a scale factor of 1,75 is a reasonable value as a lower limit. So, this means $b_{weff} = 1{,}75b_w$, resulting an average of 1,56 and CoV of 16%, see figure below for the distribution. The limitations for this model are:

- Only applicable for members within the ranges $0{,}20 \leq b_w/b_f \leq 0{,}60$ and $0{,}15 \leq h_f/h \leq 0{,}40$. Outside these ranges, the formula may lead to incorrect results.
- Only applicable for member with $0{,}4\% \leq \rho_s \leq 2\%$. In case the reinforcement ratio is lower than 0,4% flexural failure will be decisive. In case the reinforcement ratio is higher than 2% the height of the compression zone may change, leading to incorrect results.
- Only valid for slender members where $a/d \geq 3$.

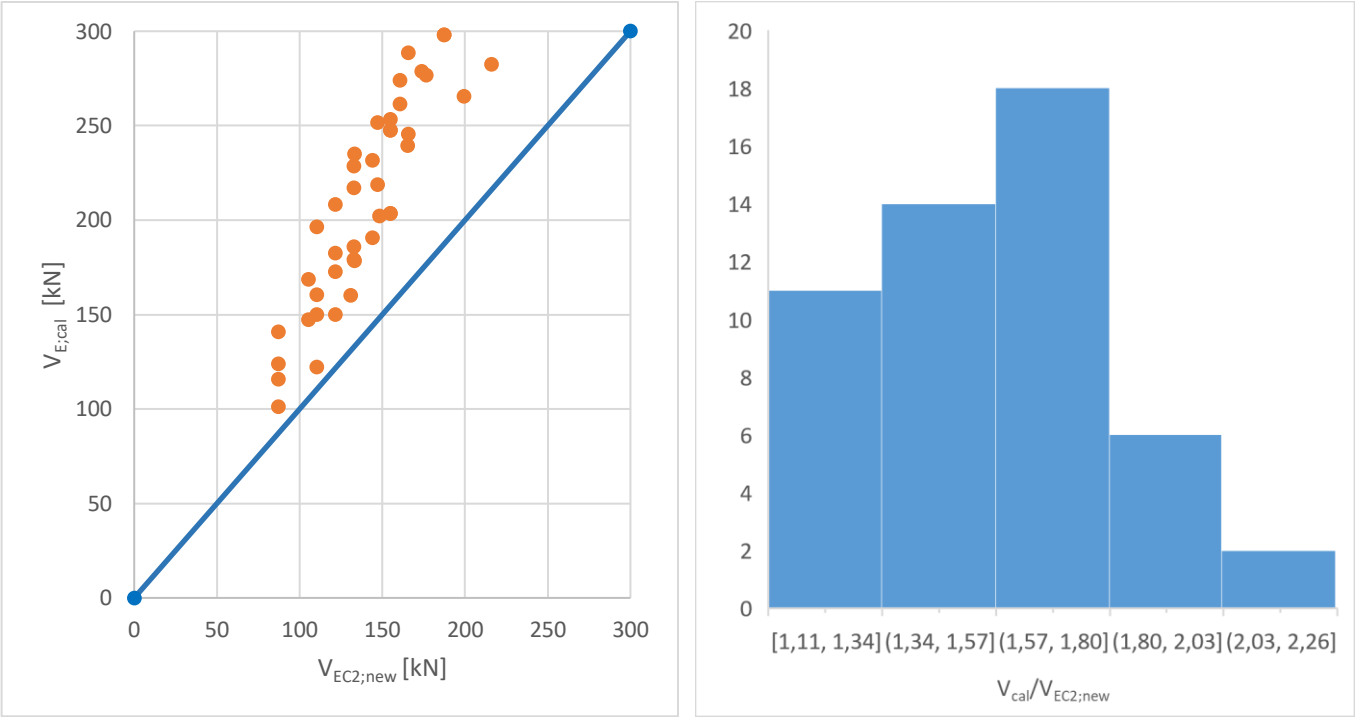

Figure 38: Distribution of $V_{cal}/V_{EC2;new}$ using $b_{weff} = 1{,}75b_w$

For plates with holes with reinforcement ratio higher than 1%, but lower than 2% the following formula for the scale factor is determined using a regression analysis:

$$sf = 1{,}75 + 3\frac{h_f}{h} - 4{,}60\frac{b_w}{b_f} \qquad (5.6)$$

Limitations:

- Formula (5.6) is only applicable for members within the ranges $0{,}20 \leq b_w/b_f \leq 0{,}60$ and $0{,}15 \leq h_f/h \leq 0{,}40$. Outside these ranges, the formula may lead to incorrect results.
- Formula (5.6) is only applicable for member with reinforcement ratio between 1% and 2%. Reinforcement ratio higher than 2% may change the height of the compression zone, leading to incorrect results.
- Formula (5.6) is only valid for slender members where $a/d \geq 3$.

The results of this model are shown in Figure 39. The average of V_{cal} / $V_{EC2;new}$ for this model is 1,43 with a CoV of 7%. It also does not lead to an overestimation of the capacity and gives reasonably good results. It is also possible to use the model with $b_{weff} = 1{,}75b_w$ for plates with holes $1\% \leq \rho_s \leq 2\%$, but is compared to the regression model less accurate.

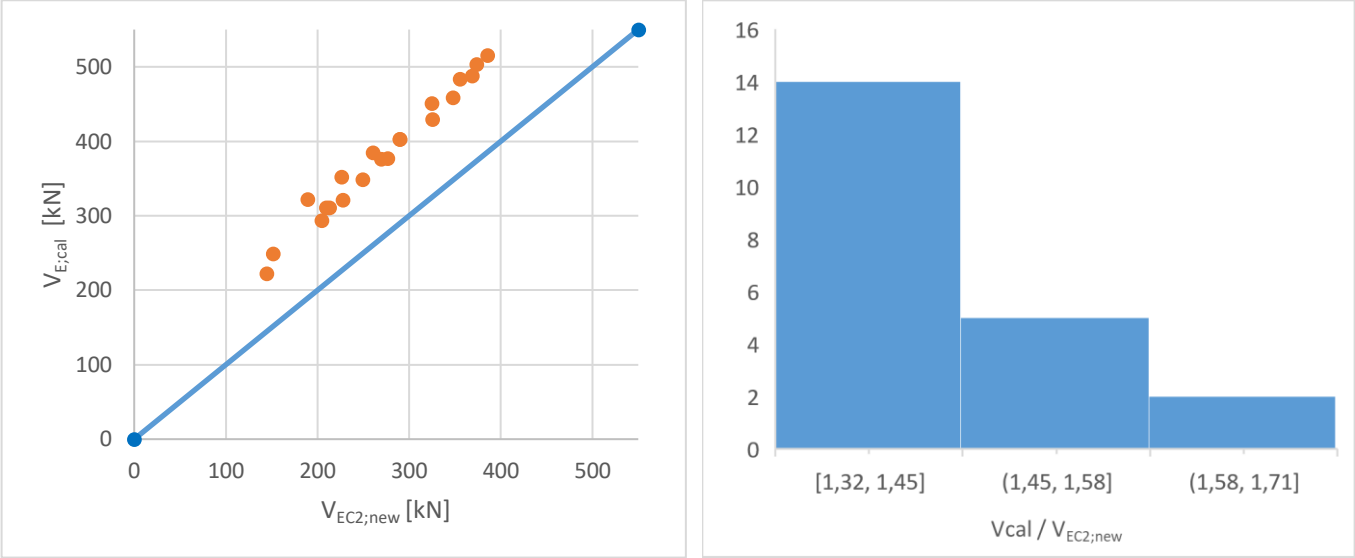

Figure 39: Distribution of Vcal/$V_{EC2;new}$ using formula (5.6)

I-beams:

The same approach is also used for the I-beams and T-beams. For I-beams with reinforcement ratio lower than 1%, the following formula is determined using a regression analysis:

$$sf = 0{,}5 + 6{,}4\frac{h_f}{h} - 1{,}4\frac{b_w}{b_f} \qquad (5.7)$$

Limitations:

- Formula (5.7) is only applicable for members within the ranges $0{,}10 \leq b_w/b_f \leq 0{,}50$ and $0{,}15 \leq h_f/h \leq 0{,}40$. Outside these ranges, the formula may lead to incorrect results.
- Formula (5.7) is only applicable for member with reinforcement ratio lower than 1%, but not lower than 0,4%, because in these cases flexural failure will be decisive.
- Formula (5.7) is based on the shear capacity with shear lag effect: $b_{f;eff} = 3b_w$. In formula (5.7) the full flange width b_f should be used.
- Formula (5.7) is only valid for slender I-beams where $a/d \geq 3$

For I-beams with $1\% \leq \rho_s \leq 2\%$ the following formula for the scale factor is determined using a regression analysis:

$$sf = 1{,}4 + 2{,}2\frac{h_f}{h} - 1{,}3\frac{b_w}{b_f} \qquad (5.8)$$

Limitations:

- Formula (5.8) is only applicable for members within the ranges $0{,}10 \leq b_w/b_f \leq 0{,}50$ and $0{,}15 \leq h_f/h \leq 0{,}40$. Outside these ranges, the formula may lead to incorrect results.
- Formula (5.8) is only applicable for member $1\% \leq \rho_s \leq 2\%$.Formula (5.8) is based on the shear capacity with shear lag effect: $b_{f;eff} = 3b_w$. In formula (5.8) the full flange width b_f should be used.
- Formula (5.8) is only valid for slender I-beams where $a/d \geq 3$

The results of both models are shown below. Formula (5.7) resulted in an average of 1,01 ($s_{f;cal}$ /$s_{f;regression}$) and CoV of 16%. The model for I-beams with $\rho_s < 1\%$ has an average of 1,22 for V_{cal} / $V_{EC2;new}$ and CoV of 19%. However, this model leads to overestimation of the shear capacity in 14% of the cases. The standard Eurocode 2 approach has in this case an average of 1,92 with a CoV of 28%.

Formula (5.8) has an average of 1,00 ($s_{f;cal}$ / $s_{f;regression}$) and CoV of 13%. Using this formula in the Eurocode 2 for I-beams with $1\% \leq \rho_s \leq 2\%$, the mean becomes 1,39 with a CoV of 14%. The model does not overestimate the shear capacity. The standard Eurocode 2 approach has in this case an average of 2,15 with a CoV of 15%.

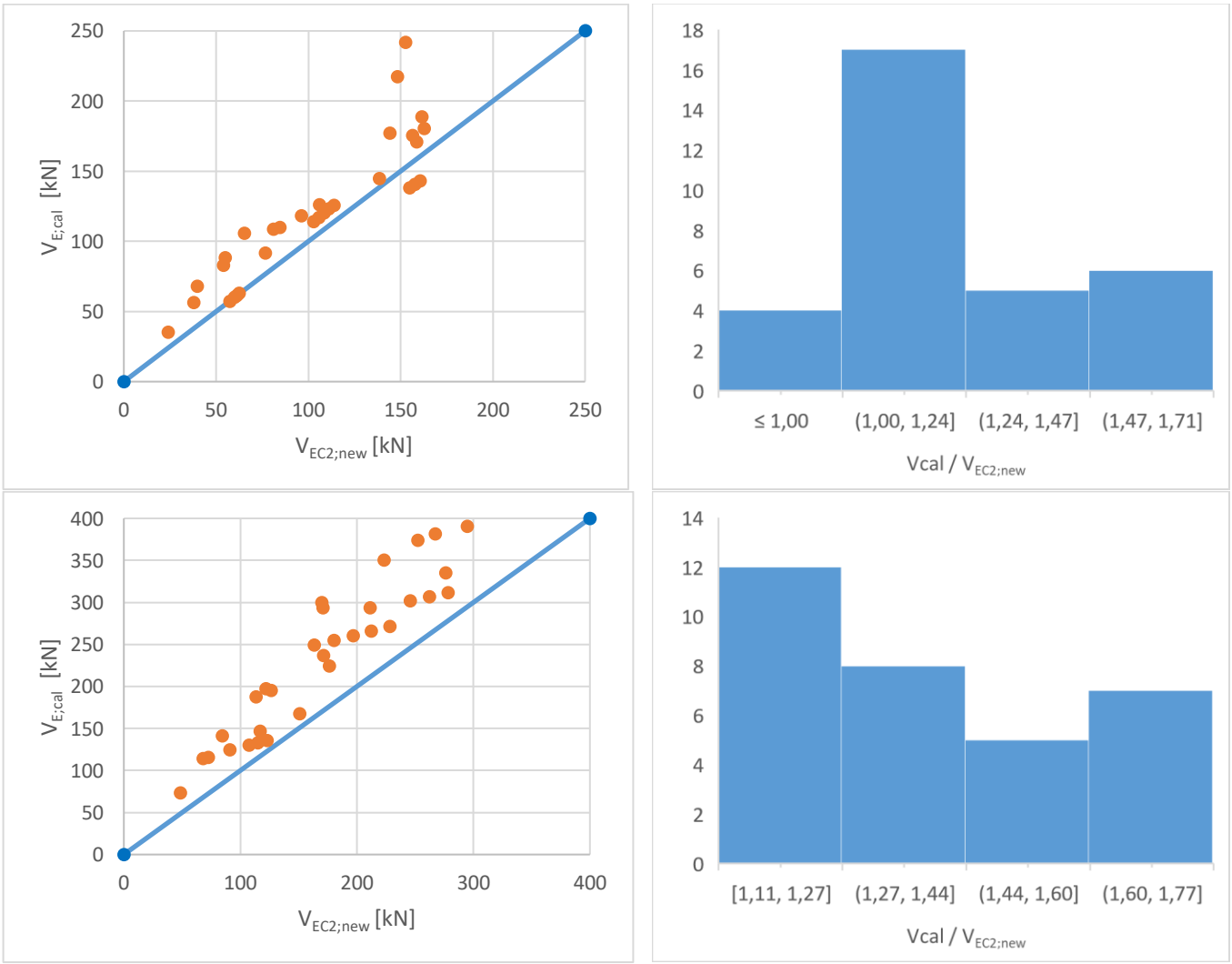

Figure 40: Results of I-beams. Top: results EC2 with formula (5.7); bottom results EC2 with formula (5.8)

In addition, a simplified method for b_{weff} for I-beams has also been developed. This is done because the model for I-beams with $\rho_s < 1\%$ overestimates the shear capacity and also that the capacity can be determined in a practical way in the engineering practice. It is basically a lower bound approach. Based on this applies:

For I-beam with $\rho < 1\%$: $b_{weff} = 1{,}25 b_w \ \ if \ \frac{h_f}{h} \leq 0{,}25$ (5.8a)

Otherwise: $b_{weff} = 4{,}2\frac{h_f}{h} + 0{,}2$ (5.8b)

For I-beam with $1\% \leq \rho \leq 2\%$: $b_{weff} = 1{,}35 b_w \ \ if \ \frac{h_f}{h} \leq 0{,}25$ (5.9a)

Otherwise: $b_{weff} = 3{,}5\frac{h_f}{h} + 0{,}5$ (5.9b)

The same limitations as for formulas (5.7) and (5.8) apply.
The results of these simplified models are shown below. Using formulas (5.8a) and (5.8b) in Eurocode 2 the average gets 1,42 with a CoV of 20%. Model for I-beams with $1\% \leq \rho_s \leq 2\%$ has an average of 1,49 and CoV of 9%.

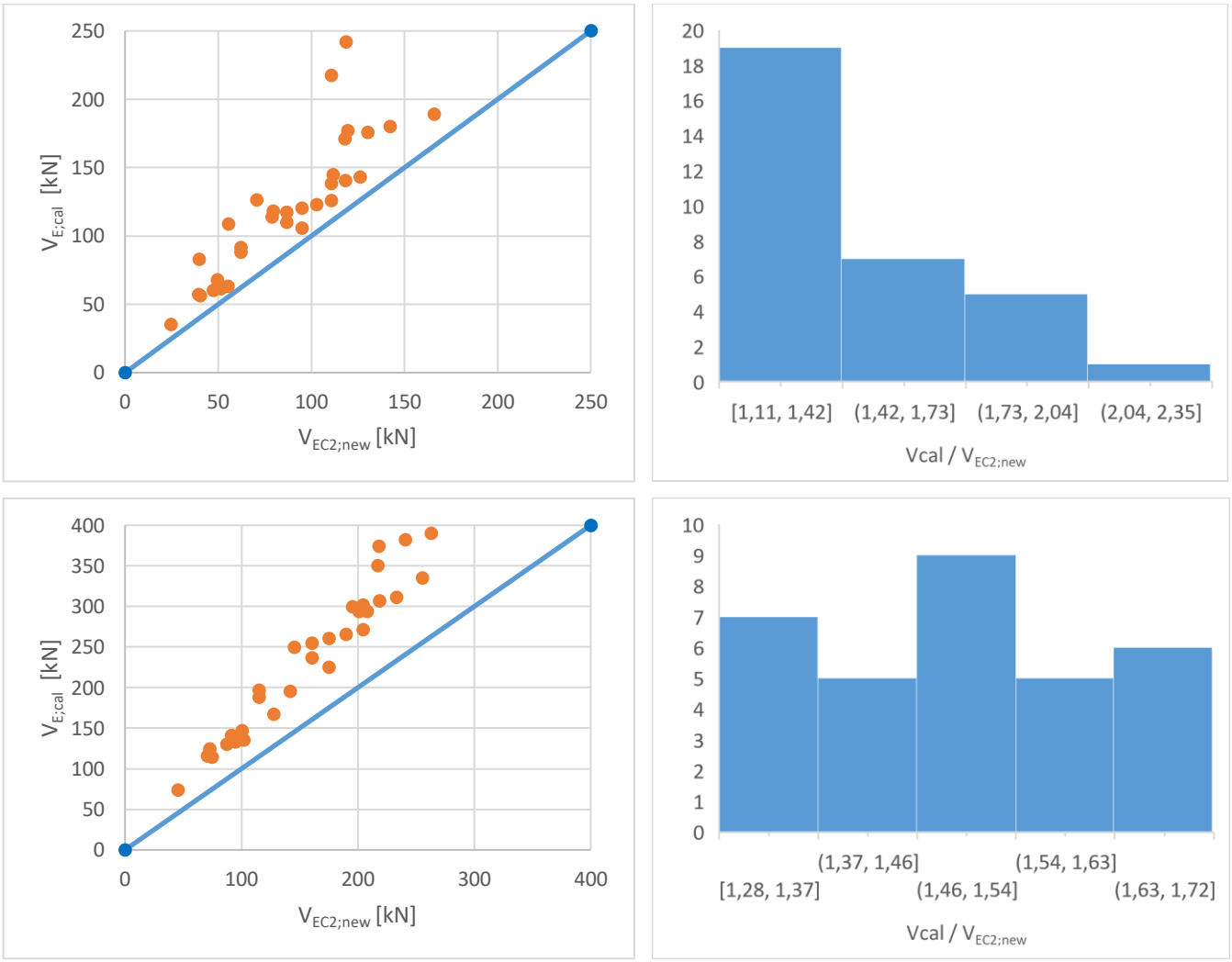

Figure 41: Simplified method for I-beams. Top: for $\rho < 1\%$, Bottom: for $1\% \leq \rho \leq 2\%$

It should be noted that for I-beams with $1\% \leq \rho_s \leq 2\%$ the approach with formula (5.8) leads to more accurate results compared to the simplified method.

T-beams:

According to the regression analysis, the relationship between scale factor and parameters b_w/b and h_f/h for T-beams could be described with:

For $\rho < 1\%$: $sf_T = 0{,}5 + 5{,}6\frac{h_f}{h} - 1{,}2\frac{b_w}{b}$ (5.10)

For $1\% \leq \rho \leq 2\%$: $sf_T = 1{,}3 + 1{,}5\frac{h_f}{h} - \frac{b_w}{b}$ (5.11)

Limitations:

- Formulas (5.10) and (5.11) are only applicable for members within the ranges $0{,}10 \leq b_w/b_f \leq 0{,}50$ and $0{,}15 \leq h_f/h \leq 0{,}40$. Outside these ranges, the formula may lead to incorrect results.
- Formula (5.10) is only applicable for member with reinforcement ratio lower than 1%, but not lower than 0,4%, because in these cases flexural failure will be decisive.
- Formula (5.11) is only applicable for member $1\% \leq \rho_s \leq 2\%$.Formula (5.11) is based on the shear capacity with shear lag effect: $b_{f;eff} = 3b_w$. In formula (5.11) the full flange width b_f should be used.
- Formulas (5.10) and (5.11) are only valid for slender T-beams where $a/d \geq 3$

The results of both models are shown below. The model with formula (5.10) has an average of 1,21 for V_{cal} / $V_{EC2;new}$ and CoV of 19%. However, this model leads to overestimation of the shear capacity in 22% of the cases. The standard Eurocode 2 approach has in this case an average of 1,75 with a CoV of 27%.

For T-beams with $1\% \leq \rho_s \leq 2\%$, by using formula (5.11) the average becomes 1,43 with a CoV of 14%. Standard Eurocode approach results for these members to an average of 1,92 and a CoV of 18%. The model does not overestimate the shear capacity.

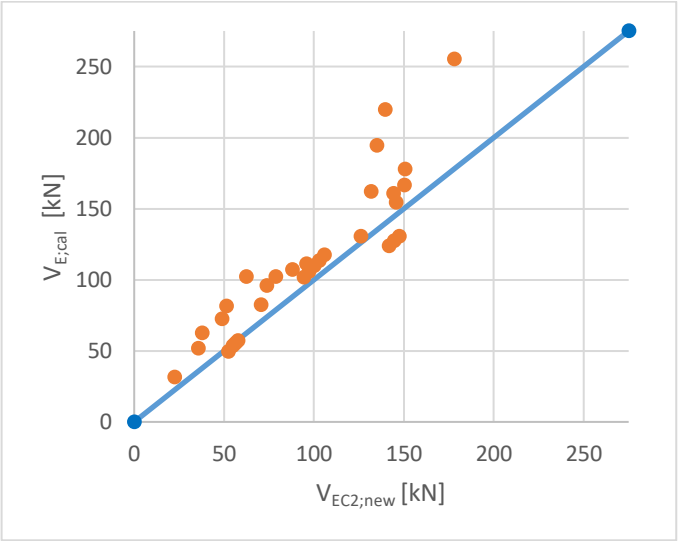

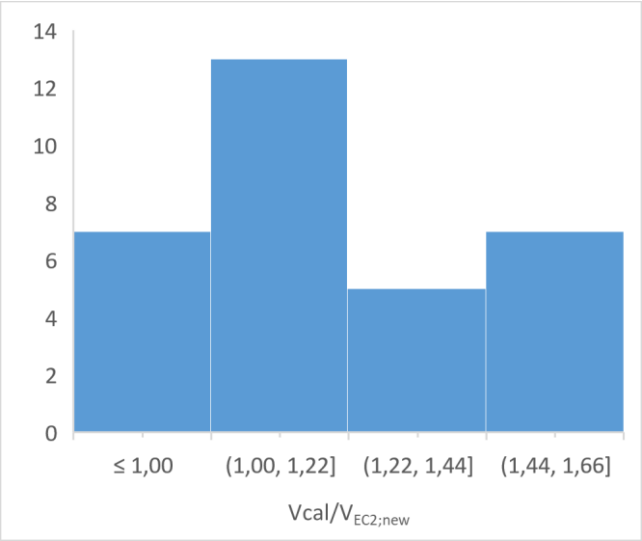

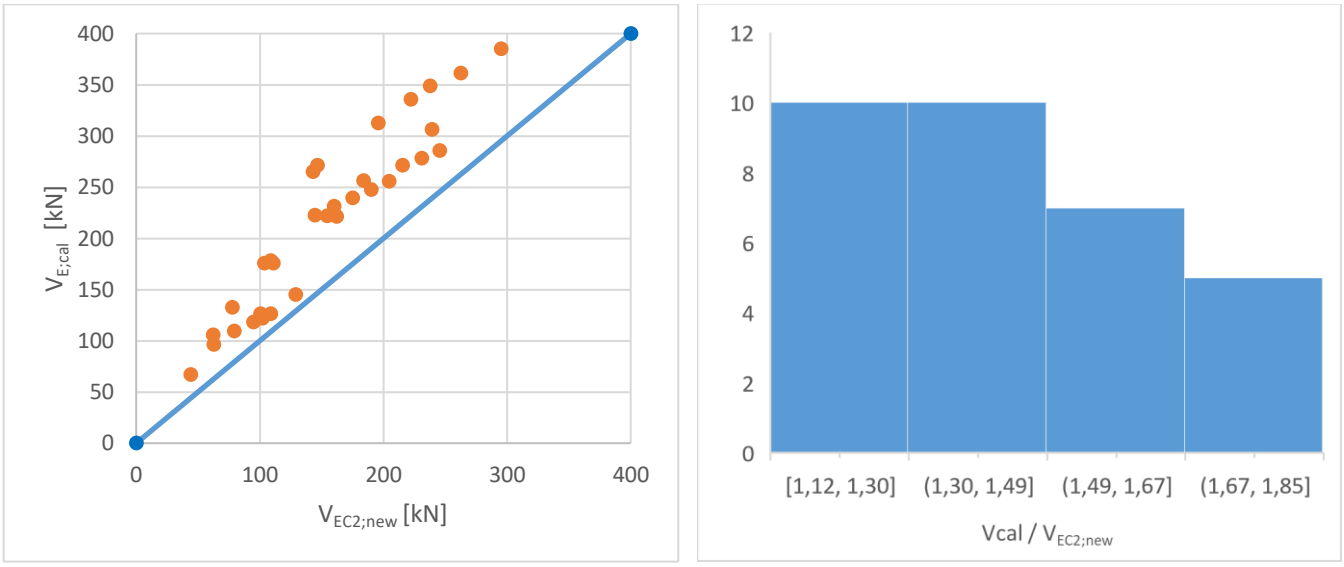

Figure 42: Results of T-beams. Top: results EC2 with formula (5.10); bottom results EC2 with formula (5.11)

Because of the overestimation of the regression model for T-beams with $\rho_s < 1\%$ and to provide the engineering practice with a practical method, a simplified model for T-beams is developed.

For T-beams with $0{,}4\% \leq \rho_s \leq 2\%$ the effective width can be calculated by:

$$b_{weff} = 1{,}15 b_w \;\; if \;\; \frac{h_f}{h} \leq 0{,}25 \qquad (5.12a)$$

Otherwise: $$b_{weff} = 3{,}85 \frac{h_f}{h} + 0{,}19 \qquad (5.12b)$$

The results of the simplified model for T-beams are shown below. The model has an average of 1,41 for V_{cal} / $V_{EC2;new}$ and CoV of 19% for members with $\rho_s < 1\%$. In case of $1\% \leq \rho_s \leq 2\%$ the model leads to an average of 1,58 with a CoV of 9%.

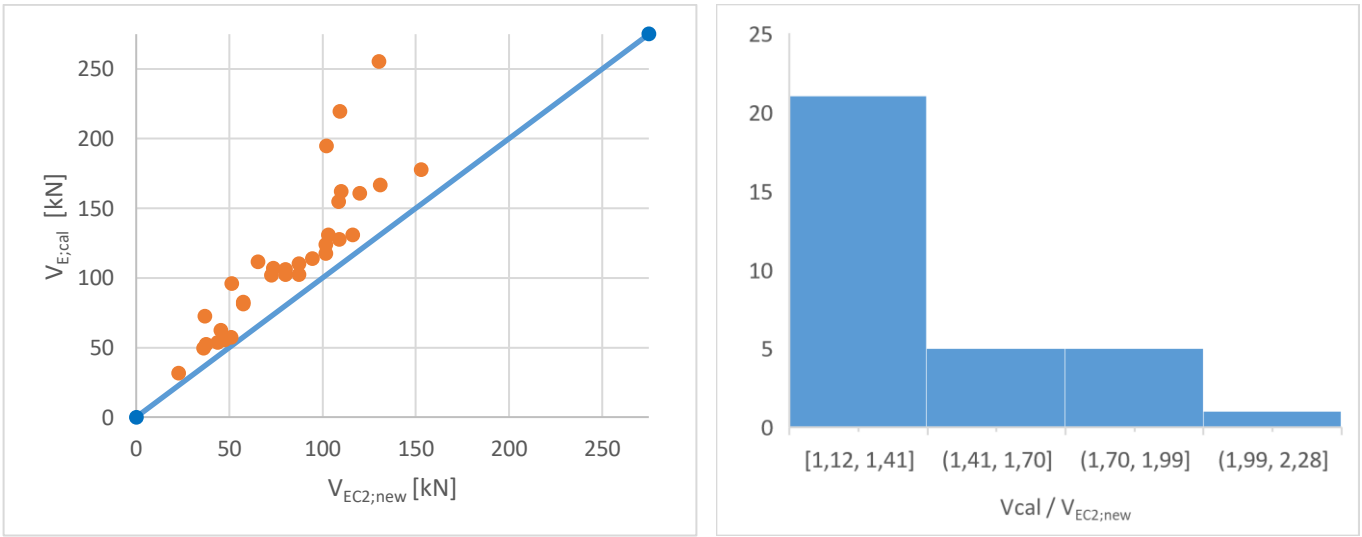

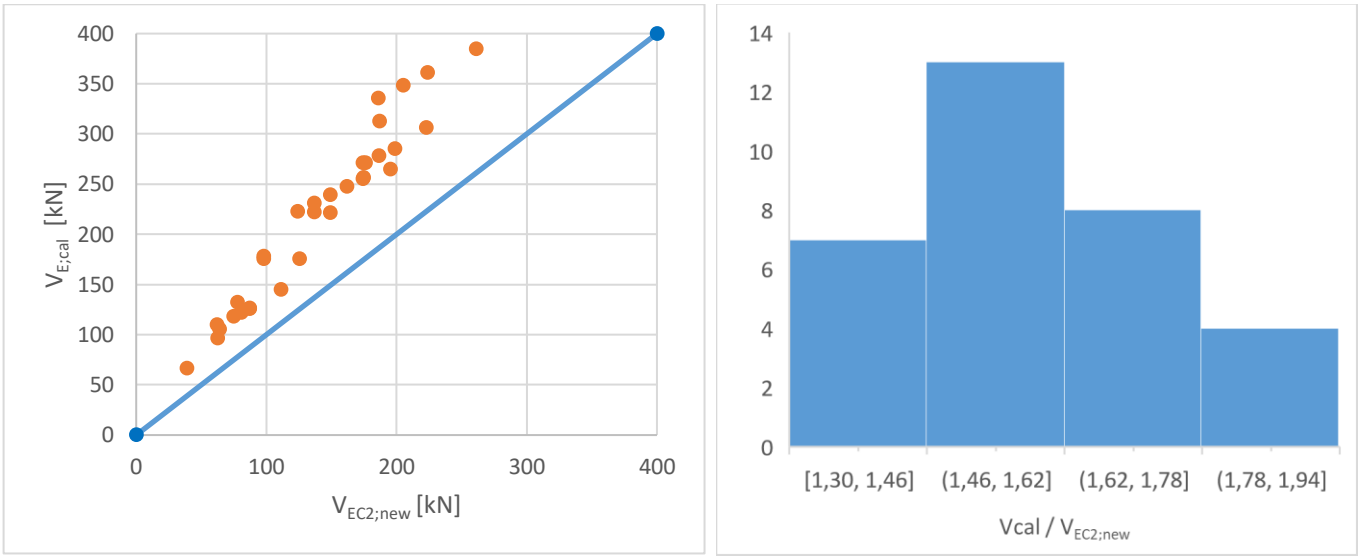

Figure 43: Results of T-beam with simplified method. Top: for ρ < 1%, Bottom: for 1% ≤ ρ ≤ 2%

It should be noted that for T-beams with $1\% \leq \rho_s \leq 2\%$ the approach with formula (5.11) leads to more accurate results compared to the simplified method.

5.3 Comparison with tests from literature

A literature review has been carried out on test results for reinforced plates with holes and I-beams. However, this has yielded little, because I-beams are generally used prestressed. No experimental research has been found for the plate with holes. One relevant study by Regan (2000) was found, in which five reinforced I-beams were tested. Three of these correspond to the typical cross-section adopted for plates with holes and the remaining are normal I-beams, see Figure 44. The results of this study will be compared with the test results. The geometry of the 5 members is shown in Table 6.

Remark: member 14.5 is a T-beam

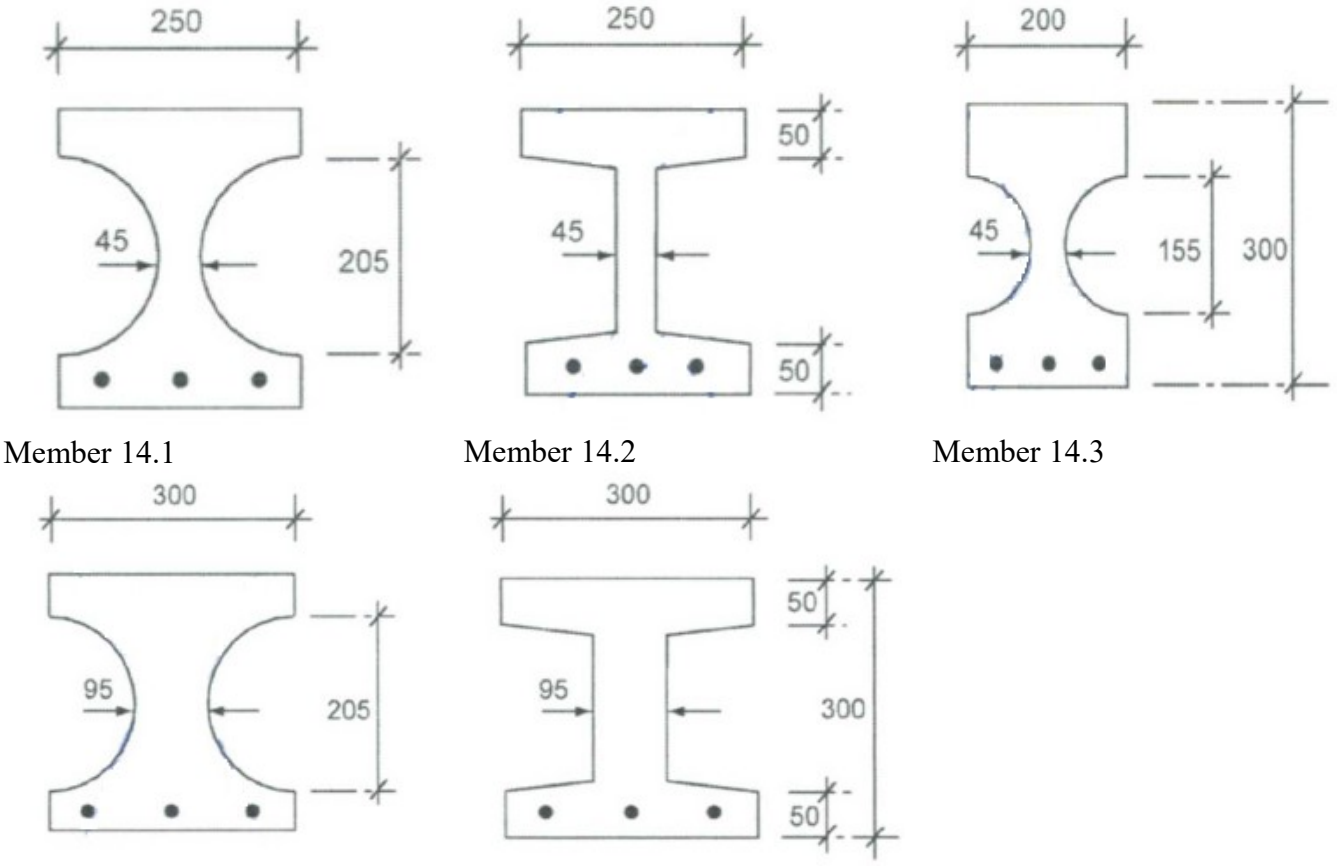

Member 14.1 Member 14.2 Member 14.3

Member 14.4 Member 14.6

Figure 44: Cross-section of the I-beams from experiment of Regan (2000)

Table 6: Cross-sectional parameters from experiment of Regan (2000), where PWH = plate with holes

Beam	Type	mvd [-]	f_c [MPa]	b_w [mm]	b_f [mm]	h_f [mm]	h [mm]	r [mm]	d [mm]	ρ_s [-]	d_r [-]	n [-]
14.1	PWH	4,9	21,1	45	250	47,5	300	102,5	276	0,0486	16	3
14.2	Ibeam	4,9	19,2	45	250	50	300	-	276	0,0486	16	3
14.3	PWH	4,9	24,1	45	200	72,5	300	77,5	276	0,0486	16	3
14.4	PWH	5,2	25,2	95	300	47,5	300	102,5	276	0,023	16	3
14.6	Ibeam	4,9	19,6	95	300	50	300	-	276	0,023	16	3

The reinforcement ratio of the beams from Table 6 is much higher than that of plates with holes. This has consequences for the height of the compression zone z_c. As explained in section 4.1.3, a z_c of $0{,}3d$ is assumed for the beams from Table 6.

The comparison of the results is shown in Table 7. This shows that the evaluation procedure of this study predicts reasonable results, the calculated capacity is quite close to the test results. Only beam 14.3 is overestimated. However, the test result of beam 14.3 is questionable, because it is much smaller than beam 14.1, while concrete strength is higher and the effective concrete area is even larger. This is against expectations. A possible reason for this may be another failure mechanism, which is not taken into account in this study. Regan has observed in his research that all beams failed in shear, but there was no visible flexural cracks or only very minor ones in the regions where the shear cracks formed. The starting point of this study, on the other hand, is that the critical shear crack originates from a flexural crack, which does not correspond with Regan's observations in the tests. This could explain the overestimation of the model, because the beam failed before a crack could develop.
Also the simplified method for b_{weff} leads reasonable results, except for member 14.3.

Table 7: Experimental results of Regan (2000) and calculated results

Beam	Type	sf [-]	V_u [kN]	V_{cal} [kN]	$V_{EC2;new}$ [kN]	V_{cal}/V_u [-]	$V_{EC2;new}/V_u$ [-]
14.1	PWH	1,75	26,2	24,0	22,6	0,91	0,86
14.2	Ibeam	1,35	21,2	20,2	16,9	0,95	0,80
14.3	PWH	1,75	19,3	26,5	23,6	1,37	1,22
14.4	PWH	1,75	42,5	33,5	39,4	0,79	0,93
14.5	Tbeam	1,15	30,1	27,3	24,0	0,91	0,80
14.6	Ibeam	1,35	37,5	30,4	28,0	0,81	0,75

In addition, the test results for reinforced T-beams from literature were collected and compared with the results according to the evaluation procedure. The following test results are used: 5 from Regan[45], 3 from Thamrin[35], 4 from Palaskas[49] and 16 from al-Alusi[50]. A total of 28 test results were therefore used for comparison of T-beams. The cross-sectional parameters and test results are included in annex III. The calculated shear capacity and the results of the tests are in good agreement.

The comparison of all collected data with the calculated ones is shown on the next page. Top results from Figure 45 are the comparison of the calculated results with test results. This shows that the evaluation procedure for non-rectangular cross-sections gives reasonably accurate results. The mean of V_{cal}/V_u is 0,94 and CoV is 16%.
The bottom part of Figure 45 is the comparison of EC2 using the simplified b_{weff} with test results. This model also predicts reasonably accurate results in comparison to the test results, where the mean is 0,79 and CoV is 21%. Less consistent compared to the own model, but still acceptable.

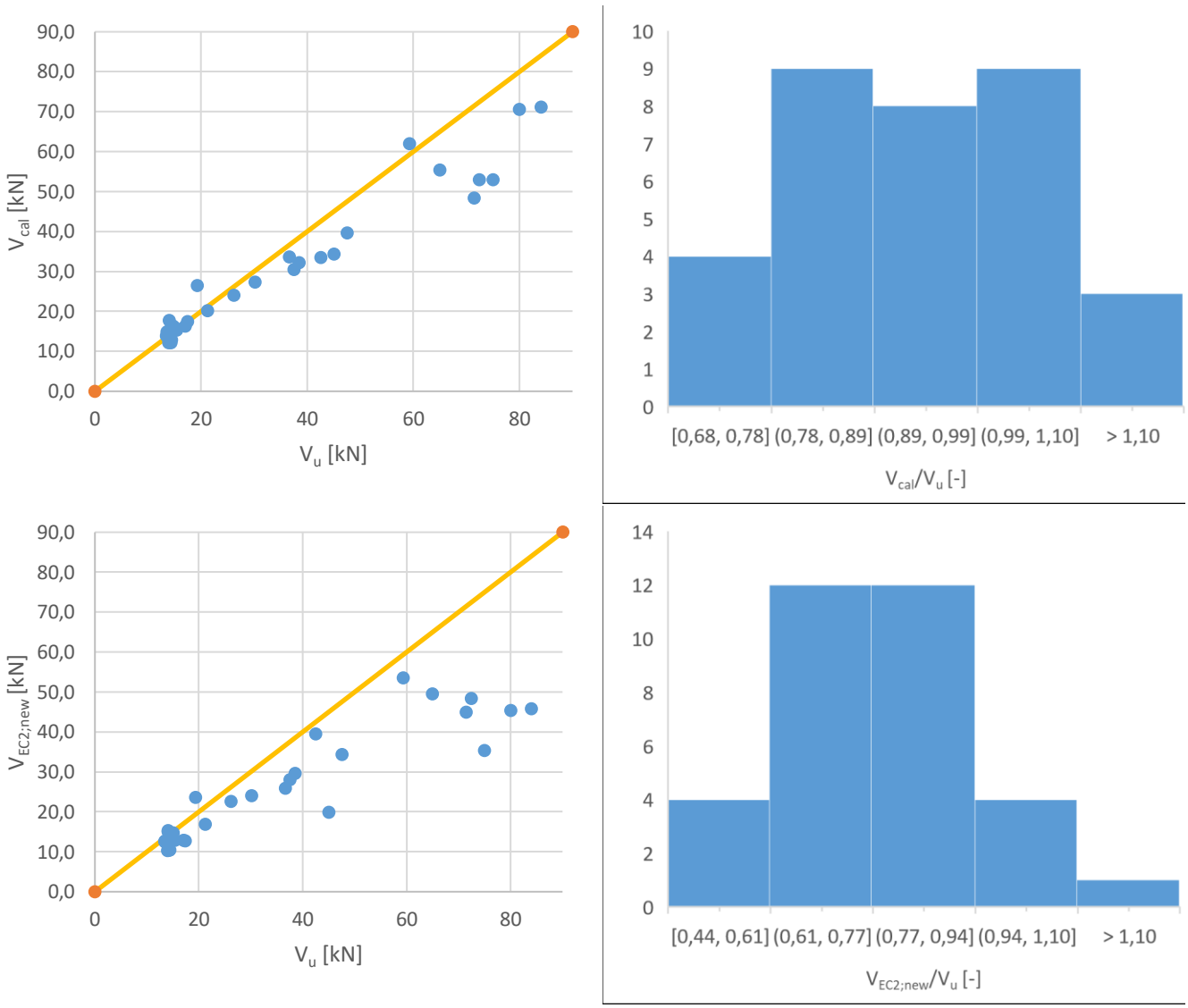

Figure 45: Comparison of the calculated results with test results: top comparison calculated results with test results; bottom comparison EC2 results with b_{weff} with test results

6. Conclusions and recommendations

6.1 Conclusions

The literature search has shown that there is a lack to knowledge regarding the shear capacity of non-rectangular cross-sections of reinforced concrete without shear reinforcement. Therefore, the primary focus of this study was to address this knowledge gap by using Yang's model as a starting point. The aim was to develop an evaluation procedure for non-rectangular cross-sections, by which the effective width for non-rectangular cross-sections could be determined and possibly included in Eurocode 2.
The evaluation procedure for rectangular cross-sections developed by Yang (2014) was adapted for plates with holes, I-beams and T-beams, which is used for the analysis.

The study results emphasized the importance of the location of the neutral axis in determining the shear resistance and has provided insights into the compression zone for plates with holes, I-beams and T-beams. It was observed that for a reinforcement ratio of 0,4%, the compression zone is $0{,}2d$ when the neutral axis is in the flange and $0{,}25d$ otherwise, ensuring internal force balance. Similarly, for I-beams and T-beams the height of the compression zone is also $0{,}2d$ if the neutral axis is inside the flange and $0{,}3d$ when it is outside the flange.
With thick flanges the neutral axis is in most cases inside the flange, while with thin flanges in the web. It was observed that thinner flanges resulted in lower shear capacity (approximately 40% less compared to thicker flange) due to reduced aggregate interlock caused by a decrease in effective depth, crack height and the smaller width over the crack height. The width of the flange played a crucial role when the neutral axis was inside the flange, resulting in higher shear capacity. This is because, in this case, the top part of the major crack is in the flange, where the shear stresses due to aggregate interlock are the highest. The contribution of aggregate interlock is equal to shear stress multiplied by the member width along the crack height, resulting in a higher contribution when the neutral axis is in the flange. In addition, it has been found that the web width also has an important influence on the shear capacity. A smaller web width leads to a smaller capacity (approximately 22% reduction compared to thicker web), because the contribution of aggregate interlock decreases.

Furthermore, the study investigated the added value of the bottom and top flanges by comparing the results of I-beams and T-beams. It was found that there is a slight difference (7%-13%) in the total shear capacity between I-beams and T-beams, with greatest differences for members with thick flanges. This is because the contribution of a thick lower flange is eliminated in case of T-beams.
On the shear transfer action level, dowel action decreases due to the reduced net width of the web in T-beams. Additionally, small differences were observed in aggregate interlock. Nevertheless, the impact of the bottom flange on the shear capacity of non-rectangular cross-sections was found to be minimal. Conversely, the top flange plays a crucial role, as the contribution of the compression zone completely depends on it. When the neutral axis is in the top flange, the aggregate interlock is strongly influenced by the width and thickness of the top compression flange.

A comparison was made between the results of the modified evaluation procedure for non-rectangular cross-sections and the shear capacity of the web only (rectangular cross-section) calculated using Yang's model. Dividing these two results provided a scale factor on the web width, which can be used in the Eurocode 2 to determine the shear capacity of non-rectangular cross-sections without shear reinforcement. This is necessary because Eurocode 2 only takes into account the smallest width of the cross-section, which leads to conservative results. The smallest differences of the shear capacity between the web-only and flange-

included scenarios were observed for members with thin flanges, while significant difference were found for thick flanges (where the neutral axis was in the flange).
The comparison between web-only scenario and web including flanges showed that the contribution of aggregate interlock to the shear capacity of non-rectangular cross-sections significantly increases when the neutral axis is in the flange. On the other hand, if the neutral axis is in the web, the contribution of aggregate interlock always increases for plates with holes due to the increasing width along the height and for I-beams slightly due to the involvement of the bottom flange. The contribution of the compression zone always increases in all cases because the area of the compression zone expands compared to the web-only scenario. However, most of the contribution comes from aggregate interlock varying between 45% to 85%.
This comparison has shown that for plates with holes the effective web width could be determined by $b_{weff} = 1{,}75b_w$. For I-beams with $\rho_s < 1\%$, the effective web width is equal to $1{,}25b_w$ if $h_f/h \leq 0{,}25$ otherwise $4{,}2h_f/h + 0{,}2$. In case of a reinforcement ratio of $1\% \leq \rho_s \leq 2\%$ the effective web width of I-beams becomes $1{,}35b_w$ if $h_f/h \leq 0{,}25$, otherwise $3{,}5h_f/h + 0{,}5$. For T-beams the effective web width could be determined by $1{,}15b_w$. The general limitations of these models are:

- Only applicable for members within the ranges $0{,}20 \leq b_w/b_f \leq 0{,}60$ for plates with holes; $0{,}10 \leq b_w/b_f \leq 0{,}50$ for I/T-beams and $0{,}15 \leq h_f/h \leq 0{,}40$ for all members;
- Only applicable for member with reinforcement ratio between 0,4% and 2%;
- Only valid for slender members where $a/d \geq 3$.

The study also conducted a literature review of test results for reinforced plates with holes, I-beams and T-beams. Limited information was available regarding plates with holes and experimental research on I-beams primarily focussed on prestressed applications. However, one relevant study by Regan (2000) was found to compare the results of the evaluation procedure with test results. In addition, the test results for reinforced T-beams from literature were collected and compared with the results according to the evaluation procedure. In short, an extensive comparison of all collected data width the calculated values showed that the evaluation procedure for non-rectangular cross-sections gave reasonably accurate results. The average ratio of calculated shear capacity (V_{cal}) to measured ultimate shear capacity during tests (V_u) was 0,94, with a Coefficient of Variation of 16%. In comparison, using the simplified effective web width b_{weff} approach with EC2, the results also showed reasonable accuracy, with an average ratio of 0,79 and a CoV of 21%. Although slightly less consistent compared to the developed model, these results are still considered acceptable.

6.2 Recommendations

1. Conduct additional tests on reinforced I-beams and plates with holes: These tests can help verify the accuracy of the model for these type of cross-sections better and provide valuable insights into the behaviour and shear capacity of such members. Also because Regan's research probably revealed another failure mechanism.
2. Investigate dowel action: The study by Autrup et al. (2020) highlighted the inaccuracies in the dowel cracking load prediction using the method applied in this research (method of Baumann and Rüsch). Therefore, it is recommended to investigate the phenomenon of dowel action and explore alternative methods or approaches that can accurately predict the dowel force in reinforced members without shear reinforcement. Also, it is not known where in the cross-section the dowel crack will occur in a plate with holes. This research will contribute to a better understanding of the structural behaviour and shear capacity.
3. Explore shear capacity of prestressed non-rectangular cross-sections: The research conducted so far has primarily focused on reinforced non-rectangular members. To broaden the knowledge base, it is

proposed to investigate the shear capacity of prestressed non-rectangular cross-sections. This research can provide insight into the behaviour of such members under shear loading and help develop design guidelines specific to prestressed non-rectangular members.

4. Extend the model for other types of loads: In this study, the model developed focussed on analysing the shear capacity of non-rectangular members without shear reinforcement under point loading. It is recommended to extend the model to other types of loads, such as distributed loads. By considering different loading scenarios, the model's applicability can be expanded, providing a tool for the engineering practice to evaluate the shear capacity of non-rectangular members in various structures.
5. Explore the influence of rebar configuration on the shear capacity. There are few insights into the mechanism how rebar configuration influences shear capacity. With this research, the behaviour can be better understood.

Pursuing these research recommendations will enable further progress in understanding and predicting the shear capacity of reinforced non-rectangular elements, contribution to the development of more precise design guidelines and improving the structural performance of such elements. With the current knowledge it is possible to make a lower bound approximation of the shear capacity of reinforced non-rectangular cross-sections without shear reinforcement, but with the help of the studies listed above it may be possible to improve and refine this lower bound.

References

[1] Kani G.N.J. (1964), The riddle of shear failure and its solution, ACI Journal 61(4), pp442-467
[2] Kani G.N.J. (1966), Basic facts concerning shear failure, ACI Journal 63(6), pp675-690
[3] Kani G.N.J. (1967), How safe are our large reinforced concrete beams, ACI Journal 64(3), pp128-141
[4] Muttoni A., Fernandez Ruiz M. (2008), Shear strength of members without transverse reinforcement as function of critical shear crack width, ACI Journal 105(2), pp163-172
[5] Fenwick R.C., Paulay T. (1968), Mechanism of shear resistance of concrete beams, Journal of the Structural Division ASCE 94(10), pp2325-2350
[6] Campana S., Anastasi A., Fernandez Ruiz M., Muttoni A. (2013), Analysis of shear-transfer actions on one-way RC members based on measured cracking pattern and failure kinematics, Magazine of Concrete Research 65(6), pp386-404
[7] Yang Y. (2014), Shear behaviour of reinforced concrete members without shear reinforcement: A new look at an old problem, PhD Thesis TU Delft
[8] Cavagnis F. (2017), Shear in reinforced concrete without transverse reinforcement: from refined experimental measurements to mechanical models, PhD Thesis École Polytechnique Federale de Lausanne
[9] Fernandez Ruiz M., Muttoni A., Sagaseta J. (2015), Shear strength of concrete members without transverse reinforcement: A mechanical approach to consistently account for size and strain effects, Engineering Structures 99, pp360-372
[10] Cavagnis F., Fernandez Ruiz M., Muttoni A. (2018), A mechanical model for failures in shear of members without transverse reinforcement based on development of a critical shear crack, Engineering Structures 157, pp300-315
[11] Walraven J. (1980), Aggregate Interlock: A theoretical and experimental analysis, PhD Thesis TU Delft
[12] Walraven J. (1981), Fundemental analysis of aggregate interlock, Journal of Structural Engineering 107, pp2245-2270
[13] Huber T., Huber P. Kolleger J. (2019), Influence of aggregate interlock on the shear resistance of reinforced concrete beams without stirrups, Engineering Structures 186, pp26-42
[14] Taylor H.P.J. (1970), Investigation of the forces carried across cracks in reinforced concrete beams in shear by interlock of aggregate, Cement and Concrete Association Technical Report No. 42.77
[15] Hamadi Y.D., Regan P.E. (1980), Behavior in shear of beams with flexural cracks, Magazine of Concrete Research 32(111), pp67-78
[16] Ulaga T. (2003), Betonbauteile mit Stab- und Lamellenbewehrung: Verbund- und Zuggliedmodellierung, PhD Thesis Zurich
[17] Guidotti R. (2010), Poinçonnement des planchers-dalles avec colonnes superposées fortement sollicitées, PhD Thesis Ecole Polytechnique Federale de Lausanne
[18] Cavagnis F., Fernadez Ruiz M., Muttoni A. (2017), An analysis of the shear-transfer actions in reinforced concrete members without transverse reinforcement based on refined experimental measurements, Structural Concrete DOI:10.1002/suco.201700145
[19] Cavagnis F., Fernadez Ruiz M., Muttoni A. (2015), Shear failures in reinforced concrete members without transverse reinforcement: An analysis of the critical shear crack development on the basis of test results, Engineering Structures 103, pp157-173
[20] Krefeld W., Thurston C. (1966), Studies of the shear and diagonal tension strength of simply supported reinforced concrete beams, ACI Journal 63(4), pp449-476
[21] Jelíc I., Pavlovic M.N., Kotsovos M.D. (1999), A study of dowel action in reinforced concrete beams, Magazine of Concrete Research 51(2), pp131-141

[22] Fernandez Ruiz M., Plumey S., Muttoni A. (2010), Interaction between bond and deviation forces in spalling failures of arch-shaped members without transverse reinforcement, ACI Journal 107(3), pp346-354
[23] Baumann T., Rüsch H. (1970), Versuche zum Studium der Stahlbetonbalkens, Deutscher Ausschuss für Stahlbeton 210
[24] Hillerborg A., Modeer M., Petersson P.E. (1976), Analysis of crack formation and crack growth in concrete by means of fracture mechanics and finite elements, Cement and Concrete Research 6(6), pp773-782
[25] Cornelissen H.A.W., Hordijk D.A., Reinhardt H.W. (1986), Exprimental determination of crack softening characteristics of normalweight and lightweight concrete, TU Delft
[26] Hordijk D.A. (1991), Local approach to fatigue of concrete, PhD Thesis TU Delft
[27] Mörsch E. (1908), Concrete-Steel Construction (Der Eisenbetonbau), Translation from the Third German Edition, The Engineering News Publishing Company (1909)
[28] Sagaseta J., R.L. Vollum (2011), Influence of aggregate fracture on shear transfer through cracks in reinforced concrete, Magazine of Concrete Research 63(2), pp119-137
[29] Kani M.W., Huggins M.W., Wittkopp R.R. (1979) Kani on shear in reinforced concrete, University of Toronto
[30] Leonhardt F., Walther R. (1962), Schubversuche an einfeldrigen Stalhbetonbalken mit und ohne Schubbewehrung, DAfStb H.151
[31] Caldentey P., Padilla P., Muttoni A., Fernandez Ruiz M. (2012), Effect of load distribution and variable depth on shear resistance of slender beams without stirrups, ACI Journal 109(5), pp595-603
[32] Jacobsen J.S., Poulsen P.N., Olesen J.F. (2012), Characterization of mixed mode crack opening in concrete, Materials and Structures 45(1) DOI: 10.1617/s11527-011-9745-5
[33] Reineck K., Bentz E.C., Fitik B., Kuchma D.A., Bayrak O. (2013), ACI-DAfStb Database of shear tests on slender reinforced concrete beam without shear reinforcement, ACI Journal 110(5), pp867-876
[34] Ribas Gonzáles C.R, Fernandéz Ruiz M. (2017), Influence of flanges on the shear-carrying capacity of reinforced concrete beams without web reinforcement, Structural Concrete 18, pp720-732
[35] Thamrin R., Tanjung J., Aryanti R., Nur O.F., Devinus A. (2016), Shear strength of reinforced concrete T-beams without stirrups, Journal of Engineering Science and Technology 11(4), pp548-562
[36] Muttoni A., Schwartz J. (1991), Behavior of beams and punching in slabs without shear reinforcement, IABSE Colloquium 62, pp703-708
[37] Ribas C., Cladera A. (2013), Exprimental study on shear strength of beam-and-block floors, Engineering Structures 57(B), pp428-442
[38] Tureyen A.K., Frosch R.J. (2003), Concrete Shear Strength: Another perspective, ACI Journal 100(5), pp609-615
[39] Tureyen A.K., Wolf T.S., Frosch R.J. (2006), Shear strength of reinforced concrete T-beams without transverse reinforcement, ACI Journal 103(5), pp656-663
[40] Bui T.T., Nana W.S.A., Limam A., Tedoldi B., Roure T. (2017), Influence of uniaxial tension and compression on shear strength of concrete slabs without shear reinforcement under concentrated loads, Construction and Building Materials 146, pp86-101
[41] Fernadez Ruiz M., Campana S., Muttoni A. (2009), Discussion ‘’Saqan E.I., Frosch R.J. (2009), Influence of flexural reinforcement on shear strength of prestressed concrete beams’’, ACI Journal Disc. 106-S07, p60
[42] Autrup F., Jorgensen H.B., Hoang L.C. (2020), Experimental investigation of dowel action in RC beams without shear reinforcement, Conference paper

[43] Muttoni A., Fernandez Ruiz M. (2019), From experimental evidence to mechanical modeling and design expressions: The Critical Shear Crack Theory for shear design, Stuctural Concrete 20, pp1464-1480
[44] Vecchio F.J., Collins M.P. (1986), The Modified Compression Field Theory for Reinforced Concrete Elements Subjected to Shear, ACI Journal 83(2), pp219-231
[45] Regan P. (2000), Aspects of diagonal tension in reinforced concrete, Structural Concrete, No. 13, pp119-132
[46] Taylor H. P. J. (1972), Shear Strength of Large Beams, Journal of the Structural Division, ASCE, No. 98, pp2484-2488
[47] Sherwood E. G., Bentz E. C. and Collins M. P.(2007), Effect of Aggregate Size on Beam-Shear Strength of Thick Slabs, ACI Structural Journal 104(2), pp180-183
[48] Deng Q., Yi W.J. and Tang F.J. (2017), Effect of Coarse Aggregate Size on Shear Behavior of Beams without Shear Reinforcement, ACI Structural Journal 114(5), pp1131-1142
[49] Palaskas M.N., Attiogbe E.K. and Darwin D. (1980), Shear Strength of Lightly Reinforced T-beams, ACI Journal No. 78, pp447-455
[50] Al-Alusi A.F. (1956), Diagonal Tension Strength of Reinforced Concrete T-beams with Varying Shear Span, Journal Proceedings 53(5), pp1067-1077
[51] Yang Y. Den Uijl J.A. (2011), Report of Experimental Research on Shear Capacity of Beams Close to Intermediate Supports, TU Delft Report 25.5-11-10,
[52] Walraven J.C. (2013), Minimum afschuifdraagvermogen van platen uit gewapend beton zonder schuifwapening: de waarde v_{min}, Rapportnummer 25.5-12-04
[53] Rijkswaterstaat GPO (2022), RTD1006 Richtlijnen Beoordeling Kunstwerken versie 1.2.1

Annex I

Layer model

In this annex the layer model to determine the grade of fullness is shown.

The theory of Jourawski is used to determine the shear stress:

$$\tau = \frac{VS}{bI}$$

where:
V is the shear force in N
S is the statical moment of the area
I is the moment of ineartia of the entire cross-section
b is the web width at the neutral axis

The shear stress has been determined for different heights in the cross-section using the formula above, where the height of a layer is 5mm. Because the layer height is so small, it is possible to approach it as a rectangular cross-section. Based on this assumption, the required parameters are determined as follows:

$$\Delta A_i = (h_i - h_{i-1}) \frac{b_w + b_{w-1}}{2}$$

$$A_i = A_{i-1} + \Delta A_i$$

$$z_i = \frac{\Delta A_i \left(h_{i-1} + \frac{h_i - h_{i-1}}{2} \right) + A_{i-1} z_{i-1}}{A_i}$$

$$S_i = A_i (z_c - z_i)$$

$$I_i = \frac{1}{12} \frac{b_i + b_{i-1}}{2} (h_i - h_{i-1})^3 + \Delta A_i \left(z_c - \left(h_{i-1} + \frac{h_i - h_{i-1}}{2} \right)\right)^2 + I_{i-1}$$

$$V = (h_i - h_{i-1}) * \frac{b_i + b_{i-1}}{2} \frac{\tau_i + t_{i-1}}{2}$$

Plate with holes

Beam parameters	
b	600
h_f	100
b_w	200
h_w	400
h	600
D	400

Ratio
h_f/h 0,17

Unit shear force:	V =		100	kN
Concrete cover	c =		30	mm
Rebar diameter	d_r =		20	mm
Effective depth	d =		560	mm
Height of the compression zone:	z_c =	0,2d =	112	mm
Internal lever arm	z =		504	mm

Layer	h_i [mm]	ΔA_i [mm²]	A_i [mm²]	z_i [mm]	S_i [mm³]	b_i [mm]	I_i [mm⁴]	τ_i [MPa]	τ x b [N/mm]	V [N]
1	0	0	0	0	0	600	0,00E+00	0	0	
2	5	3000	3000	3	328500	600	3,60E+07	0,10	58	146
3	10	3000	6000	5	642000	600	6,87E+07	0,19	114	432
4	15	3000	9000	8	940500	600	9,85E+07	0,28	167	704
5	20	3000	12000	10	1224000	600	1,25E+08	0,36	218	963
6	25	3000	15000	13	1492500	600	1,49E+08	0,44	266	1209
7	30	3000	18000	15	1746000	600	1,71E+08	0,52	311	1441
8	35	3000	21000	18	1984500	600	1,90E+08	0,59	353	1660
9	40	3000	24000	20	2208000	600	2,06E+08	0,65	393	1865
10	45	3000	27000	23	2416500	600	2,21E+08	0,72	430	2058
11	50	3000	30000	25	2610000	600	2,33E+08	0,77	464	2236
12	55	3000	33000	28	2788500	600	2,44E+08	0,83	496	2402
13	60	3000	36000	30	2952000	600	2,53E+08	0,88	525	2554
14	65	3000	39000	33	3100500	600	2,60E+08	0,92	552	2693
15	70	3000	42000	35	3234000	600	2,66E+08	0,96	576	2818
16	75	3000	45000	38	3352500	600	2,71E+08	0,99	597	2930
17	80	3000	48000	40	3456000	600	2,74E+08	1,03	615	3029
18	85	3000	51000	43	3544500	600	2,77E+08	1,05	631	3115
19	90	3000	54000	45	3618000	600	2,79E+08	1,07	644	3187
20	95	3000	57000	48	3676500	600	2,80E+08	1,09	654	3245
21	100	3000	60000	50	3720000	600	2,81E+08	1,10	662	3291
22	105	2778	62778	52	3746389	511	2,81E+08	1,30	667	3344
23	110	2466	65243	54	3757484	475	2,81E+08	1,41	669	3343
24	112	939	66182	55	3758423	464	2,81E+08	1,44	669	1338
25	112	0	66182	55	3758423	464	2,81E+08	1,44	669	0
26		66181,97					5,62E+08			

Vc = 50,00 kN

Grade of fullness $\alpha = \frac{V_c}{\tau_m z_c b_w} =$ **0,67**

Comparison with only web (rectangular cross-section):

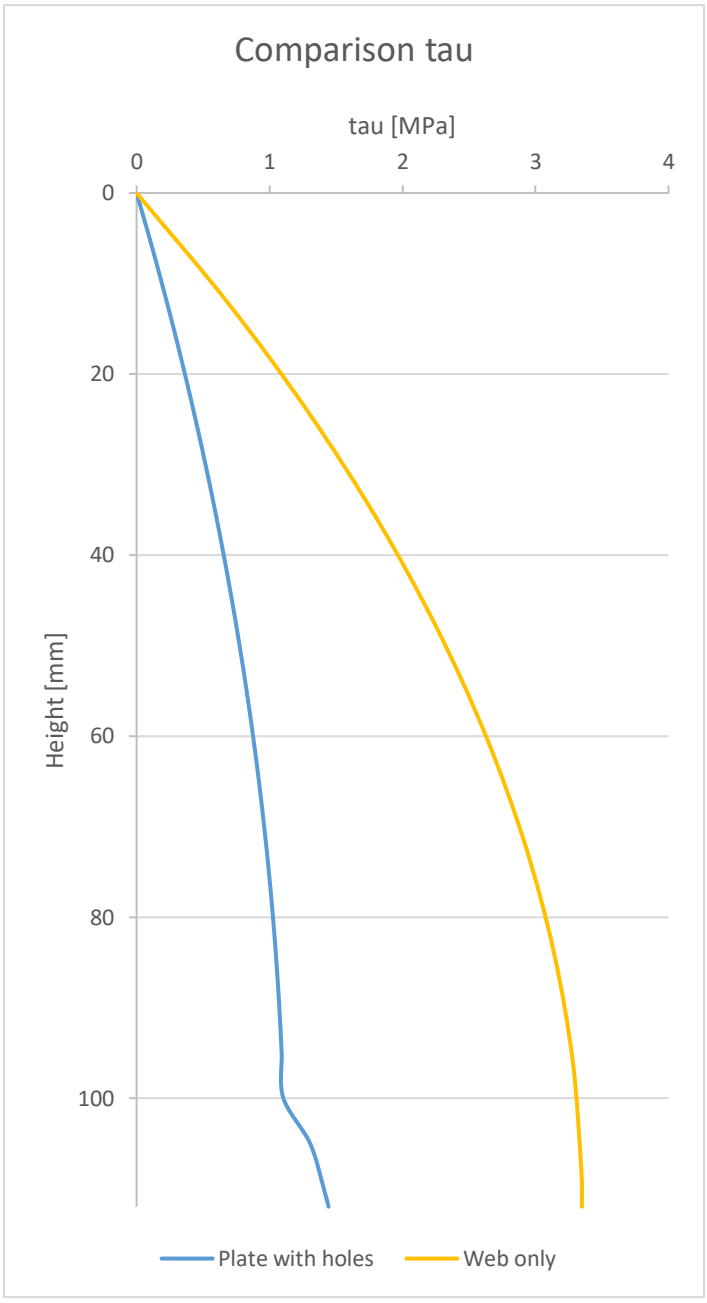

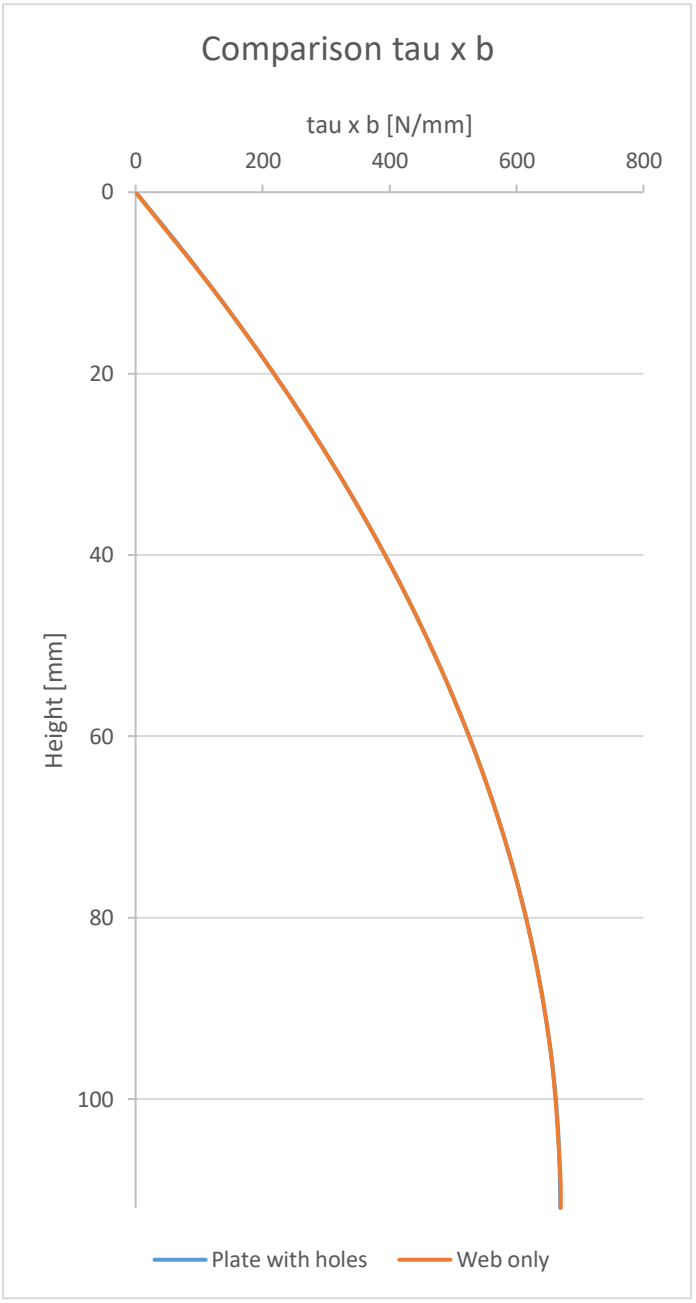

Annex II

Matlab Code

In this annex the Matlab scripts wherein the evaluation procedure is integrated for plates with holes, I-beams and T-beams are shown. For rectangular cross-sections, see PhD Thesis Yang (2014).

Plates with holes:

```
function [V, Vdw, Vai, Vc] = Vm(mvd, da, fc, bw, h, dr, hf, b, r, rho)
global Es Ec
Es = 210000; % elastic modules of steel in MPa
Ec = 40000; % elastic modules of concrete in MPa, only effecting the
% crack height calculation, thus a rough estimation is sufficient.
ne = Es/Ec; % ratio between Es and Ec for crack height calculation
d = 0.9*h; %rough estimation of the effective height
Ac = b*h-(pi*r^2)-(h-d)*b; % effective concrete area
As = rho*Ac; %reinforcement area appr. 0,4% for plates
delta = min((3.3555e-5.*d+.005), .025);%critical shear displacement
if rho<0.01
    if hf<= 0.25*d %height of the compression zone
        zc = 0.25*d;
    else
        zc = 0.2*d;
    end

else
    if hf<= 0.35*d %height of the compression zone
        zc = 0.35*d;
    else
        zc = 0.3*d;
    end
end
scr = d-zc; % major crack height
lcrm = scr./1.28; % average crack spacing of major cracks
z = (2*d + scr)/3; % internal level arm
V1 = 1.5*d*bw; % first guess of shear resistance
V0 = 0; count = 0; % initiation of iteration
while abs(V0-V1) > 10
M0 = V1*d*mvd; % cross sectional moment
w = M0/z/As/Es*lcrm; % estimation of average crack width
V0 = V1;
Vdw = V_dw(bw, fc, dr, b); %dowel action
Vai = V_ai(delta, w, da, scr, fc, hf, b, r, h, d); % aggregate interlock
Vc = V_c(z, d, V0); % shear force in compression zone
V1 = Vai + Vc + Vdw; % summation of total shear force
V = V1;
if count == 1000 % maximum iteration number is 100
    disp("Calculation didn't converge")
break
end
count = count+1;
end
end
```

```
%-------------------------------------------------------------------------
function Vai = V_ai(delta, w, da, scr, fc, hf, b, r, h, d)
% shear resistance contributed by aggregate interlock, based on eq..(4.13)
w0 = 0.01; % crack width at crack tip
dw = (w0-w)/100; % increment of crack width in the linear crack profile
CrackProfile = (w: dw: w0); % crack profile, divided into 100 sections
n = numel(CrackProfile);
L = scr/n;
fc = min(fc,60); % limitation for high strength concrete
tau = zeros(size(CrackProfile));
bwi = zeros(size(CrackProfile));
for l = 1:n
    hL = l * L;
[~,tau(l)]=AI_walraven(CrackProfile(l), delta, da, fc);
% Walraven's aggregate interlocking formula
    if hL<=(hf-0.1*h)
        bwi(l)=b;
    elseif hL>=(d-hf)
        bwi(l)=b;
    elseif hL>(hf-0.1*h)
        bwi(l)=abs(b-2*sqrt((r^2)-((hL+0.1*h)-hf-r)^2));
    end
%Adding the term of bwi
end
Vai = -sum(tau.*bwi.*L);
end

%-------------------------------------------------------------------------
function Vdw = V_dw(bw, fc, dr, b)
% maximum dowel action force, based on eq..(4.17)
Vdw = 1.64*min((bw*1.25),b-3*dr)*dr*(fc).^.333;
end

%-------------------------------------------------------------------------
function Vc = V_c(z, d, V)
% shear force contrition in compression zone, based on eq..(4.3)
Vc = 2*(d-z)/z*V;
end

%=========================================================================
```

I-beams:

```
function [V, Vdw, Vai, Vc] = Vm(mvd, da, fc, bw, h, dr, hf, b, rho)
global Es Ec
Es = 210000; % elastic modules of steel in MPa
Ec = 40000; % elastic modules of concrete in MPa, only effecting the
% crack height calculation, thus a rough estimation is sufficient.
ne = Es/Ec; % ratio between Es and Ec for crack height calculation
d = 0.9*h; %rough estimation of the effective height
Ac = 2*b*hf+(h-2*hf)*bw-(h-d)*b; % effective concrete area
As = rho*Ac; %reinforcement area
delta = min((3.3555e-5.*d+.005), .025); %critical shear displacement
if rho<0.01
    if hf<= 0.3*d %height of the compression zone
        zc = 0.3*d;
    else
        zc = 0.2*d;
    end

else
    if hf<= 0.4*d %height of the compression zone
        zc = 0.4*d;
    else
        zc = 0.3*d;

    end
end
scr = d-zc; % major crack height
lcrm = scr./1.28; % average crack spacing of major cracks
z = (2*d + scr)/3; % internal level arm
V1 = 1.5*d*bw; % first guess of shear resistance
V0 = 0; count = 0; % initiation of iteration
while abs(V0-V1) > 10
M0 = V1*d*mvd; % cross sectional moment
w = M0/z/As/Es*lcrm; % estimation of average crack width
V0 = V1;
Vdw = V_dw(bw, fc, dr, b); %dowel action
Vai = V_ai(delta, w, da, scr, fc, hf, b, bw, h, d); % aggregate interlock
Vc = V_c(z, d, V0, hf, rho); % shear force in compression zone
V1 = Vai + Vc + Vdw; % summation of total shear force
V = V1;
if count == 1000 % maximum iteration number is 100
    disp("Calculation didn't converge")
break
end
count = count+1;
end
end

%-------------------------------------------------------------------------
function Vai = V_ai(delta, w, da, scr, fc, hf, b, bw, h, d)
% shear resistance contributed by aggregate interlock, based on eq..(4.14)
w0 = 0.01; % crack width at crack tip
dw = (w0-w)/100; % increment of crack width in the linear crack profile
CrackProfile = (w: dw: w0); % crack profile, divided into 100 sections
n = numel(CrackProfile);
L = scr/n;
```

```
fc = min(fc,60); % limitation for high strength concrete
tau = zeros(size(CrackProfile));
bwi = zeros(size(CrackProfile));
for l = 1:n
    hL = l * L;
[~,tau(l)]=AI_walraven(CrackProfile(l), delta, da, fc);
% Walraven's aggregate interlocking formula
    if hL<=(hf-0.1*h)
        bwi(l)=b;
    elseif hL>=(d-hf)
        bwi(l)=b;
    else
        bwi(l)=bw;
    end
%Adding the term of bwi
end
Vai = -sum(tau.*bwi.*L);
end

%-------------------------------------------------------------------------
function Vdw = V_dw(bw, fc, dr, b)
% maximum dowel action force, based on eq..(4.16)
Vdw = 1.64*min(bw,b-3*dr)*dr*(fc).^.333;

end

%-------------------------------------------------------------------------
function Vc = V_c(z, d, V, hf, rho)
% shear force contrition in compression zone, based on eq..(4.7)
if rho<0.01
    if hf<= 0.3*d %height of the compression zone
        zc = 0.3*d;
    else
        zc = 0.2*d;
    end

else
    if hf<= 0.4*d %height of the compression zone
        zc = 0.4*d;
    else
        zc = 0.3*d;
    end
end

if hf>=zc
    Vc = 2*(d-z)/z*V; %compression zone if neutral axis is in de flange
else
    Vc = (3/4)*(zc/z)*V;%compression zone if neutal axis is below hf
end
end

%=========================================================================
```

T-beams:

```
function [V, Vdw, Vai, Vc] = Vm(mvd, da, fc, bw, h, dr, hf, b, rho)
global Es Ec
Es = 210000; % elastic modules of steel in MPa
Ec = 40000; % elastic modules of concrete in MPa, only effecting the
% crack height calculation, thus a rough estimation is sufficient.
ne = Es/Ec; % ratio between Es and Ec for crack height calculation
d = 0.9*h; %rough estimation of the effective height
Ac = b*hf+(h-hf)*bw-(h-d)*bw; % effective concrete area
As = rho*Ac; %reinforcement area
delta = min((3.3555e-5.*d+.005), .025); %critical shear displacement
if rho<0.01
    if hf<= 0.3*d %height of the compression zone
        zc = 0.3*d;
    else
        zc = 0.2*d;
    end

else
    if hf<= 0.4*d %height of the compression zone
        zc = 0.4*d;
    else
        zc = 0.3*d;
    end
end
scr = d-zc; % major crack height
lcrm = scr./1.28; % average crack spacing of major cracks
z = (2*d + scr)/3; % internal level arm
V1 = 1.5*d*bw; % first guess of shear resistance
V0 = 0; count = 0; % initiation of iteration
while abs(V0-V1) > 10
M0 = V1*d*mvd; % cross sectional moment
w = M0/z/As/Es*lcrm; % estimation of average crack width eq..(4.8)
V0 = V1;
Vdw = V_dw(bw, fc, dr, As); %dowel action
Vai = V_ai(delta, w, da, scr, fc, hf, b, bw, h, d); % aggregate interlock
Vc = V_c(z, d, V0, hf, rho); % shear force in compression zone
V1 = Vai + Vc + Vdw; % summation of total shear force
V = V1;
if count == 100 % maximum iteration number is 100
    disp("Calculation didn't converge")
break
end
count = count+1;
end
end

%-------------------------------------------------------------------------
function Vai = V_ai(delta, w, da, scr, fc, hf, b, bw, h, d)
% shear resistance contributed by aggregate interlock, based on eq..(4.14)
w0 = 0.01; % crack width at crack tip
dw = (w0-w)/100; % increment of crack width in the linear crack profile
CrackProfile = (w: dw: w0); % crack profile, divided into 100 sections
n = numel(CrackProfile);
L = scr/n;
fc = min(fc,60); % limitation for high strength concrete
```

```
tau = zeros(size(CrackProfile));
bwi = zeros(size(CrackProfile));
for l = 1:n
    hL = l * L;
[~,tau(l)]=AI_walraven(CrackProfile(l), delta, da, fc);
% Walraven's aggregate interlocking formula eq..(3.30)
    if hL>=(d-hf)
        bwi(l)=b;
    else
        bwi(l)=bw;
    end
%Adding the term of bwi
end
Vai = -sum(tau.*bwi.*L);
end

%-------------------------------------------------------------------------
function Vdw = V_dw(bw, fc, dr, As)
% maximum dowel action force, based on eq..(4.15)
n = As/(pi*(dr/2)^2);
if ceil(n) <= 3
    br = dr * ceil(n);
elseif ceil(n)>= 4
    br = dr * 3;
end
Vdw = 1.64*(bw-br)*dr*(fc).^.333;

end

%-------------------------------------------------------------------------
function Vc = V_c(z, d, V, hf,rho)
% shear force contrition in compression zone, based on eq..(4.7)
if rho<0.01
    if hf<= 0.3*d %height of the compression zone
        zc = 0.3*d;
    else
        zc = 0.2*d;
    end

else
    if hf<= 0.4*d %height of the compression zone
        zc = 0.4*d;
    else
        zc = 0.3*d;
    end
end

if hf>=zc
    Vc = 2*(d-z)/z*V; %compression zone if neutral axis is in de flange
else

    Vc = (3/4)*(zc/z)*V; %compression zone if neutal axis is below hf

end
end
%=========================================================================
```

Annex III

Shear Database

In this annex the collected test results from literature are shown. In total 32 tests found and used during this study. The data is selected considering the following criteria:

- Ratio of shear slenderness divided by the effective depth a/d should be bigger than 2,5
- Reinforced non-rectangular cross-sections, especially plates with holes, I-beams and T-beams

The model predicts accurate results, with an average of 0,94 and Coefficient of Variation of 16%. The calculations according to EC2 assuming b_{weff} also gives a good match with the test results. The average of this model is 0,79 and CoV is 21%.

Reference	Beam	Type	mvd [-]	f_c [Mpa]	b_w [mm]	b_f [mm]	h_f [mm]	h [mm]	r [mm]	d [mm]	ρ_s [-]	n [-]	A_c [mm^2]	A_s [mm^2]	b_w/b_f [-]	h_f/h [-]	sf [-]	d_r [mm]	d_a [mm]	V_u [kN]	V_{cal} [kN]	$V_{EC2;new}$ [kN]	V_{cal}/V_u [-]	$V_{EC2;new}/V_u$ [-]
Regan	**14.1**	PWH	4,9	21,1	45	250	47,5	300	102,5	276	0,0486	3	35994	604	0,18	0,16	1,75	16	20	26,2	24,0	22,6	0,91	0,86
	14.2	Ibeam	4,9	19,2	45	250	50	300	-	276	0,0486	3	28000	604	0,18	0,17	1,35	16	20	21,2	20,2	16,9	0,95	0,80
	14.3	PWH	4,9	24,1	45	200	72,5	300	77,5	276	0,0486	3	36331	604	0,23	0,24	1,75	16	20	19,3	26,5	23,6	1,37	1,22
	14.4	PWH	5,2	25,2	95	300	47,5	300	102,5	276	0,023	3	49794	603	0,32	0,16	1,75	16	20	42,5	33,5	39,4	0,79	0,93
	14.5	Tbeam	4,9	21,4	95	300	50	300	-	262	0,0242	2	35140	602	0,32	0,17	1,15	16	20	30,1	27,3	24,0	0,91	0,80
	14.6	Ibeam	4,9	19,6	95	300	50	300	-	276	0,023	3	41800	961	0,32	0,17	1,35	20	20	37,5	30,4	28,0	0,81	0,75
	1.2	Tbeam	2,62	32	200	400	75	300	-	264	0,012	2	67800	804	0,50	0,25	1,15	16	20	84	71,1	45,8	0,85	0,55
	1.3	Tbeam	2,62	31,2	200	400	75	300	-	264	0,012	2	67800	804	0,50	0,25	1,15	16	20	80	70,6	45,4	0,88	0,57
	1.4	Tbeam	2,7	28,1	200	400	75	300	-	272	0,006	2	69400	402	0,50	0,25	1,15	16	20	75	53,0	35,3	0,71	0,47
	1.6	Tbeam	2,7	28,7	100	400	75	300	-	272	0,008	2	49700	402	0,25	0,25	1,15	16	20	45	34,3	19,9	0,76	0,44
Thamrin	**T-01E**	Tbeam	3,7	32	125	250	70	250	-	219	0,010	2	36125	265	0,50	0,28	1,27	13	20	36,6	33,6	25,9	0,92	0,71
	T-02E	Tbeam	3,7	32	125	250	70	250	-	219	0,015	3	36125	398	0,50	0,28	1,27	13	20	38,5	32,2	29,6	0,84	0,77
	T-03E	Tbeam	3,8	32	125	250	70	250	-	212	0,025	3	35250	664	0,50	0,28	1,27	13	20	47,5	39,6	34,2	0,83	0,72
Palaskas	**No2**	Tbeam	4,14	32,8	191	610	102	457	-	374	0,007	3	114172	494	0,31	0,22	1,15	13	19	72,38	53,0	48,3	0,73	0,67
	A00	Tbeam	3,92	32,7	191	610	102	457	-	395	0,007	3	118183	494	0,31	0,22	1,15	13	19	64,98	55,3	49,5	0,85	0,76
	B00	Tbeam	3,88	32	191	610	102	457	-	399	0,005	3	118947	371	0,31	0,22	1,15	11	19	71,42	48,4	44,9	0,68	0,63
	C00	Tbeam	3,96	29,4	191	610	102	457	-	391	0,009	3	117419	703	0,31	0,22	1,15	15	19	59,28	62,0	53,5	1,05	0,90
Al-Alusi	**11**	Tbeam	3,32	29	76	330	32	146	-	127	0,026	2	17741,9	255	0,23	0,22	1,15	13	6	17,4	17,5	12,7	1,00	0,73
	2	Tbeam	3,45	28	76	330	32	146	-	127	0,015	2	17741,9	142	0,23	0,22	1,15	10	6	14,4	12,9	10,4	0,90	0,72
	3	Tbeam	4	27	76	330	32	146	-	127	0,015	2	17741,9	144	0,23	0,22	1,15	10	6	14,3	12,1	10,3	0,84	0,72
	10	Tbeam	4	29	76	330	32	146	-	127	0,027	2	17741,9	261	0,23	0,22	1,15	13	6	14,7	16,3	12,8	1,10	0,87
	4	Tbeam	4,01	27	76	330	32	146	-	127	0,015	2	17741,9	145	0,23	0,22	1,15	10	6	13,9	12,1	10,3	0,87	0,74
	13	Tbeam	4,02	29	76	330	32	146	-	127	0,027	2	17741,9	263	0,23	0,22	1,15	13	6	17,0	16,3	12,9	0,96	0,76
	18	Tbeam	4,39	27	76	330	32	146	-	127	0,027	2	17741,9	256	0,23	0,22	1,15	13	6	14,0	15,2	12,5	1,08	0,89
	7	Tbeam	4,5	25	76	330	32	146	-	127	0,027	2	17741,9	262	0,23	0,22	1,15	13	6	13,5	14,8	12,3	1,10	0,91
	24	Tbeam	4,51	28	76	330	32	146	-	127	0,027	2	17741,9	262	0,23	0,22	1,15	13	6	15,4	15,3	12,8	0,99	0,83
	17	Tbeam	5,36	30	76	330	32	146	-	127	0,027	2	17741,9	256	0,23	0,22	1,15	13	6	13,8	14,4	12,9	1,04	0,93
	8	Tbeam	5,5	26	76	330	32	146	-	127	0,027	2	17741,9	262	0,23	0,22	1,15	13	6	13,4	13,8	12,5	1,03	0,93
	19	Tbeam	5,5	31	76	330	32	146	-	127	0,042	2	17741,9	407	0,23	0,22	1,15	16	6	14,0	17,7	15,2	1,26	1,09
	25	Tbeam	5,79	26	76	330	32	146	-	127	0,029	2	17741,9	276	0,23	0,22	1,15	13	6	13,5	13,8	12,6	1,02	0,93
	9	Tbeam	6,5	32	76	330	32	146	-	127	0,027	2	17741,9	262	0,23	0,22	1,15	13	6	14,1	13,7	13,3	0,97	0,94
	20	Tbeam	6,54	27	76	330	32	146	-	127	0,042	2	17741,9	407	0,23	0,22	1,15	16	6	15,0	15,8	14,6	1,05	0,98
	23	Tbeam	7,76	28	76	330	32	146	-	127	0,044	2	17741,9	426	0,23	0,22	1,15	16	6	14,0	15,2	15,0	1,08	1,07